

AD 762 112

AD-762 112

MODEL TESTS OF LINED TUNNELS IN A JOINTED ROCK MASS

ILLINOIS UNIVERSITY

PREPARED FOR
ARMY CONSTRUCTION ENGINEERING RESEARCH LABORATORY

MAY 1973

Distributed By:

NTIS

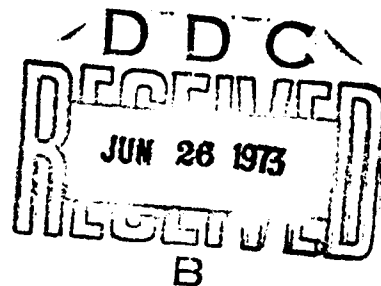
National Technical Information Service
U. S. DEPARTMENT OF COMMERCE

TECHNICAL REPORT M-41

MODEL TESTS OF LINED TUNNELS
IN A JOINTED ROCK MASS
(STRENGTHENING OF ROCK BY CHEMICAL ADHESIVE GROUTING)

by
A. J. Hendron, Jr.
and
Paul Engeling

May 1973



Department of the Army
CONSTRUCTION ENGINEERING RESEARCH LABORATORY
P.O. Box 4005
Champaign, Illinois 61820

Approved for public release; distribution unlimited.

UNCLASSIFIED

Security Classification:

DOCUMENT CONTROL DATA - R & D

(Security classification of title, body of abstract and indexing annotation must be entered when the overall report is classified)

1. ORIGINATING ACTIVITY (Corporate author) Construction Engineering Research Laboratory P.O. Box 4005 Champaign, Illinois 61820	2a. REPORT SECURITY CLASSIFICATION Unclassified
	2b. GROUP

3. REPORT TITLE
MODEL TESTS OF LINED TUNNELS IN A JOINTED ROCK MASS

4. DESCRIPTIVE NOTES (Type of report and inclusive dates)
Technical Report

5. AUTHOR(S) (First name, middle initial, last name)
A. J. Hendron, Jr.
Paul Engeling

6. REPORT DATE May 1973	7a. TOTAL NO. OF PAGES 75 76	7b. NO. OF REFS 60
----------------------------	---------------------------------	-----------------------

8a. CONTRACT OR GRANT NO. DACA 23-70-C-0050	9a. ORIGINATOR'S REPORT NUMBER(S) CERL-TR-M-41
b. PROJECT NO. 6.21.04A 4A062104A880	
c. d.	9b. OTHER REPORT NO(S) (Any other numbers that may be assigned this report) AD# obtainable from address block 1.

10. DISTRIBUTION STATEMENT
Approved for public release; distribution unlimited.

11. SUPPLEMENTARY NOTES
Copies of this report are obtainable from National Technical Information Service, Springfield, Virginia 22151

12. SPONSORING MILITARY ACTIVITY
Department of the Army

13. ABSTRACT

Model laws governing the design of geomechanical model studies of underground openings in rock subjected to static loads are developed using dimensional analysis and the theory of models. The significant variables influencing the behavior of rock considered in this study are the free-field stresses, the properties of the discontinuities in the rock mass, the opening geometry, and the structural liner supporting the opening. The prototype chosen for study is a short section of a long circular tunnel which is underground at a depth of more than four tunnel diameters.

The development of geomechanical modeling techniques for the construction and testing of jointed rock models is described. The strength properties of the intact model material and of the joint surfaces are also presented. The models were tested in plane strain (zero strain parallel to the tunnel axis) by the use of a controlled rigid longitudinal loading head.

Five jointed models were tested to determine the effect of tunnel liner stiffness and the ratio of joint spacing to tunnel diameter on the behavior of tunnel liners in jointed rock masses. The model tunnels were lined with plexiglass liners of varying thickness to simulate reinforced concrete liners in a jointed rock mass. The effect of the ratio of the tunnel diameter to joint spacing on structural behavior was studied by testing three different size tunnels in the model rock mass composed of 1-in. square joint blocks. The structural behavior of the models was assessed by means of quantitative measurements such as measurement of the diameter changes of the liner, the extensometer measurements of displacements in the rock mass behind the tunnel wall.

The observed model behavior was analyzed and compared to a previously developed elasto-plastic analysis. The analyses showed that elastic theory was sufficiently accurate for calculating the diametrical strains of the lined tunnels up to diametrical strains of about 1.2%. For diametrical strains above 1.2%, the elasto-plastic theory was used successfully to calculate the tunnel diametrical strains within an error of about $\pm 15\%$.

KEY WORDS
geomechanical models jointed rock models elasto-plastic analysis

ABSTRACT

Model laws governing the design of geomechanical model studies of underground openings in rock subjected to static loads are developed using dimensional analysis and the theory of models. The significant variables influencing the behavior of rock considered in this study are the free-field stresses, the properties of the discontinuities in the rock mass, the opening geometry, and the structural liner supporting the opening. The prototype chosen for study is a short section of a long circular tunnel which is underground at a depth of more than four tunnel diameters.

The development of geomechanical modeling techniques for the construction and testing of jointed rock models is described. The strength properties of the intact model material and of the joint surfaces are also presented. The models were tested in plane strain (zero strain parallel to the tunnel axis) by the use of a controlled rigid longitudinal loading head.

Five jointed models were tested to determine the effect of tunnel liner stiffness and the ratio of joint spacing to tunnel diameter on the behavior of tunnel liners in jointed rock masses. The model tunnels were lined with plexiglass liners of varying thickness to simulate reinforced concrete liners in a jointed rock mass. The effect of the ratio of the tunnel diameter to joint spacing on structural behavior was studied by testing three different size tunnels in the model rock mass composed of 1-in. square joint blocks. The structural behavior of the models was assessed by means of quantitative measurements such as measurement of the diameter changes of the liner, the extensometer measurements of displacements in the rock mass behind the tunnel wall.

The observed model behavior was analyzed and compared to a previously developed elasto-plastic analysis. The analyses showed that elastic theory was sufficiently accurate for calculating the diametrical strains of the lined tunnels up to diametrical strains of about 1.2%. For diametrical strains above 1.2%, the elasto-plastic theory was used successfully to calculate the tunnel diametrical strains within an error of about $\pm 15\%$.

CONTENTS

	ABSTRACT	
	FOREWORD	
	LIST OF FIGURES, TABLES	
1	INTRODUCTION	1
	Justification for Geomechanical Model Studies	
	Scope of Study	
2	GEOMECHANICAL MODELING TECHNIQUES	3
	Development of Jointed Models	
	Free-Field Strain Measurement	
3	TEST RESULTS	11
	Presentation of Test Results	
4	ANALYSIS OF TEST RESULTS	29
5	CONCLUSIONS	35
	REFERENCES	
	APPENDIX A: SIMILITUDE CONSIDERATIONS	
	APPENDIX B: DESCRIPTION OF MODEL LOADING APPARATUS	
	DISTRIBUTION	
	DD FORM 1473	

FIGURES

Number		Page
1	Jointed model configuration used in Joint Block #6, #7 and #8	5
2	Jointed model configuration used in Joint Block #9 and #10	5
3	Compaction of 20" X 20" X 3" block of model material	6
4	Diamond-blade saw used to cut joint blocks	6
5	Grain size distribution of fine Sangamon River sand	7
6	Triaxial shear strength properties of intact model material	8
7	Results of direct shear tests on joint surfaces of model material	8
8	Jointed model ready for test	9
9	Locations of extensometer in jointed test blocks	10
10	Extensometer ready for installation in test block	11
11	Detail of extensometer measurement setup	12
12	Extensometer exposed after test	13
13	Average vertical model stress-strain curves for JB #6	15
14	Diametrical strain of liner at four different diameters for JB #6	16
15	Dimensionless plot of diametrical strain of liner as a function of vertical free-field strain of model for JB #6	17
16	Stress-strain curves for JB #7	19
17	Diametrical strain of tunnel liner at four different diameters for JB #7	20
18	Stress-strain curves for JB #8	21
19	Diametrical strain of tunnel liner at four different diameters for JB #8	22
20	Stress-strain curves for JB #9	24
21	Diametrical strain of tunnel liner at three different diameters for JB #9	25
22	Stress-strain curves for JB #10	26
23	Diametrical strain of tunnel liner at four different diameters for JB #10	27
24	Average stress-strain curves for JB #7, JB #8, JB #9 and JB #10	28
25	Average diametrical strain of tunnel liner as a function of model pressure for JB #7, JB #8, JB #9 and JB #10	30
26	Dimensionless plot of average diametrical strain of tunnel liner as a function of average vertical strain of model for JB #7, JB #8, JB #9 and JB #10	31
27	Ratio of insitu strength to laboratory strength as a function of tunnel diameter to joint spacing	32
28	Stress-strain curve used for plexiglass liners	33
29	Diametrical strain of tunnel liner as a function of model pressure - measured results compared to theory	34

FIGURES (continued)

Number		Page
30	Diametrical strain of tunnel liner as a function of model pressure--measured results compared to theory	36
A1	Stress distribution some distance from tunnel	41
A2	Approximate stress distribution some distance from tunnel	41
A3	Failure envelope considered typical for rock	43
A4	Stress-strain curve considered typical for rock	43
A5	Prototype and model Mohr envelopes	48
A6	Dimensionless prototype and model Mohr envelopes	48
A7	Prototype and model stress-strain curves	49
A8	Dimensionless prototype and model stress-strain curve	49
B1	Detail of lateral triangular loading elements	52
B2	Sketch of lateral loading element assembly	53
B3	An instrumented No. 3 loading element	54
B4	Entire set of instrumented lateral loading elements	54
B5	Calibration of lateral loading elements	55
B6	Sketch of possible cantilevered lateral reaction system	56
B7	Plan and section of top head	57
B8	Loading machine	58
B9	Loading frame assembly	59
B10	A lateral loading assembly	60
B11	Longitudinal end reaction in σ_v direction	61
B12	Lower longitudinal reaction head and concrete pedestal	62
B13	Schematic diagram of base and loading element assembly	63
B14	Top longitudinal reaction head	64

TABLES

I	Summary of model blocks tested	14
A1	Significant variables	40
A2	Dimensionless Pi terms	46
A3	Model laws	47

MODEL TESTS OF LINED TUNNELS IN A JOINTED ROCK MASS

1 INTRODUCTION

Justification for Geomechanical Model Studies. The current volume of underground construction activity for military and civil work is unprecedented in history, and is expected to expand significantly in the future. Moreover, the size and complexity of underground structures is steadily increasing. Although significant advances have been made in recent years, our understanding of the behavior of underground openings is poor because the problem is extremely complex and highly indeterminate due to the discontinuous nature of jointed rock masses. A more comprehensive understanding of the interaction of various structural liners with jointed rock masses is necessary if future underground works are to be designed and constructed rationally and economically.

Among the variables which exert a significant influence on the behavior of underground openings in rock are the following: natural free-field stresses in rock mass; artificial, superimposed loads coming either from within the opening or applied to the rock mass at some distant point; mechanical properties of the intact rock material; the nature of discontinuities in the rock mass, such as joints, faults, and bedding planes; the geometry of the opening; the structural liner or rock bolts supporting the opening; and the techniques and sequence by which the opening is constructed.

Analytical methods of predicting the behavior of underground openings in rock are quite limited in applicability because the jointed rock mass is generally discontinuous; the construction procedures are of great significance but are often indeterminate; and the system consisting of the underground structure and the surrounding rock mass is also highly indeterminate. Solutions from the theory of elasticity are directly applicable only to a limited number of rock masses whose properties approach the assumptions of elastic theory because joint spacings are large and the stress levels imposed are below failure stresses for the rock mass.

Numerical analyses utilizing finite element techniques and electronic computers are much more versatile and are becoming quite sophisticated. They are

capable of considering to varying degrees such properties as openings of any shape, anisotropy, non-homogeneous layering, non-linear elastic-plastic frictional material properties, and discontinuities in the rock mass (see for example Reyes,¹ Goodman,² and Zienkiewicz.³). At present, however, restrictions of computer size, development of finite element techniques, and our ability to accurately determine and describe the actual complex properties of the intact rock material, the rock mass, and the underground structures limit the usefulness of this method of analysis.

Hence, in addition to the use of theoretical and analytical techniques in studying and predicting the behavior of underground openings, it is necessary to use empirical techniques in field and laboratory experimentation. Limited field data concerning the behavior of underground openings subjected to static and dynamic loadings are available, but it is not possible to extrapolate these data directly to predict the behavior at other sites where the pertinent variables have different values. In order to do this one must have a quantitative basis for determining how changes in the variables will influence the behavior of the opening. To develop empirically such quantitative relationships between the pertinent variables and the behavior of the opening, data must be obtained over a wide range of the variables. The cost and impracticality of obtaining data from many full-scale field construction sites limits the usefulness of this approach. Field data does, however, offer the only ready means of studying the influence of construction techniques. In addition, concepts and predictions derived from other methods of study must ultimately be checked by field observations to substantiate or disprove their validity and usefulness.

¹ S.F. Reyes, *Elastic Plastic Analysis of Underground Openings by the Finite Element Method*, Ph. D. Thesis (University of Illinois, 1966).

² R.E. Goodman, "On the Distribution of Stresses Around Circular Tunnels in Non-Homogeneous Rocks," *Proceedings, 1st International Congress, Vol 2* (Int. Soc. of Rock Mec., 1966) pp 249-255; R. E. Goodman, R.L. Taylor and T. L. Brekke, "A Model for the Mechanics of Jointed Rock," *Proceedings ASCE*, Vol 94, No. 1 (May 1968) pp 637-659.

³ O.C. Zienkiewicz, "Continuum Mechanics as an Approach to Rock Mass Problems," *Rock Mechanics in Engineering Practice*, Stagg and Zienkiewicz, ed. (John Wiley & Sons, 1968).

A most promising technique for studying the influence of many of the pertinent variables appears to be the use of geomechanical models. In this technique, a small scale model of the underground opening is constructed in a material which accurately models the properties of the actual rock mass in the field. The model is then loaded in such a manner as to reproduce the stress state which exists in the real prototype underground. If the requirements of similitude are satisfied, the behavior of the model then reproduces the behavior of the prototype in all respects: distribution of stresses, distribution of strains and deformations both elastic and inelastic, and failure modes. There are relatively few theoretical limitations on this technique. Its usefulness appears to depend mostly upon the skill and ingenuity of the investigator in solving the many practical and technical problems involved in trying to satisfy the requirements of similitude, particularly in modeling the details of the underground structure and of the geologic environment of the prototype. These problems are not insignificant.

The validity and usefulness of structural models is well established in many phases of engineering research and design. The most notable examples in civil engineering probably are the structural model tests of arch dams and other structures at such places as Laboratório Nacional de Engenharia Civil in Lisbon, Portugal and Istituto Sperimentale Modelli e Strutture in Bergamo, Italy. The next step beyond structural modeling is the use of geomechanical models in which not only the proposed engineering structure is modeled, but an attempt is also made to model the details of the geologic environment in which the structure is to exist. For example, the in-situ stress state, the strength and deformability of the different rock formations, and the frequency, orientation, and strength and deformation characteristics of discontinuities such as joints, bedding planes, and faults are modeled as accurately as is possible and practical. The structure and surrounding geologic environment are envisioned as a single interacting unit in which the behavior of the structure itself cannot be predicted without giving due consideration to the behavior of the surrounding geologic environment.

The use of geomechanical models appears to be the only technique available analytical or experimental for determining the behavior of underground openings through all stages of loading and deformation, both elastic and inelastic, up to failure.

The theoretical basis of model studies in general

(for example, Marpay,⁴ Langhaar,⁵) and of structural and geomechanical models in particular (for example, Preece and Davies,⁶ Rocha,⁷ Fumagalli,⁸ Mandel,⁹) has been well established. The basis for geomechanical model studies of underground openings in rock (not considering time-dependent behavior) has been discussed and developed to varying degrees by experimenters such as Barron and Laroque,¹⁰ Everling,¹¹ Hobbs,¹² Hoek,¹³ and Fumagalli.¹⁴

Some critical aspects of similitude requirements such as boundary loading conditions and model material properties generally have not been adequately satisfied by the investigators above, however, and their

-
- ⁴ G. Murphy, *Similitude in Engineering* (Ronald Press, 1950).
 - ⁵ H.L. Langhaar, *Dimensional Analysis and Theory of Models* (John Wiley & Sons, 1951).
 - ⁶ B.W. Preece and J.W. Davies, *Models for Structural Concrete* (C.R. Books Ltd., London, 1964).
 - ⁷ M. Rocha, "Model Tests in Portugal," *Civ. Engr. and Pub. Work Rev.*, Vol 53, No. 619 (January 1958) pp 49-53, and No. 620 (February 1958) pp 179-182; "Structural Model Techniques - Some Recent Developments," *Stress Analysis*, Zienkiewicz and Hollister, ed (John Wiley & Sons, 1965).
 - ⁸ E. Fumagalli, "Communication Sur Les Materiaux Pour Modeles Statiques de Barrages en Beton," *5th International Congress on Large Dams*, Vol 4, C. 26 (Paris, 1955) pp 1039-1074; "The Use of Models in Reinforced Concrete Structures," *Magazine of Concrete Research*, Vol 12, No. 35 (July 1960) pp 63-72; and "Modeles Geomechaniques des Reservoirs Artificiels: Materiaux, Technique D'Essais, Ex- ampler de Reproduction Sur Modeles," ISMES Pub. No. 26 (Bergamo, Italy, October 1964); "Model Simulation of Rock Mechanics Problems," *Rock Mechanics in Engineering Practice*, Ch II, Stagg and Zienkiewicz, ed. (John Wiley & Sons, 1968).
 - ⁹ J. Mandel, "Tests on Reduced Scale Models in Soil and Rock Mechanics, A Study of the Conditions of Similitude," *International Journal of Rock Mechanics and Mining Science*, Vol 1, No. 1 (1964) pp 31-42.
 - ¹⁰ K. Barron and G. Laroque, "Development of a Model for a Mine Structure," *Proc. Rock Mechanics Symposium* (McGill University, Montreal, 1962).
 - ¹¹ G. Everling, "Model Tests Concerning the Interaction of Ground and Roof Support in Gate-Roads," *Int. Journ. Rock Mech. and Min. Sci.*, Vol 1, No. 3 (1964) pp 319-326.
 - ¹² D.W. Hobbs, "Scale Model Studies of Strata Movement Around Mine Roadways, Apparatus, Technique, and Some Preliminary Results," *Int. Journ. of Rock Mech. and Min. Sci.*, Vol 3, No. 3 (May 1966) pp 101-128; "Scale Model Studies of Strata Movement Around Mine Roadways - I, II, III," *Int. Journ. of Rock Mech. and Min. Sci.*, Vol 5, No. 3 (May 1968) pp 219-251.
 - ¹³ E. Hoek, *Rock Fracture Under Static Stress Conditions*, CSIR Report MEG 383 (Nat. Mech. Eng. Res. Inst., Pretoria, South Africa, 1965).
 - ¹⁴ E. Fumagalli, "Model Simulation of Rock Mechanics Problems."

work is of limited value in a general understanding of the influence of the variables affecting the behavior of underground openings in rock. For example, in the studies cited above the rock tunnels studied were subjected to plane stress rather than the plane strain loading which tunnels are subjected to in the field. In addition, the model materials used by the investigators listed above had angles of internal friction ranging from 5° to 20° under significant stresses and thus would lead to an underestimation of the strength of rock materials around tunnels in the field.

Heuer and Hendron¹⁵ have overcome these difficulties by developing a device to subject model tunnels to plane strain loading and by developing a model material with an angle of internal friction comparable to many real rock materials. In addition, techniques have been developed for acquiring detailed quantitative measurements of the behavior of the rock mass behind the tunnel wall.¹⁶ Recent developments also enable the modeling of the interaction of structural linings with jointed rock masses.¹⁷

Scope of Study. In this study a number of models were tested to study their behavior. The models were lined with plexiglass liners of varying thicknesses to simulate reinforced concrete tunnel liners in a jointed rock mass. The effect of the ratio of the tunnel diameter to joint spacing on structural behavior was also studied by testing three different size openings in the model rock mass composed on 1-in. square joint blocks. The structural behavior of the model was assessed by means of quantitative measurements such as clip gage measurements of diameter changes of the liner, and model extensometers to measure displacements in the rock mass behind the tunnel wall.

¹⁵R.E. Heuer and A.J. Hendron, *Geomechanical Model Study of the Behavior of Underground Openings in Rock Subjected to Static Loads: Report 1, Development of Modeling Techniques*, Contract Report N-69-1 (U.S. Army Engineer Waterways Experiment Station [WES], October 1969).

¹⁶R.E. Heuer and A.J. Hendron, *Geomechanical Model Study...Report 1*; R.E. Heuer, "Geomechanical Model Study of the Behavior of Underground Openings in Rock Subjected to Static Loads," Ph.D. Thesis (University of Illinois, 1971); and Heuer and Hendron, *Geomechanical Model Study of the Behavior of Underground Openings in Rock Subjected to Static Loads: Report 2, Tests on Unlined Openings in Intact Rock*, Contract Report N-69-1 (WES, 1971).

¹⁷A.J. Hendron, Jr., P. Engeling, A.K. Aiyer, and S. Paul, *Geomechanical Model Study of the Behavior of Underground Openings in Rock Subjected to Static Loads Report 3* (WES [in publication]).

The similitude requirements governing the choice of model rock material and the model structural liner are given in Appendix A. Although this analysis was developed in previous studies by Heuer and Hendron, it is repeated in Appendix A to give the reader a better understanding of the basis for the choice of the structural linings tested in this study.

The methods and details of constructing the jointed models are described in Chapter 2, which also reviews strength properties of the intact model material and gives strength properties of the joint surfaces. Details of the model instrumentation are also included. (Appendix B describes the model loading apparatus.) Chapter 3 discusses selection of the model structural linings and reports results of the experimental measurements. An analysis of the data and the conclusions which can be drawn from these tests is in Chapter 4.

2 GEOMECHANICAL MODELING TECHNIQUES

The model material, the techniques of model construction, and the instrumentation and loading equipment used on this contract (DACA 23-70-C-0050) were all developed on a previous contract (DACA 39-67-C-0009) with the U.S. Army Engineer Waterways Experiment Station. Complete discussions of these earlier phases of the project are given by Heuer and Hendron, Heuer, and Hendron et al. The remainder of this chapter is a brief discussion of the modeling techniques used in this phase of the project.

Development of Jointed Models. The loading frame used was designed to test 24" × 24" × 8" models in plane strain (no strain along the axis of the tunnel). The model tunnels tested on this study were 4, 6, and 8 inches in diameter and were drilled through the center of the 24" × 24" faces. Thus, the model tunnel simulates a section in the axial direction. All of the jointed models were constructed to have two sets of mutually perpendicular joints oriented parallel to the tunnel axis. Figures 1 and 2 show the joint configurations used in the models tested in this study. The models were tested with the 24" × 24" faces horizontal, and thus the longitudinal direction is vertical in the model whereas it would generally be the horizontal direction in the field. The models were tested in this orientation because it greatly simplified the design of the loading apparatus.

Figures 1 and 2 show that a large number of joint blocks were required for the construction of a single model. Two possible methods could be used to manufacture such a large number of joint blocks: they could either be cast in a mold to the proper shape, or they could be sawed out of larger blocks of model material. Because of the large amount of time-consuming work anticipated in a sawing process, it was decided first to try molding the blocks by vibrating a sand-water-plaster mix in a mold. The anticipated model blocks would be required to have a low cohesion, c , so they could be failed by the testing machine and a high angle of shearing resistance, ϕ , to accurately simulate the properties of rock. It was necessary for the blocks to have a very dense packing of sand grains to prevent collapse of their structure at high confining pressures.¹⁸ Also it was desired to use the same kind of sand and plaster in the vibrated model material as had been used in the compacted model material used in the solid model blocks.¹⁹

Attempts to make joint blocks by vibrating material in a mold proved to be futile because the blocks were too fragile to be removed from the mold. (These were 2" x 2" x 8" blocks). The failure to successfully extrude the vibrated joint blocks was due largely to the very low cohesive strength of the material.

After attempts at molding joint blocks failed it was decided to make joint blocks by sawing them out of larger compacted blocks. Steel molds 20" x 20" x 6" were used to compact 20" x 20" x 3" blocks using the same compaction procedure and the same mix proportions as used by Heuer and Hendron on 24" x 24" x 8" solid model blocks (Fig. 3). A decided advantage of this procedure is that the intact material of the joint blocks would be essentially identical to the intact material composing the solid models tested previously by Heuer. This model material developed by Heuer and Hendron is probably the best reported to date for modeling the properties of rock.

After compaction, the blocks are allowed to air dry for three days, then put into an oven to dry at 105°F for about a week. When the 20" x 20" x 3" blocks are properly cured, they are strong enough to be handled easily without breaking. They also saw very easily. A metal surface grinder with a moving table was

converted into a saw for accurately cutting joint blocks (Fig. 4). Diamond blades are used quite successfully for sawing joint blocks with this machine—it has been possible to saw blocks as small as 1/2" x 1/2" x 8". A jig was also made to fit the saw for cutting the triangular cross-section blocks used around the edges of models which have joints oriented at 45° to the principal directions of loading (Fig. 1).

Since exactly the same material was used in the joint blocks as was used by Heuer and Hendron in the solid blocks, a new series of material properties tests was not necessary. The standard mix is made in the ratio of 1.2/1/9/.01 (water/plaster/sand/retarder) by weight. The plaster used is white molding plaster. The sand is the fine fraction of a Pleistocene sand deposit obtained from the Sangamon River valley near Mahomet, Illinois. The grain size distribution of the fine Sangamon River sand is shown in Fig. 5. The retarder used is sodium phosphate (Na_2HPO_4) in the dibasic anhydrous powder form.

The sand, plaster and retarder are mixed together dry for about 5 minutes in a concrete mixer. The water is then added while the mixer is running and the batch is mixed wet for about 5 minutes. When the wet mix is homogeneous, it is placed in the mold in about 1/2-in. thick layers and compacted with a pneumatic tamper by the same method used by Heuer and Hendron.

The intact shear strength properties of the model material are shown in Fig. 6. The angle of internal friction is $\phi = 33^\circ$ and the unconfined compressive strength is $q_u \cong 555$ psi.

The Mohr failure envelope for the intact material in Fig. 6 is essentially a straight line up to confining pressures as high as 1000 psi. This is in marked contrast to the behavior of most previous model materials which approach $\phi = 0^\circ$ behavior at high pressure. Since a high frictional shearing resistance is one of the most important properties of jointed rock masses, it is essential that a model rock material have high frictional resistance.

A series of three direct shear tests were run on 2" x 6" sawed joint surfaces of the model material. These tests were conducted in the direct shear machine in the University of Illinois rock mechanics laboratory. Tests were run at normal stresses of 50 psi, 150 psi, and 400 psi. The measured maximum shear strength in each case respectively was 33.3 psi, 97.5 psi, and 230 psi. These three points are plotted in Fig. 7, which shows that the effective angle of shearing resistance on the

¹⁸R.E. Heuer, *Geomechanical Model Study*.

¹⁹R.E. Heuer and A.J. Hendron, *Geomechanical Model Study...Report 1*.

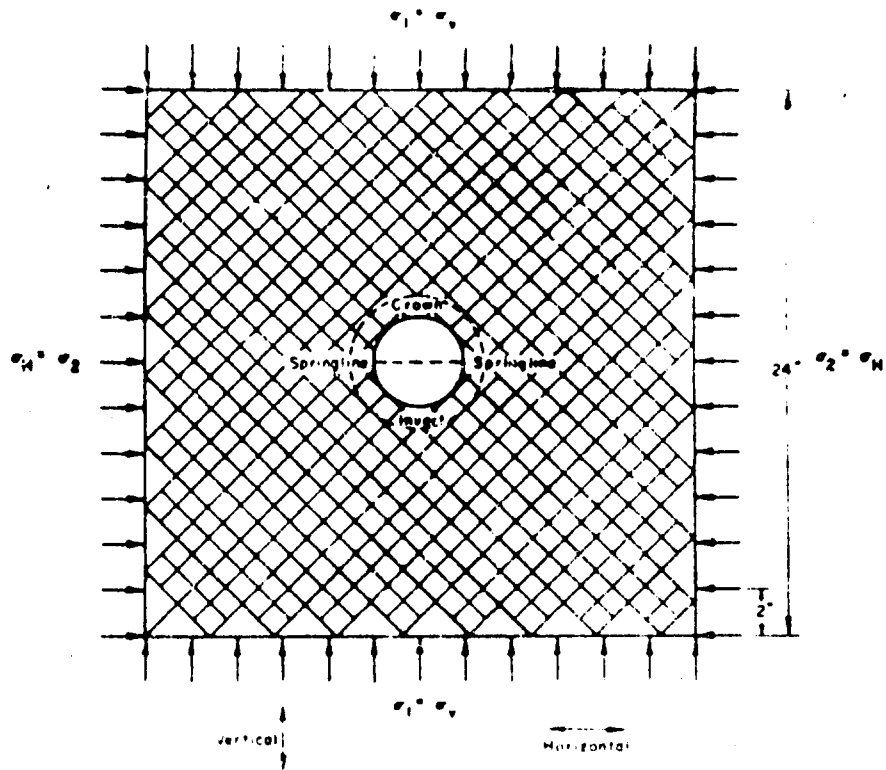


Figure 1. Jointed model configuration used in Joint Block #6, #7 and #8.

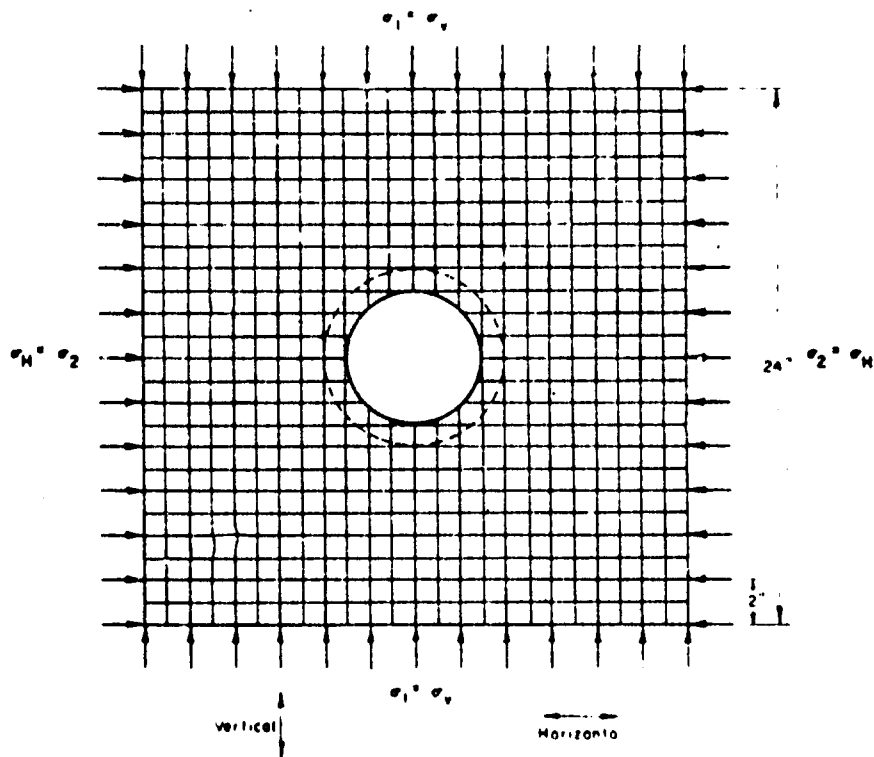


Figure 2. Jointed model configuration used in Joint Block #9 and #10.

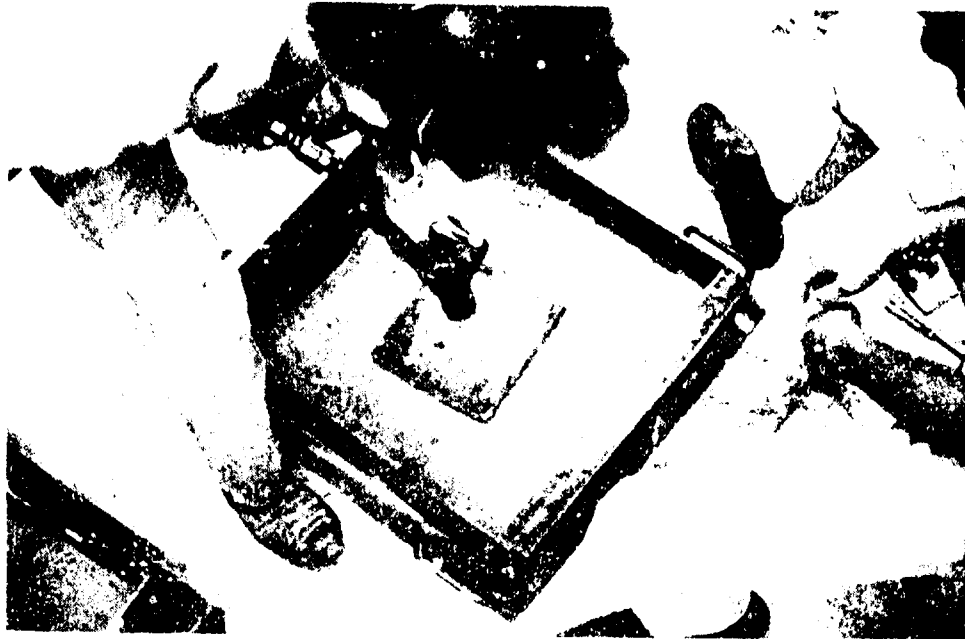


Figure 3. Compaction of 20" x 20" x 3" block of model material.

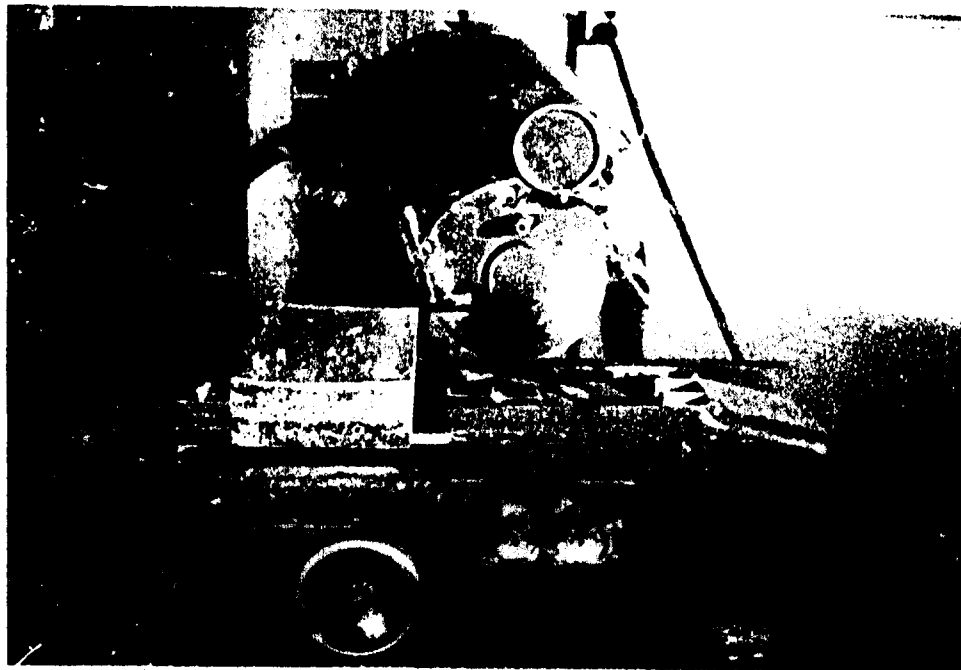


Figure 4. Diamond-bladed saw used to cut joint blocks.

Best Available Copy

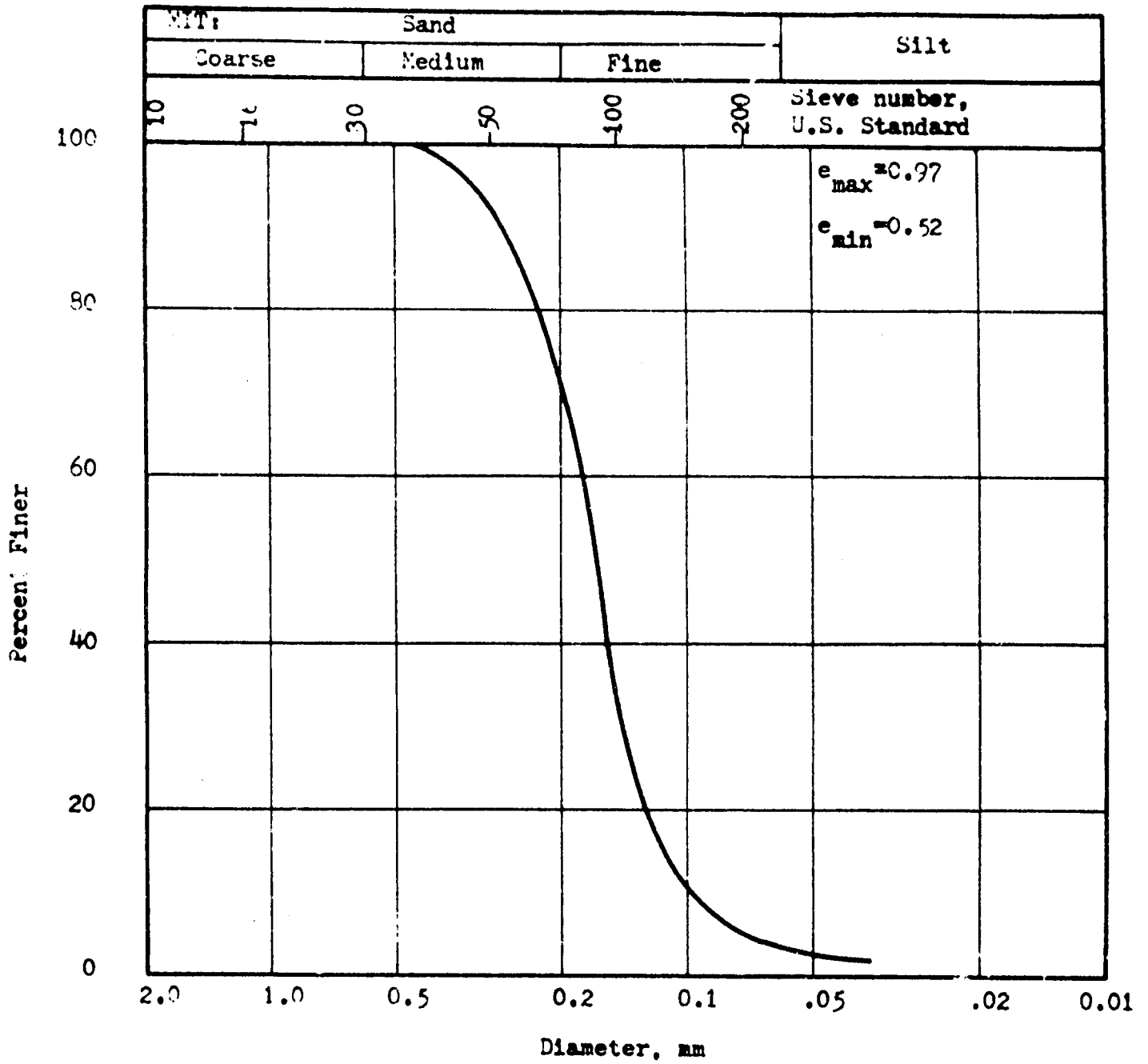


Figure 5. Grain size distribution of fine Sangamon River sand.

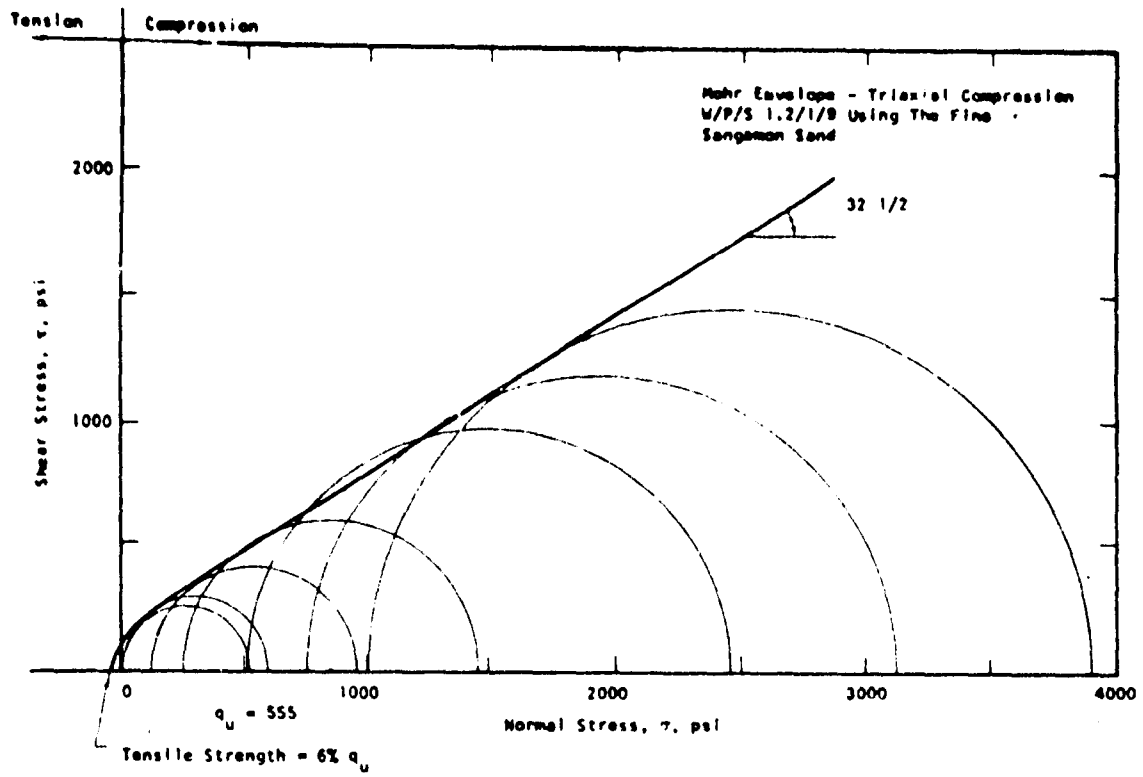


Figure 6. Triaxial shear strength properties of intact model material.

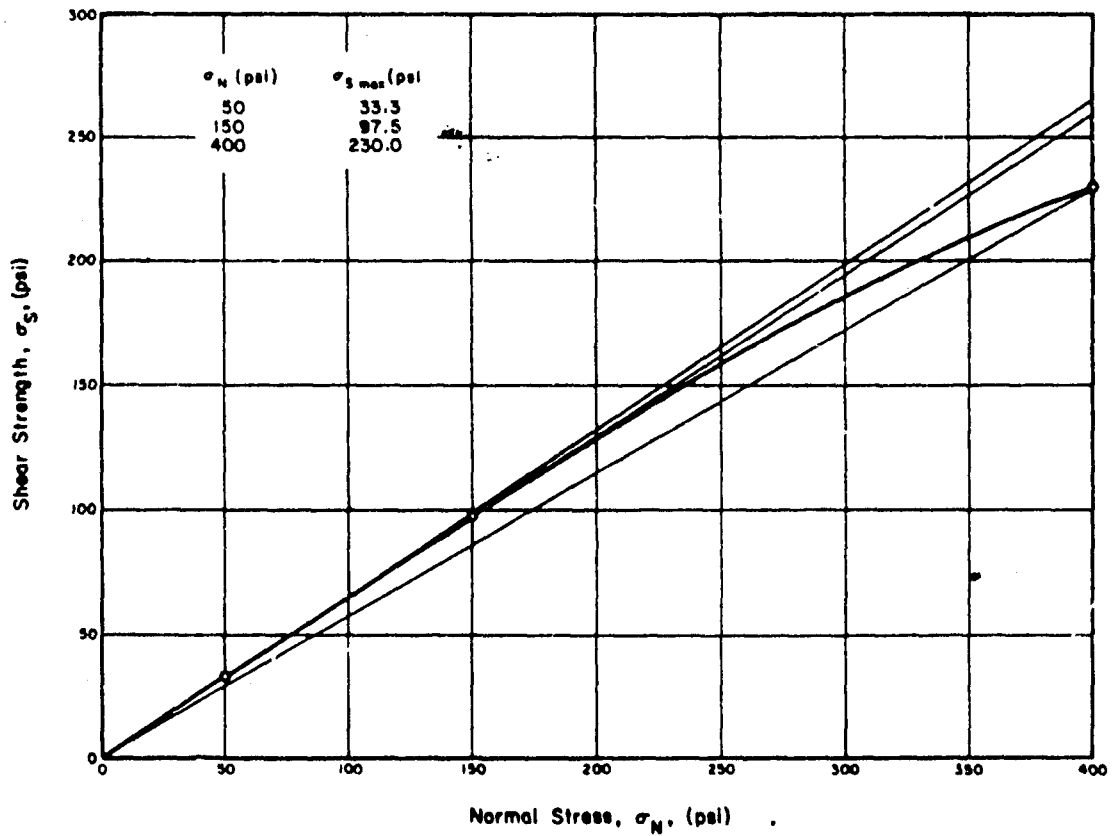


Figure 7. Results of direct shear tests on joint surfaces of model material.

joint surfaces decreases from 33° to 29° with increasing normal pressures. All three direct shear specimens had flat-top shear strength vs. deformation curves for a given normal pressure. In all three cases, the residual shear strength after 3 cm of slip along the joint was essentially the same as the peak shear strength. These tests indicate that a value of the angle of shearing resistance for use in an analysis of the jointed models should be slightly lower than the value obtained in the triaxial tests of intact samples shown in Fig. 6. For the theoretical elasto-plastic analysis, the appropriate angle of frictional resistance should be taken as the angle of frictional resistance along the joints, not the angle of internal friction derived from triaxial tests on intact samples of the model material (Hendron and Ayer.²⁰)

The sawing tolerance on the blocks is about $\pm .01$ in. This means that in a model with 7-in. joint spacing, if all of the blocks on one row are 0.01 in. too thin and on the next row they are all 0.01 in. too thick, the maximum offset of the joints across the model would accumulate to as much as 0.24 in., which is intolerable. The test blocks must therefore be constructed by selecting the blocks so that they fit together to make straight joint lines with minimum offsets in both directions (Fig. 8). The blocks are constructed on edge on a table and then moved block by block into the testing machine. Each of the external faces of the constructed block is flattened by grinding and is thoroughly cleaned of dust with compressed air before placing it in the testing machine.

The jointed models are placed in the testing machine on a friction reducing sandwich composed of a sheet of teflon plastic sandwiched between two sheets of 4 mil polyethylene plastic placed directly on the base plate of the testing machine. The plastic sheets are used to reduce friction between the model and the base plate of the testing machine.

When the model is constructed in the testing machine, the loading elements are put in place and a small seating load of about 25 psi is applied in both the horizontal and vertical directions. With the seating load held constant, the 4-in. diameter tunnel is cored and cleaned out thoroughly with a vacuum cleaner. The joints intersecting the tunnel are then sealed with a

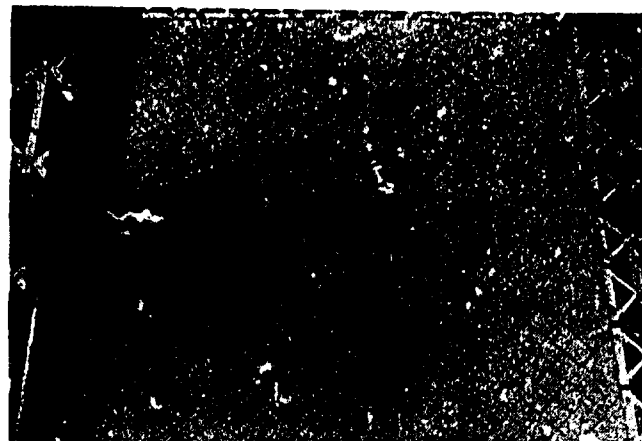


Figure 8. Jointed model ready for test.

small bead of silastic caulking compound which is allowed to cure for two days. The tunnel wall is then painted with SR-4 strain gage cement for waterproofing purposes and the cement is allowed to cure for one day. The instrumented tunnel liner is then installed in the tunnel and the base of the liner is sealed with silastic. When the silastic has cured, the liner is grouted-in with a liquid grout consisting of one part water to one part sulfaset rock bolt cement by weight. The grout is cured for one day and then the loading head is placed on top of the model using two layers of 4 mil polyethylene sheet and a layer of plaster to get close contact between the model and the testing head. This procedure for placement of the loading head is the same as that used by Heuer.

Free-Field Strain Measurement. In the jointed blocks, strain gage measurement on the intact blocks are meaningless as measure of the free-field strain of the model due to closure along the joints. Thus buried extensometers were used in the jointed models to measure the average relative displacement of two points across the block. Average strains of the block were obtained by dividing the relative displacement between the points by the distance between the points, ($\epsilon = \Delta L/L$). Fig. 9 shows the locations of extensometers and their identification code.

The buried extensometers are simply metal rods grouted with epoxy into holes bored into the model to the specified depth. The extensometer holes are bored with a masonry bit. Plastic tubing is used to contain the epoxy until it is extruded by pushing the extensometer into position in the model. Figure 10 shows a series of extensometers ready to be filled with epoxy

²⁰A.J. Hendron and A.K. Ayer, *Stresses and Strains Around a Cylindrical Tunnel in an Elasto-Plastic Material with Dilatancy*, Technical Report (Omaha District, U.S. Army Corps of Engineers, January 1971 [in publication]).

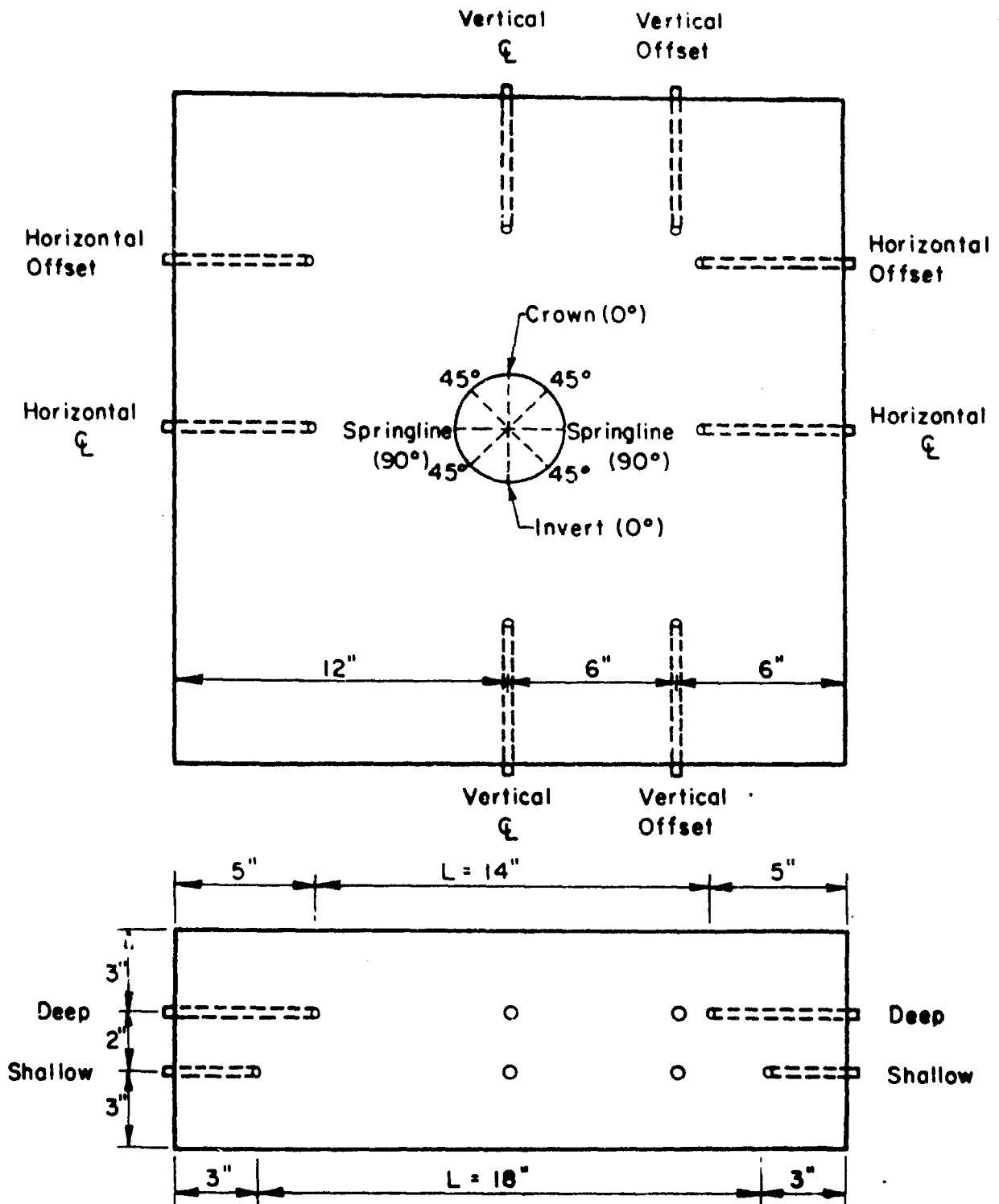


Figure 9. Locations of extensometers in jointed test blocks.

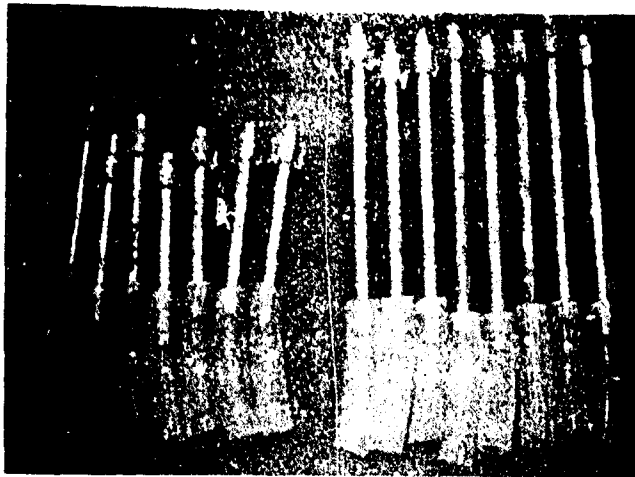


Figure 10. Extensometers ready for installation in test block.

and installed. The extensometers are composed of a piece of 1/4-in. diameter metal rod with a seating hole drilled in the end. Two pieces of plastic tubing are used to make a cup to contain the epoxy on one end of the extensometer and another piece is used as a spacer to center the rod in the hole near the face of the model (Fig. 11a). A typical overall installation of two buried extensometers is shown in Fig. 11b. The epoxy is very viscous and will not flow out when the extensometers are held in a horizontal position. Figure 12 shows an extensometer as it was exposed after a test. The model must be under a seating load when the extensometer holes are drilled and when the extensometers are grouted in place.

The movements of the extensometers are measured with beryllium-copper clip gages like those used to measure diameter changes in the tunnels of the previous tests.²¹ These gages consist of 5-in. curved strips of beryllium-copper with seating points on the ends. Each strip is gaged with four strain gages wired on a four-arm bridge. These clip gages can be accurately calibrated with a standard strain indicator and they are linear over a range of about 1 in. deflection. Figure 11b is a detail of the setup used to measure the movements of the buried extensometers.

Each of the clip gages is calibrated before and after each test while wired to the same terminals used during

the test. There are small changes in the calibration of the gages from test to test and continual recalibration is necessary to detect changes in the system before running a test.

3 TEST RESULTS

Table 1 summarizes the model tests completed in this study. The five tests completed are designated as JB #6 through JB #10. JB #6 was tested at an N value of 2/3 as a continuation of the first series of jointed models (JB #1 through JB #5) tested under a previous contract (DACA 39-67-C-0009).²² JB #7 through JB #10 constitute the second related series of jointed models tested. All the models in this second series were tested at a principal stress ratio $N = \sigma_h/\sigma_v = 1$ so that the results could be compared to an elasto-plastic theory with dilatancy developed by Hendron and Aiyer. Comparisons between this theory and the model test results are presented in Chapter 6.

The usual type of liner of interest for practical protective structures problems is a reinforced concrete integral liner in rock. For example, consider an 18-in. thick reinforced concrete liner in a 20-ft diameter opening. The circumferential stiffness of the liner would be approximately $E_t/R = \frac{3 \times 10^6 \text{ psi} \times 18 \text{ in.}}{10 \text{ ft} \times 12 \text{ in./ft}} = 450,000$

psi and the jointed rock mass might have an effective plane strain deformation modulus of about $E_r = 1-2 \times 10^6$ psi. These figures would give a linear stiffness to rock mass stiffness ratio of $\frac{E_t/R}{E_r} = \frac{450,000 \text{ psi}}{1-2 \times 10^6 \text{ psi}} =$

0.45 - 0.225. In these model tests, three sizes of plexiglass liners were used as shown in Table 1. The circumferential stiffness of these liners varied from 16,700 psi to 25,000 psi, whereas the range of model stiffness, E_m , for models JB #7 through JB #10 was 61,000 psi to 64,300 psi (Table 1). The ratio of the circumferential stiffness of the liner, E_t/R , to the plane strain stiffness of the model, E_m , varied from 0.261 to 0.410 (Table 1). Thus the models had a circumferential stiffness to rock mass stiffness ratio similar to that of the prototype structure mentioned above. The ratio of the bending stiffness, EI/R^3 , to the circumferential stiffness, E_t/R , determines whether a liner will fail by

²¹ R.E. Heuer, *Geomechanical Model Study*.

²² A.J. Hendron et al, *Geomechanical Model Study...Report 3*.

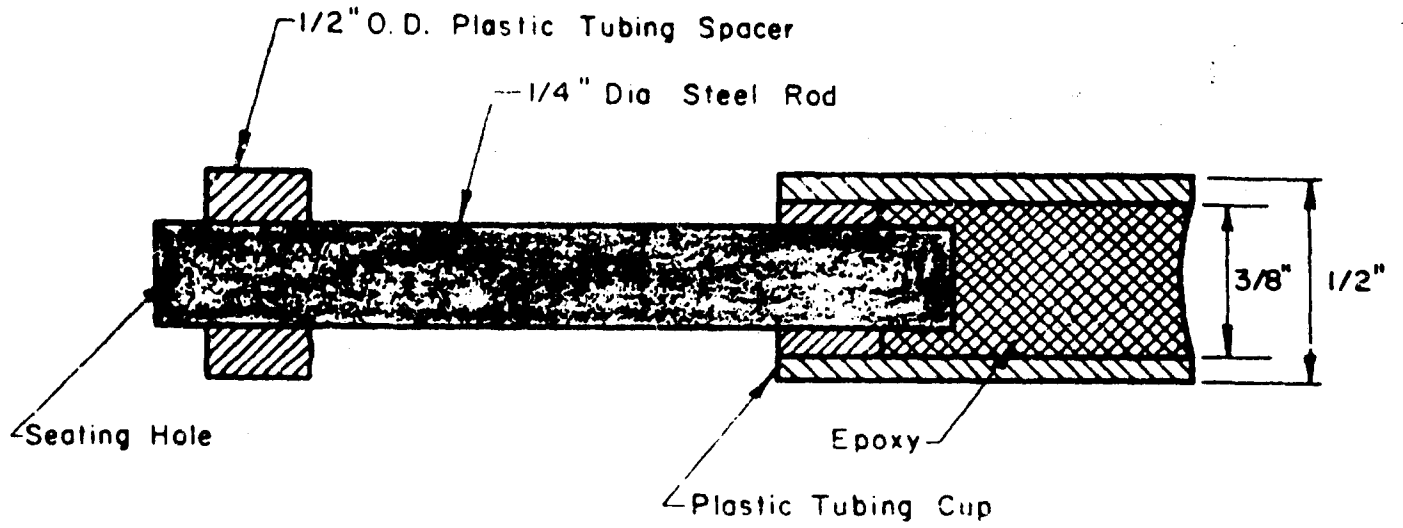


Figure 11a. Detail of buried extensometer.

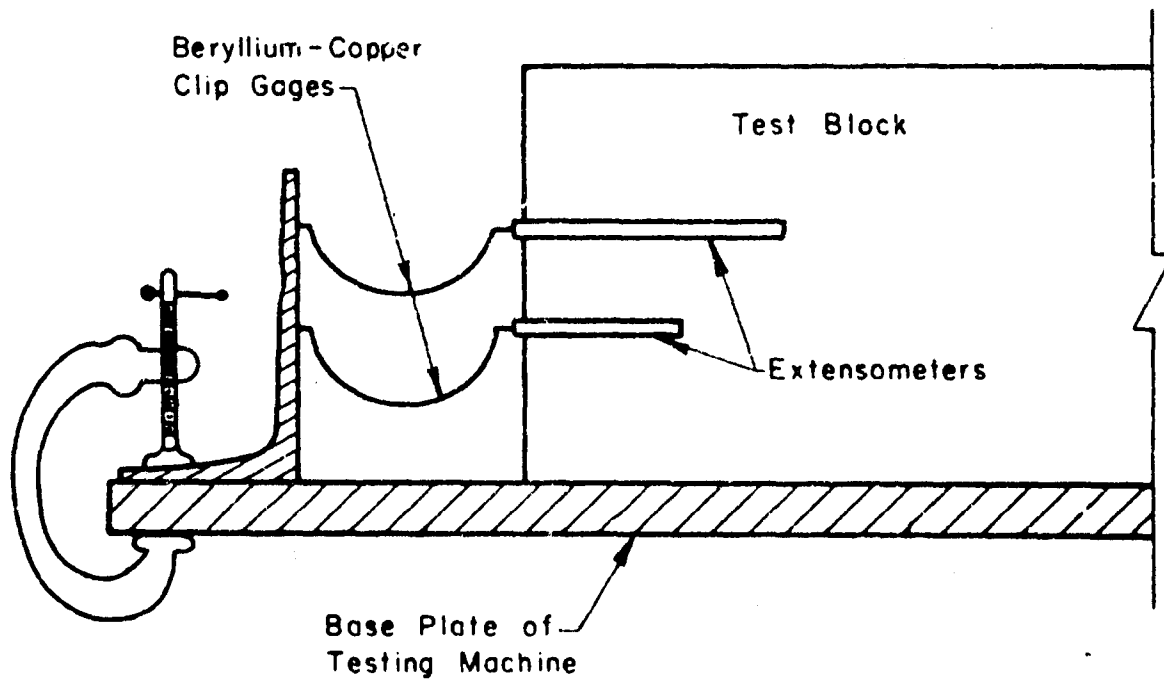


Figure 11b. Detail of extensometer measurement setup.



Figure 12. Extensometer exposed after test.

buckling or by simple circumferential compression failure. This ratio is dependent only on the value of t/R . The value of t/R for the prototype cited above is 0.15 while values for the liners used in the models are 0.0625 and 0.046. Thus the model liners are more likely to buckle than is the 18-in. thick concrete liner in the 20-ft diameter example prototype structure. In the model tests, none of the plexiglass liners buckled and two of them failed in circumferential compression as a prototype concrete liner would. Thus the selection of plexiglass liners prevented a buckling mode of failure which had previously been experienced with aluminum liners.²³

The remainder of this chapter consists of a systematic presentation and discussion of the data obtained in the testing of the models JB #6 through JB #10.

Presentation of Test Results

Joint Block #6. #6 was identical to JB #5²⁴ except that a plexiglass liner was used in JB #6 and an aluminum liner was used in JB #5. The change to plexiglass was made because the bending stiffness ($EI/R^3 = 4.5$ psi) of the aluminum liners was too low and the circumferential stiffness ($Et/R = 175,000$ psi) was too high to model reinforced concrete liners in rock. As a result the aluminum liners buckled before the ultimate thrust capacity of the aluminum section was developed. Also, the circumferential stiffness of the

aluminum liner was about 4.5 times as great as the stiffness of the jointed model in the vertical direction, which caused the liner to attract excessive load by arching. Thus it was desirable to increase the bending stiffness of the liner in JB #6 to reduce the chance of buckling failure. It was also desirable to decrease the thrust stiffness of the liner to a value less than the modulus of the surrounding model rock mass so that the test would more accurately model real prototype structures in jointed rock masses. A 4-in. diameter plexiglass liner 1/8-in. thick has a calculated thrust stiffness of 25,000 psi and a calculated bending stiffness of 8.15 psi. These stiffnesses are based upon a Young's modulus of the plexiglass, E , of 400,000 psi. The value of E was determined by testing an 8-in. long sample of the 4-in. diameter liner in uniaxial compression using SR-4 strain gages to measure the strains. The average vertical model stiffness of JB #5 was $E_m = 38,000$ psi and thus the thrust stiffness of this liner was lower than the model stiffness as desired.

With the aid of the information above JB #6 was constructed using 1-in. joint blocks oriented at 45° to the loading directions; and a 4-in. diameter plexiglass liner 1/8-in. thick. JB #6 was tested at a principal stress ratio $N = \sigma_h/\sigma_v = 2/3$ to compare with six previous tests²⁵ conducted at $N = 2/3$.

Figures 13 through 15 are summary plots of the data obtained in the testing of JB #6. Figure 13 is a plot of the vertical stress-strain curves of the model. The stress-strain curve designated as "vertical-shallow" was obtained from a pair of extensometers buried 3 in. deep in opposite vertical faces of the model as shown in Fig. 9 and represents the average strain over the central 18 in. of the vertical model centerline. Thus the "vertical-deep" stress-strain curve is more affected by strain concentrations due to the tunnel and the "vertical-shallow" stress-strain curve is more representative of the free-field strain of the model. After initial seating movements, both of the vertical stress-strain curves are almost linear up to a vertical model stress of 1200 psi. Above 1200 psi they both show the strain to increase at a slightly increasing rate with pressure. The separation of the two vertical stress-strain curves indicates that the movements of the deep extensometers were affected by the presence of the tunnel.

The diametrical extensometers in JB #6 were placed at angles of 10° , 35° , 55° , and 80° from the

²³ A.J. Hendron et al, *Geomechanical Model Study...Report 3.*

²⁴ A.J. Hendron et al, *Geomechanical Model Study...Report 3.*

²⁵ A.J. Hendron et al, *Geomechanical Model Study...Report 3.*

Table 1
Summary of Model Blocks Tested

Test Block	Tunnel Diameter (in.)	Liner Properties*	Joint Spacing (in.)	Joint Orientation	$N = \frac{\sigma_h}{\sigma_v}$	E_m (psi)	$\frac{Et/r}{E_m}$
JB #6	4	plexiglass t = 0.125 in. Et/R = 25,000 psi EI/R ³ = 8.15 psi	1	45°	2/3	54,000	0.463
JB #7	4	plexiglass t = 0.125 in. Et/R = 25,000 psi EI/R ³ = 8.15 psi	1	45°	1	64,300	0.389
JB #8	6	plexiglass t = 0.125 in. Et/R = 16,700 psi EI/R ³ = 2.4 psi	1	45°	1	64,000	0.261
JB #9	6	plexiglass t = 0.125 in. Et/R = 16,700 psi EI/R ³ = 2.4 psi	1	90°	1	52,500	0.268
JB#10	8	plexiglass t = 0.250 in. Et/R = 25,000 psi EI/R ³ = 8.15 psi	1	90°	1	61,000	0.410

* liner stiffnesses calculated for a 1 in. length of the liner.

crown and invert diameter instead of the usual 0°, 45°, and 90° used in the other tests. The extensometers were oriented this way to help determine the actual shape of the tunnel liner after deformation. Fig. 14 is a plot of these diametrical strains labeled as to the angle they make with the crown and invert direction. These curves show that the liner was actually more flexible than the model as even the springline diameter was compressed in this test.

Fig. 15 is a dimensionless plot of the diametrical strain of the liner on four different diameters as a function of the vertical free-field strain. In this plot, the vertical-shallow stress-strain curve was used as the free-field stress-strain curve. Presentation of the data in this manner is helpful for an immediate comparison of the diametrical strain $\Delta D/D$ with the free-field strain in the rock mass. Note that at strains less than 1% the diametrical strains along the 10° diameter and the 35° diameter are nearly equal to the free-field strain. As the free field strain increases above 1%, inelastic action of the model rock mass surrounding the liner results in the diametrical strains increasing at an increasing rate

with respect to the free-field strain. At free-field strains of 2-3% the diametrical strains along these two diameters are about 1.5-1.8 as great as the free-field strain. The diametrical strains on the 55° diameter and the 80° diameter are less than the free-field strain because of ovaling. At higher loads, the 80° diameter would have shown an actual increase over its original length due to ovaling of the liner caused by testing at $N = 2/3$.

Joint Block #7. The second series of jointed models (JB #7 through JB #10) was tested at a principal stress ratio $N = \sigma_h/\sigma_v = 1$ specifically to compare the test results to a theoretical elasto-plastic analysis with dilatancy which was developed by Hendron and Aiyer. The theory is valid for calculating stresses and strains around a cylindrical opening in a homogeneous elasto-plastic material with dilatancy under symmetrical plane-strain conditions for a principal stress ratio $N = \sigma_h/\sigma_v = 1.0$. The required loading conditions are satisfied in this series of model tests. One purpose of these model tests is to provide test data for tunnels in jointed media so that appropriate values of shear strength parameters for jointed masses may be determined for use

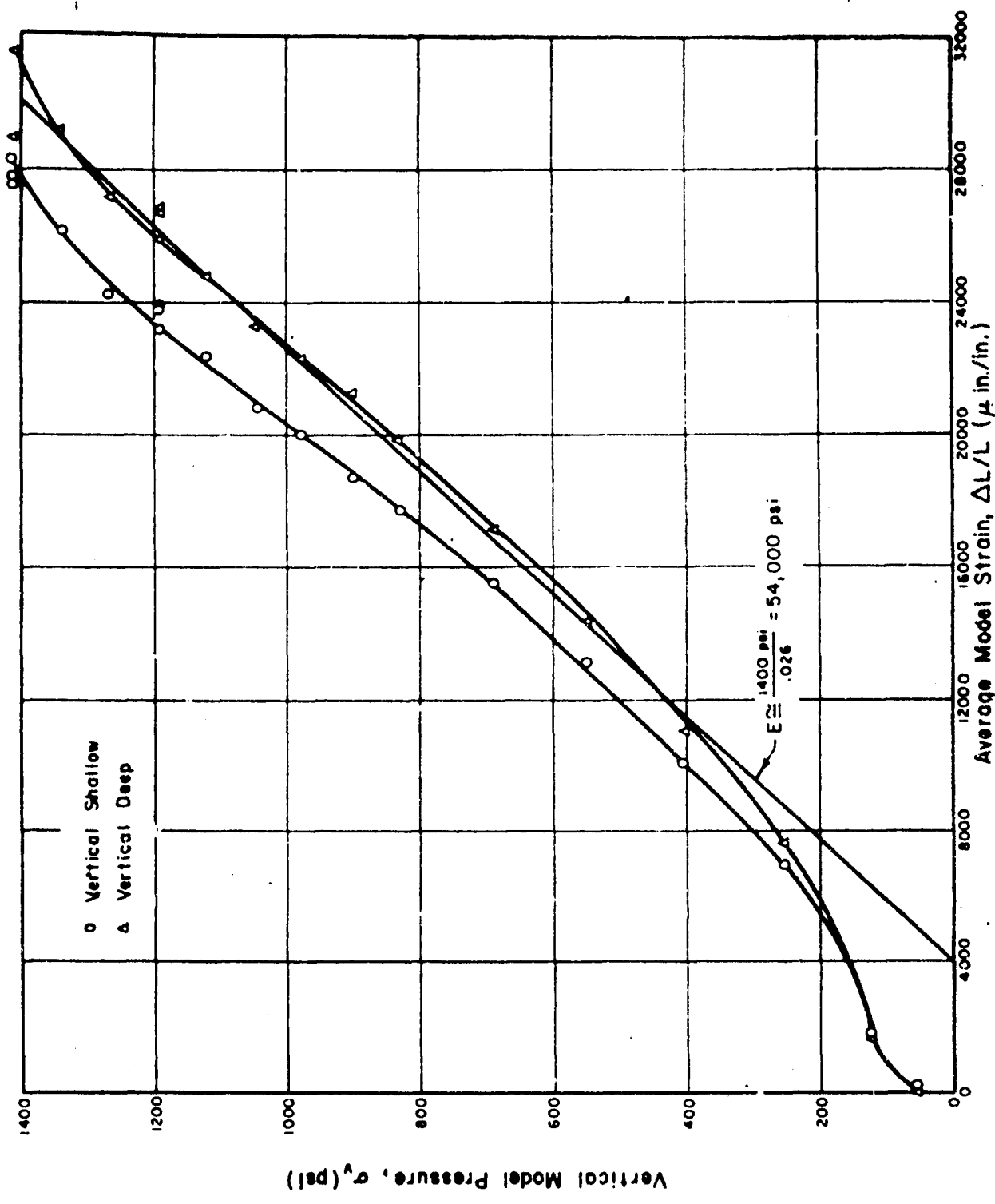


Figure 13. Average vertical model stress-strain curves for JB #6.

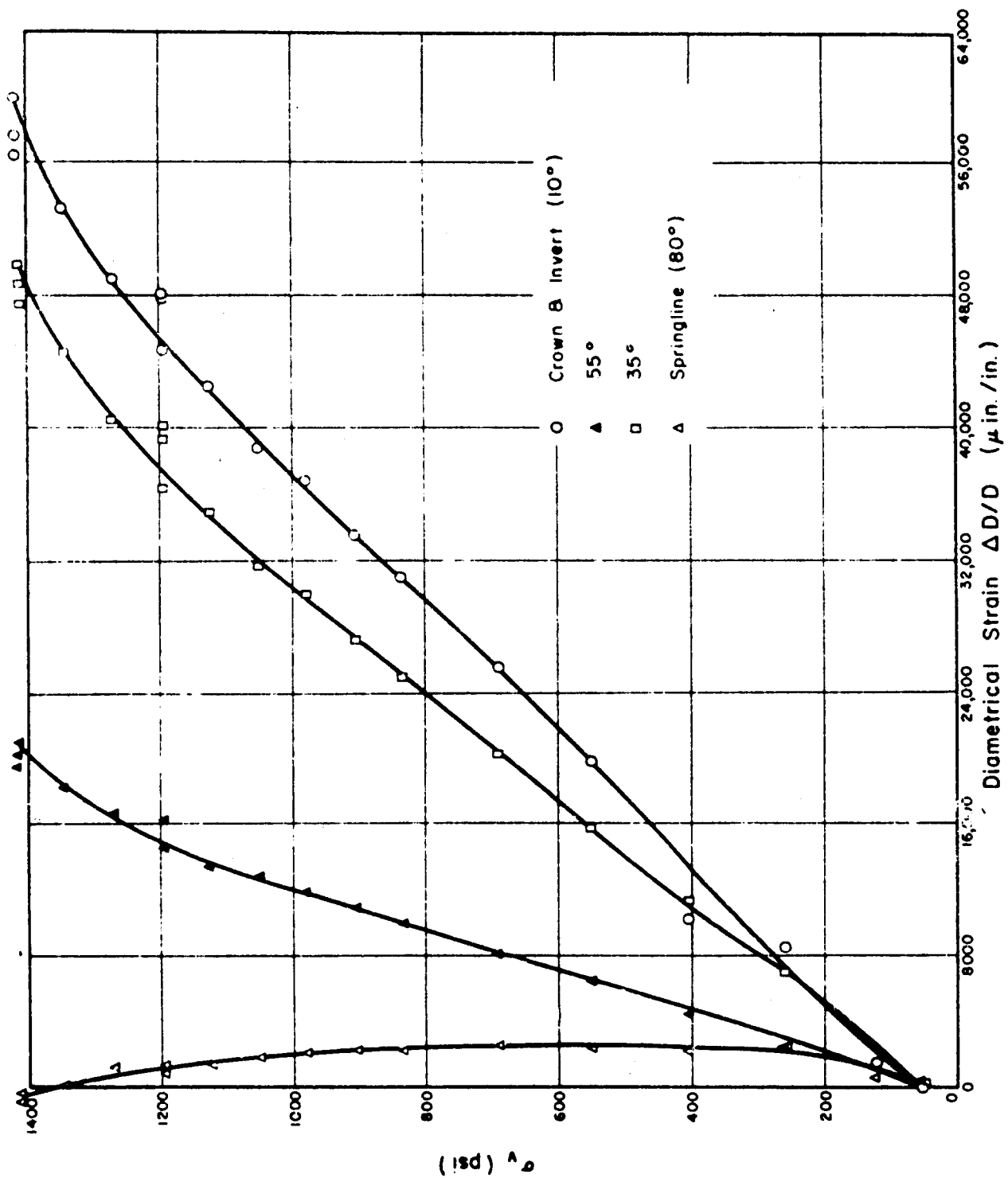


Figure 14. Diametrical strain of liner at four different diameters for JB #6.

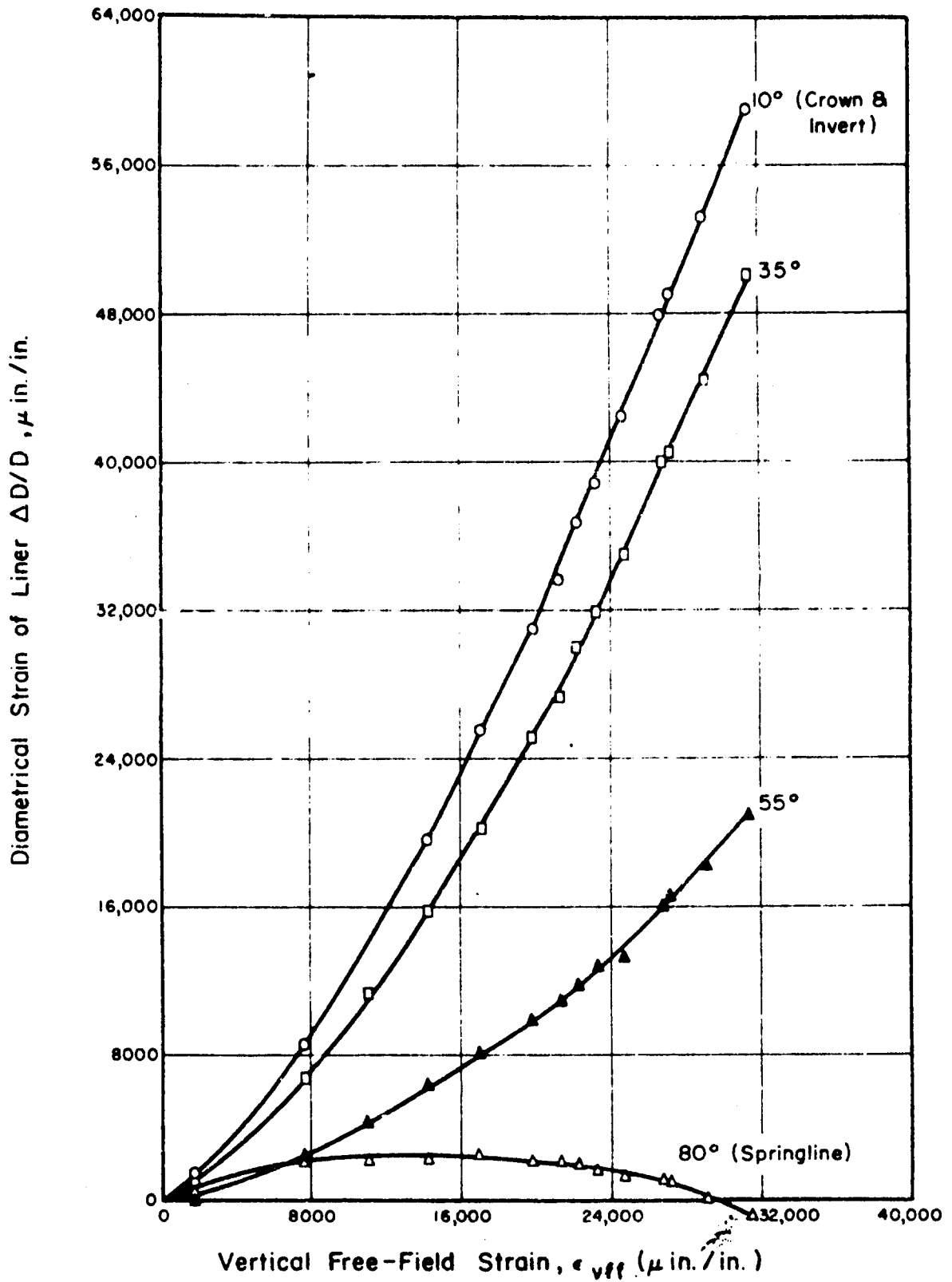


Figure 15. Dimensionless plot of diametrical strain of liner as a function of vertical free-field strain of model for JB #6.

in this theory which will yield realistic results for tunnels in jointed masses. This theory has already been used to predict the non-linear diameter changes of tunnel liners in solid models of the same model material where the models were subjected to stresses high enough to cause inelastic behavior around the tunnel.²⁶

JB #7 was constructed of 1 in. joint blocks oriented at 45° to the loading directions. The tunnel was 4 in. diameter and was lined with a 1/8-in. thick plexiglass liner. The circumferential stiffness, E_t/R , of this liner was 25,000 psi and the bending stiffness, EI/R^3 , was 8.15 psi. JB #7 was tested at a principal stress ratio $N = \sigma_h/\sigma_v = 1$ to a peak model pressure of 1420 psi. Figures 16 and 17 are summary plots of the data obtained in the testing of JB #7.

Fig. 16 is a plot of the average model stress-strain curves of JB #7 as measured by four separate pairs of external extensometers. The shallow extensometers measured over a gage length of 18 in. while the deep extensometers measured over a gage length of 14 in. An average of these four stress-strain curves of JB #7 gives an average plane-strain deformation modulus, E_m , of the jointed mass of 64,300 psi. Thus the ratio of the thrust stiffness of the liner to the stiffness of the model $\frac{E_t/R}{E_m}$ was 0.388. The vertical deformation modulus of JB #6 was 54,000 psi. JB #7 was stiffer than JB #6 because JB #7 was tested at $N = 1$ while JB #6 was tested at $N = 2/3$. Under testing at $N = 1$, the vertical plane-strain stiffness of identical models is higher due both to increased confinement of the model and to a lack of shearing deformations along the joint surfaces. If these curves (Fig. 16) were all true free-field stress-strain curves (unaffected by the presence of the liner), then they should all be coincident for testing at $N = 1$. In Fig. 16 the deep stress-strain curves show more strain than the corresponding shallow stress-strain curves because of the effects of the tunnel. Also in Fig. 16 the horizontal stress-strain curves show about 15% more strain than the vertical stress-strain curves. This relationship was not expected and can be explained only by experimental error.

Fig. 17 is a plot of the diametrical strain of the liner as a function of model pressure at four different diameters spaced 45° apart in the liner. These four curves are very nearly coincident thus indicating that

the model was behaving almost like a homogeneous isotropic medium in spite of the joints. Note that up to a pressure of about 600 psi the behavior of the liner was essentially elastic and at pressures above 600 psi the liner strains began to increase at an increasing rate with pressure. This indicates inelastic movement and yielding of the rock mass around the tunnel liner.

Joint Block #8. JB #8 was constructed with a 1-in. joint spacing with the joints oriented at 45° to the loading directions. The tunnel in JB #8 was 6 in. in diameter and was lined with a 1/8-in. thick plexiglass liner. The calculated circumferential stiffness, E_t/R , of this liner was 16,700 psi and the calculated bending stiffness, EI/R^3 , was 2.4 psi. JB #8 was tested at a principal stress ratio $N = \sigma_h/\sigma_v = 1$ to a peak model pressure of about 1320 psi. At this pressure the liner began to collapse and the test was terminated to prevent destruction of the clip gages inside the tunnel liner. Figures 18 and 19 are summary plots of the data obtained in the testing of JB #8.

Fig. 18 is a plot of the average model stress-strain curves of JB #8 as measured by four separate pairs of external extensometers. The shallow extensometers measured over a gage length of 18 in. while the deep extensometers measured over a gage length of 14 in. An average of these four stress-strain curves of JB #8 gives a deformation modulus of the jointed mass, E_m , of 64,000 psi. Thus the ratio of the calculated circumferential stiffness of the liner to the stiffness of the model $\frac{E_t/R}{E_m}$ for JB #8 was 0.260 as compared to 0.388 for JB #7. Fig. 18 shows that again in JB #8 the horizontal strains of the model were slightly greater than the vertical strains. This difference must again be explained by experimental error; possibly a systematic error since it is in the same direction as it was in JB #7. In JB #8, the deep extensometers again measured more strain than the shallow extensometers. This strain gradient is due to the strain concentration caused by the tunnel.

Fig. 19 is a plot of the diametrical strain of the liner as a function of model pressure at four different diameters spaced 45° apart in the liner. These four curves are nearly coincident thus indicating that the model was behaving almost like a homogeneous isotropic medium in spite of the joints. The liner sustained the model pressure of 1270 psi continuously without further significant deformation in spite of the fact that it was on the verge of failure and actually failed at 1320 psi.

²⁶ Hendron et al, *Geomechanical Model Study... Report 3.*

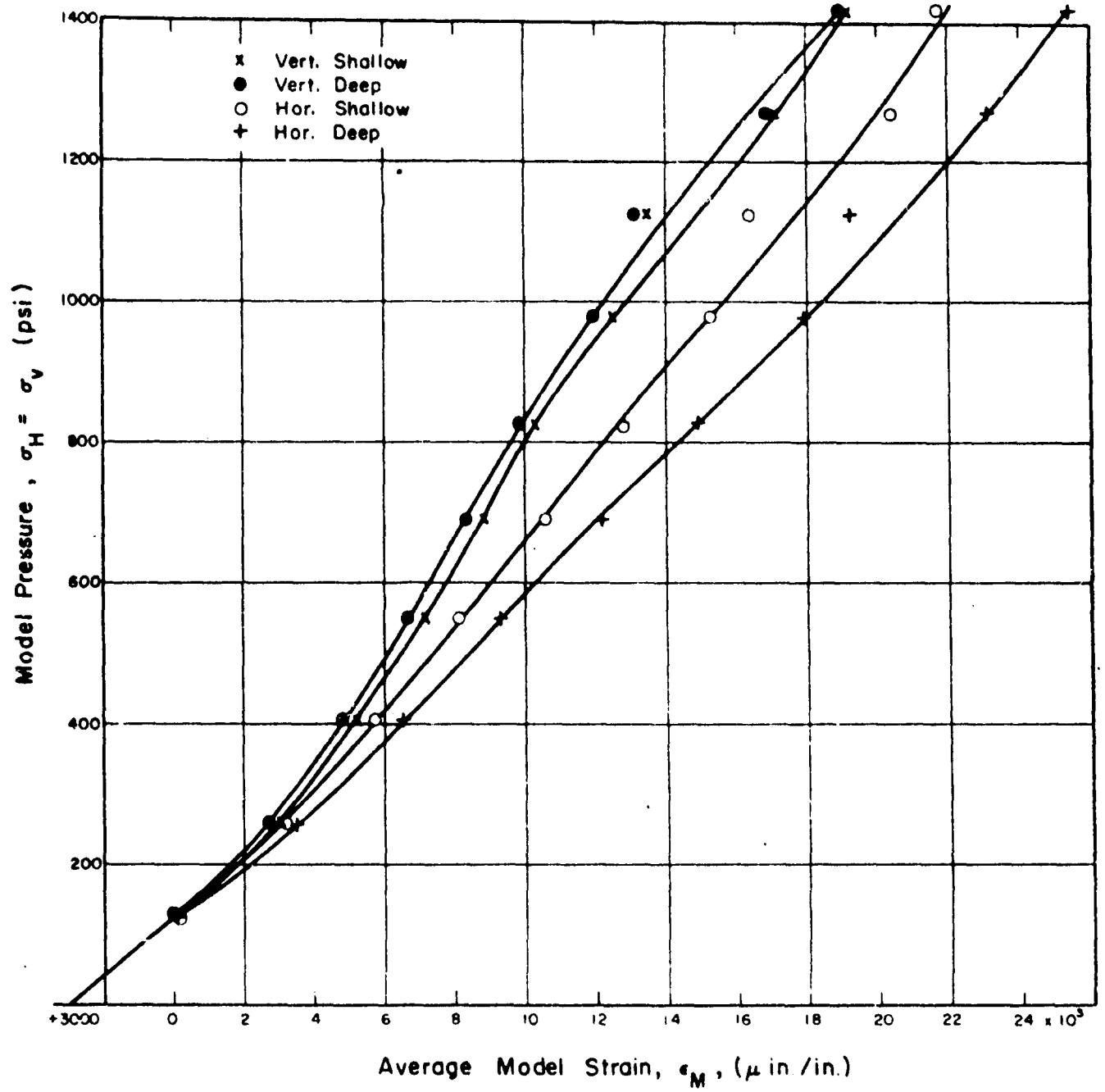


Figure 16. Stress-strain curves for JB #7.

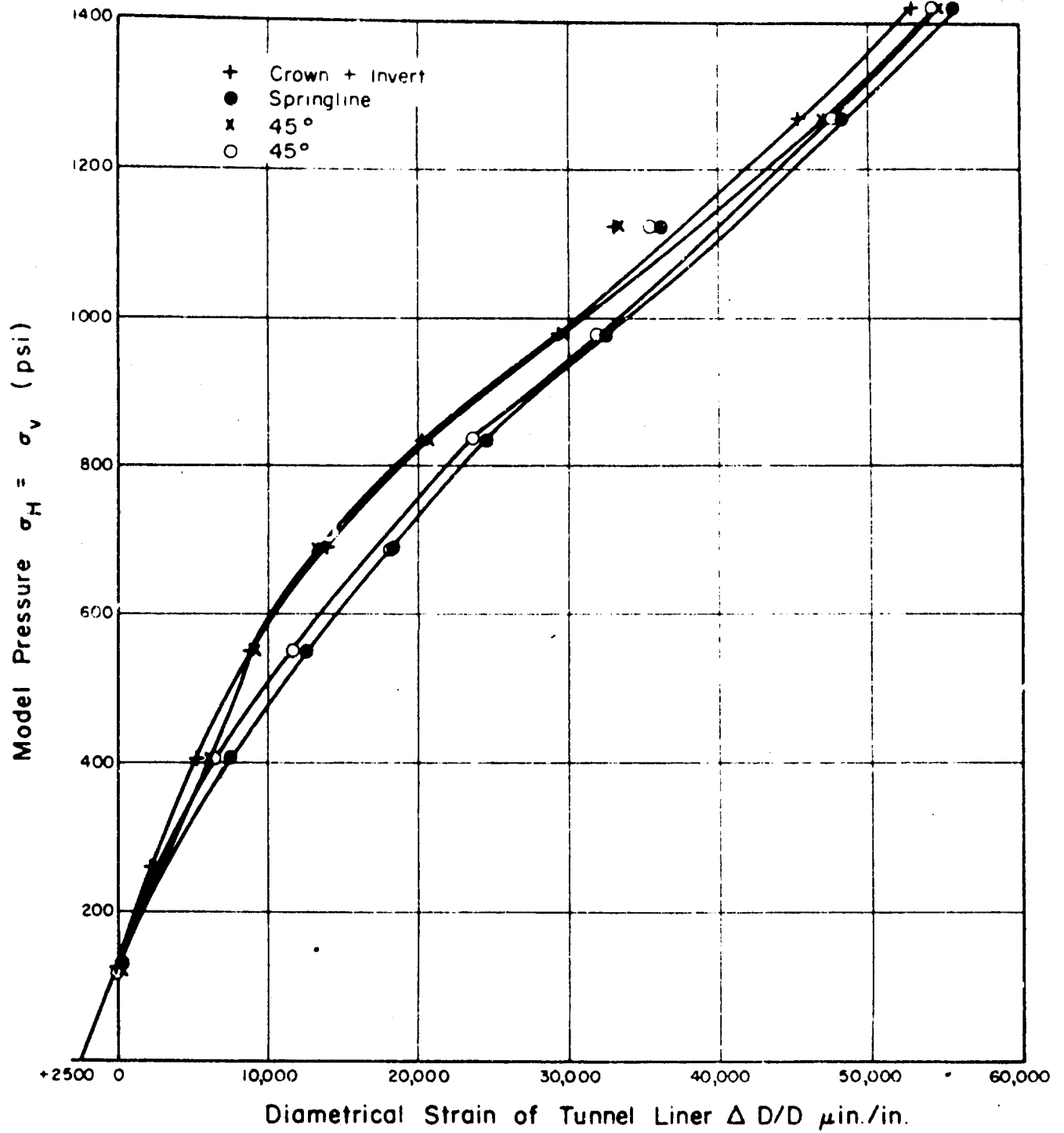


Figure 17. Diametrical strain of tunnel liner at four different diameters for JB #7.

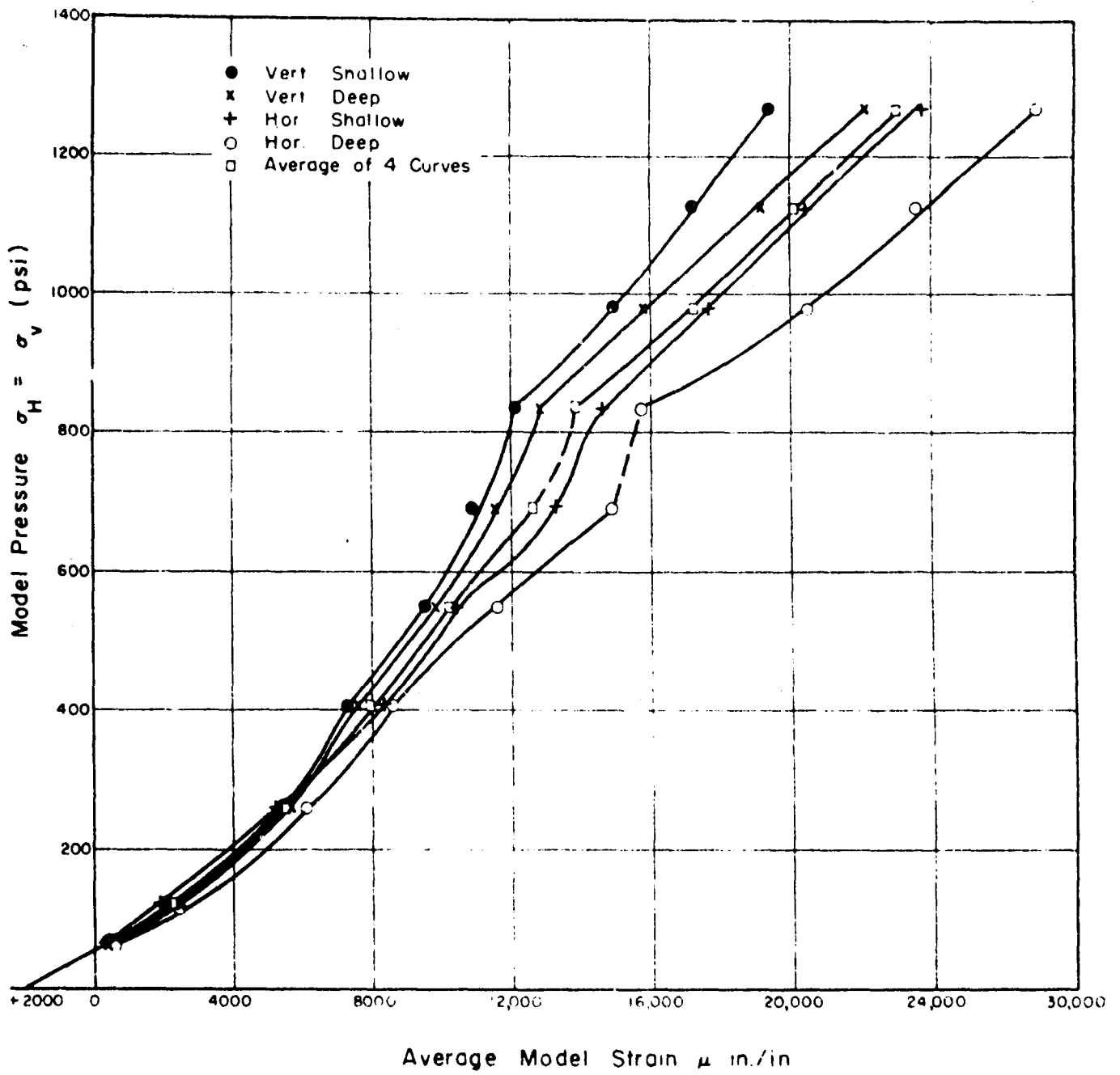


Figure 18. Stress-strain curves for JB #8.

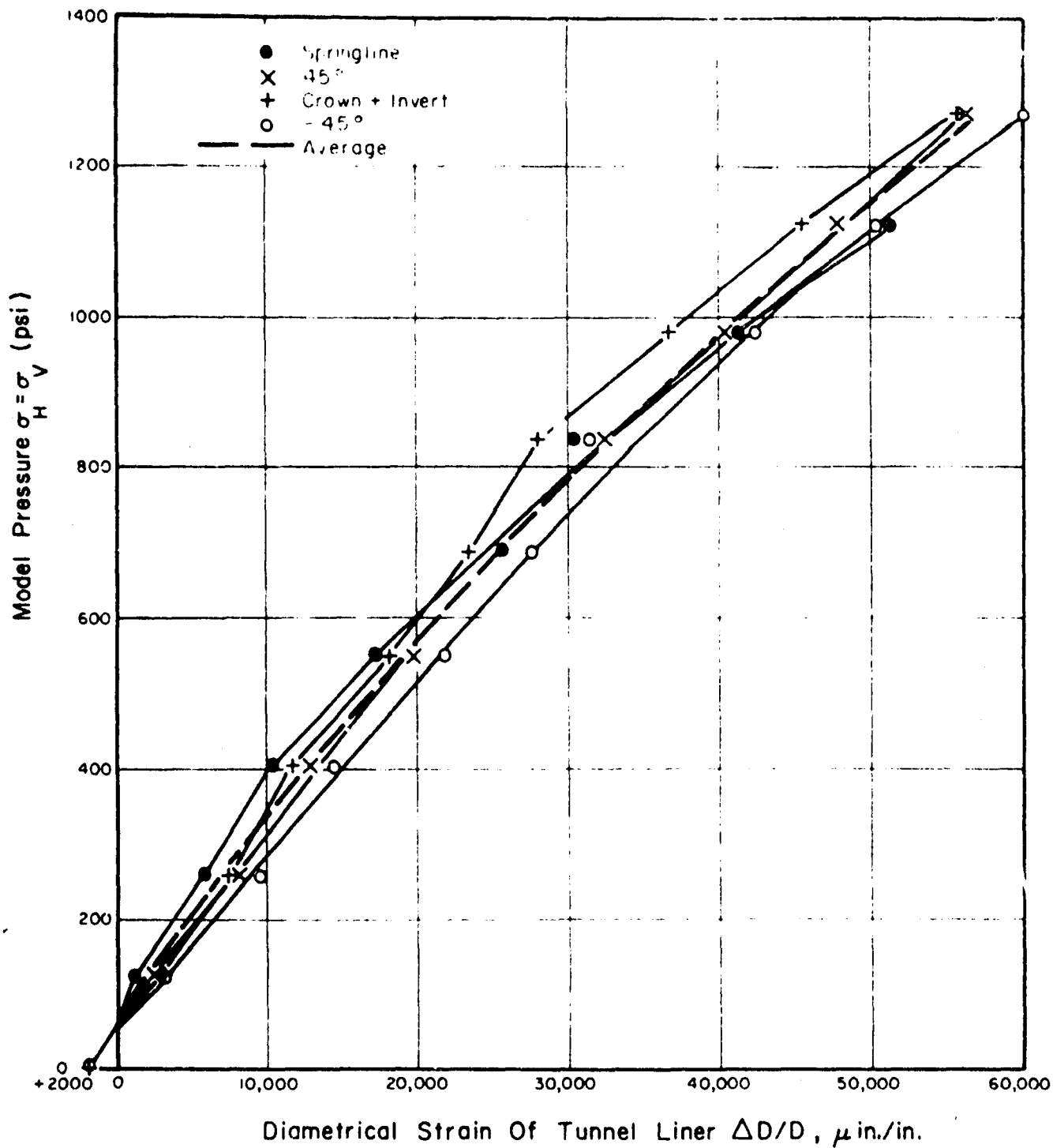


Figure 19. Diametrical strain of tunnel liner at four different diameters for JB #8.

Joint Block #9. JB #9 was constructed with a 1-in. joint spacing with the joints oriented parallel to the loading directions. The tunnel in JB #9 was 6 in. in diameter and was lined with a 1/8 in. thick plexiglass liner. The calculated circumferential stiffness of this liner, E_t/R , was 16,700 psi and the calculated bending stiffness, E_t/R^3 , was 2.4 psi. JB #9 was tested at a principal stress ratio $N = \sigma_h/\sigma_v = 1$ to a peak model pressure of about 1310 psi, at which pressure the liner suddenly cracked loudly and the test was terminated to prevent complete collapse of the tunnel and consequent destruction of the clip gages inside the tunnel liner. Figures 20 and 21 are summary plots of the data obtained in the testing of JB #9.

Fig. 20 is a plot of the average model stress-strain curves of JB #9 as measured by four separate pairs of external extensometers. The shallow extensometers measured over a gage length of 18 in. while the deep extensometers measured over a gage length of 14 in. An average of these four stress-strain curves of JB #9 gives an average plane-strain deformation modulus of the jointed mass of about 62,500 psi. Thus the ratio of the calculated circumferential stiffness of the liner to the stiffness of the model, $\frac{E_t/R}{E_m}$ for JB #9 was 0.267 as compared to 0.260 for JB #8. Fig. 20 shows that the horizontal strains in JB #9 were again slightly greater than the vertical strains. This difference is almost surely a systematic experimental error. The loading frame and the hydraulic elements of the loading system have been checked and no cause for such a systematic error was found. In JB #9 the deep extensometers again measured more strain than the shallow extensometers due to the strain gradients near the tunnel.

Fig. 21 is a plot of the diametrical strain of the tunnel liner as a function of model pressure on three different diameters. The change in slope of each curve at a stress level of 400 psi indicates that inelastic action in the rock mass surrounding the tunnel was initiated at this stress level. Inelastic action also started at about 400 psi in JB #8. Inelastic action began at about 600-700 psi in JB #7 which had a 4-in. tunnel. Since models JB #8 and JB #9 had 6-in. diameter tunnels and yielded at lower stress levels than JB #7, the decrease in rock mass strength with increasing tunnel size is illustrated by these tests. This point will be discussed in the next chapter.

Joint Block #10. JB #10 was constructed with a 1 in. joint spacing with the joints oriented parallel to

the loading directions. The tunnel in JB #10 was 8 in. in diameter and was lined with a 1/4-in. thick plexiglass liner. Using a Young's modulus of the plexiglass in the circumferential direction of 400,000 psi, the calculated circumferential stiffness of the liner, $\frac{E_t/R}{E_m}$ was 25,000

psi and the calculated bending stiffness, E_t/R^3 , was 8.15 psi. JB #10 was tested at a principal stress ratio $N = \sigma_h/\sigma_v = 1$ to a peak model pressure of 1420 psi without failing. Figures 22 and 23 are summary plots of the data obtained in the testing of JB #10.

Fig. 22 is a plot of the average model stress-strain curves of JB #10 as measured by four pairs of external extensometers. An average of these four stress-strain curves of JB #10 gives an average plane-strain deformation modulus of the jointed mass of about 61,000 psi. Thus the ratio of the calculated thrust stiffness of the tunnel liner to the average stiffness of the model, E_t/R was 0.410. Fig. 22 shows that again in JB #10 the horizontal strains were greater than the vertical strains. The deep extensometers also measured more strain than the shallow extensometers because of the strain concentrations near the tunnel.

Fig. 23 is a plot of the diametrical strain of the tunnel liner as a function of the model pressure along four different tunnel diameters. The data shown in this figure is different than for the previous joint blocks discussed because there was no definite pressure at which yielding was apparent. Furthermore the average diametrical strain at 1400 psi was about 3% for this 8-in. tunnel liner, whereas the 4-in. tunnel tested in JB #7 showed about 5% strain at comparable stress levels. This was not expected because both tunnel liners were selected for having the same circumferential stiffness, E_t/R , and the 8-in. tunnel liner should have shown larger strains because the ratio of tunnel diameter to joint spacing was 8.0 rather than the value of 4.0 used in JB #7.

Comparisons of Test Data From JB #7 through JB #10. Figures 24 through 26 are summary plots of average data obtained in the tests of JB #7 through JB #10. The relative behavior of the various tunnel liners may be compared directly on these figures. All of these models (JB #7 through JB #10) were tested at a principal stress ratio $N = \sigma_h/\sigma_v = 1$ and all had joints spaced at 1 in. in two mutually perpendicular directions. Thus all variables in these four tests were held constant except the tunnel size and liner stiffness.

Fig. 24 is a plot of the average stress-strain curve

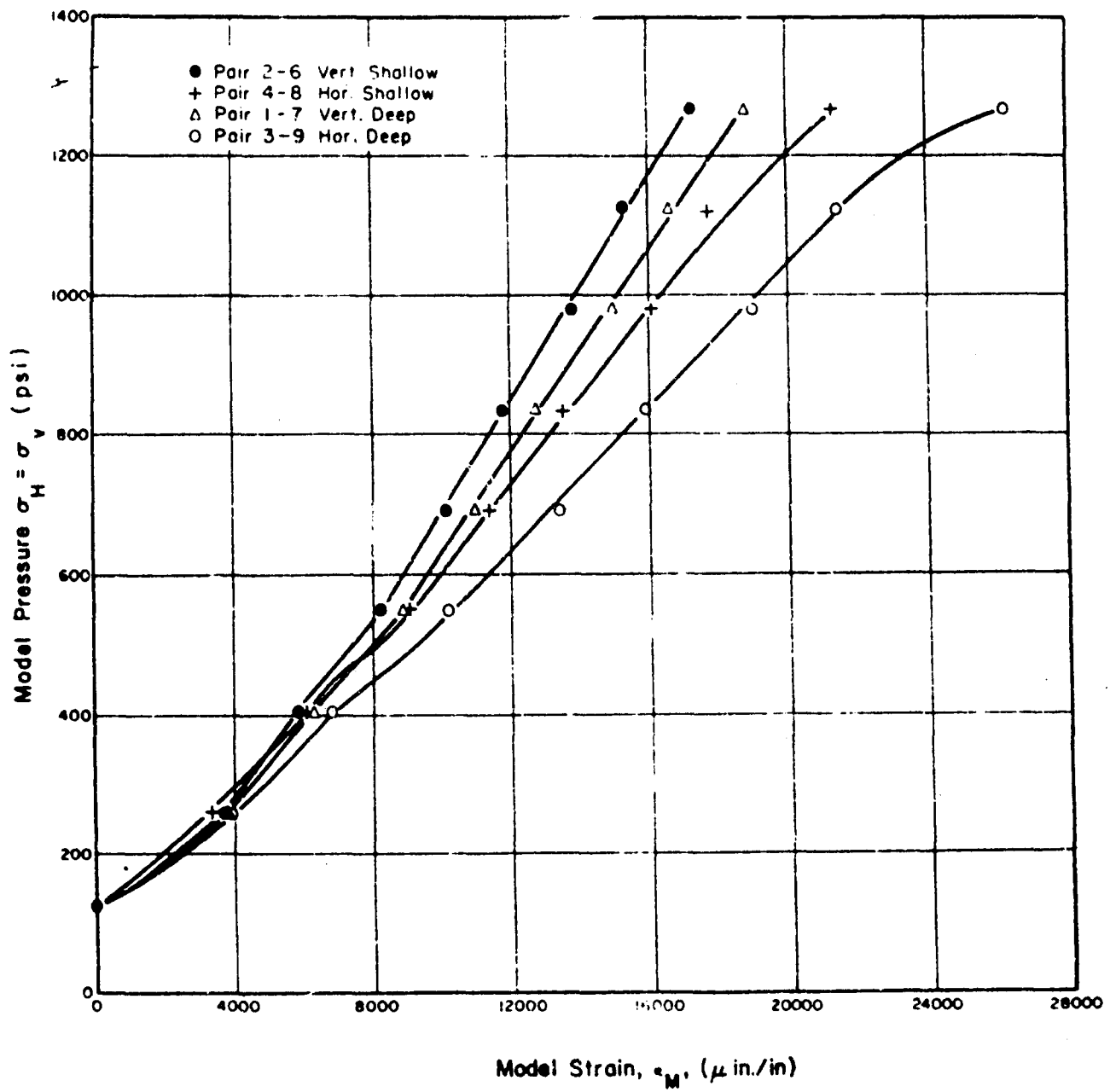


Figure 20. Stress-strain curves for JB #9.

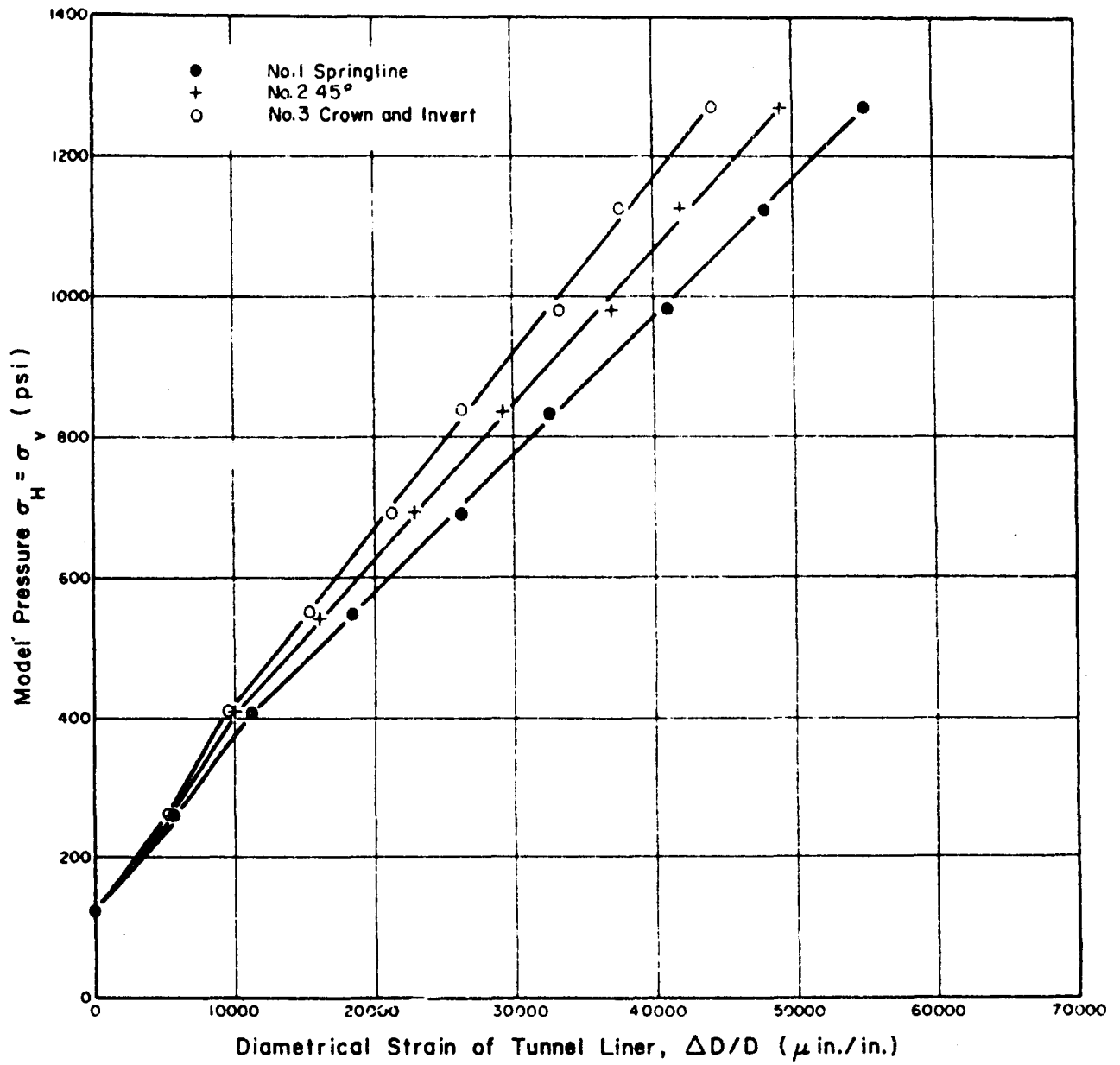


Figure 21. Diametrical strain of tunnel liner at three different diameters for 1B #9.

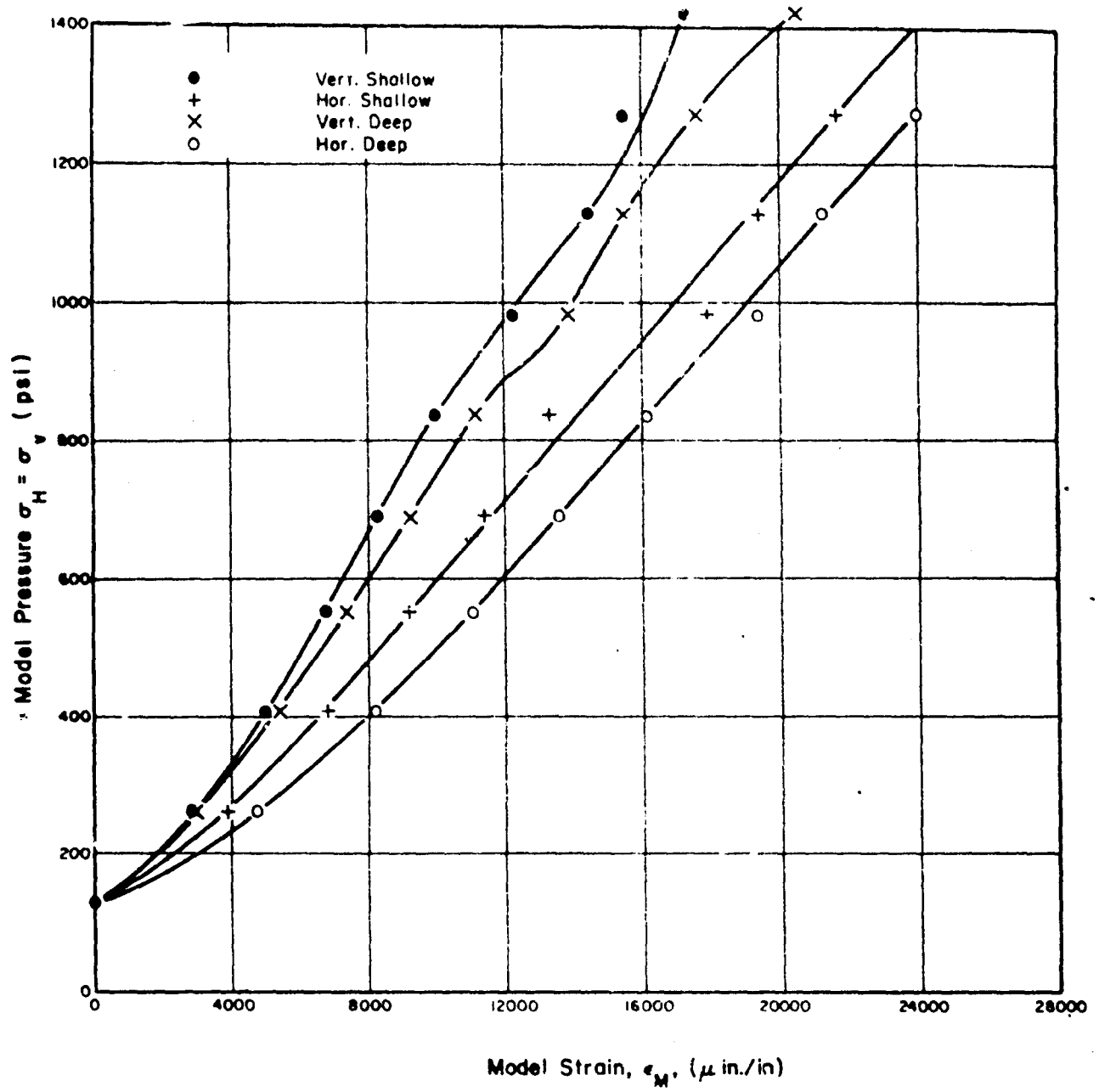


Figure 22. Stress-strain curves for JB #10.

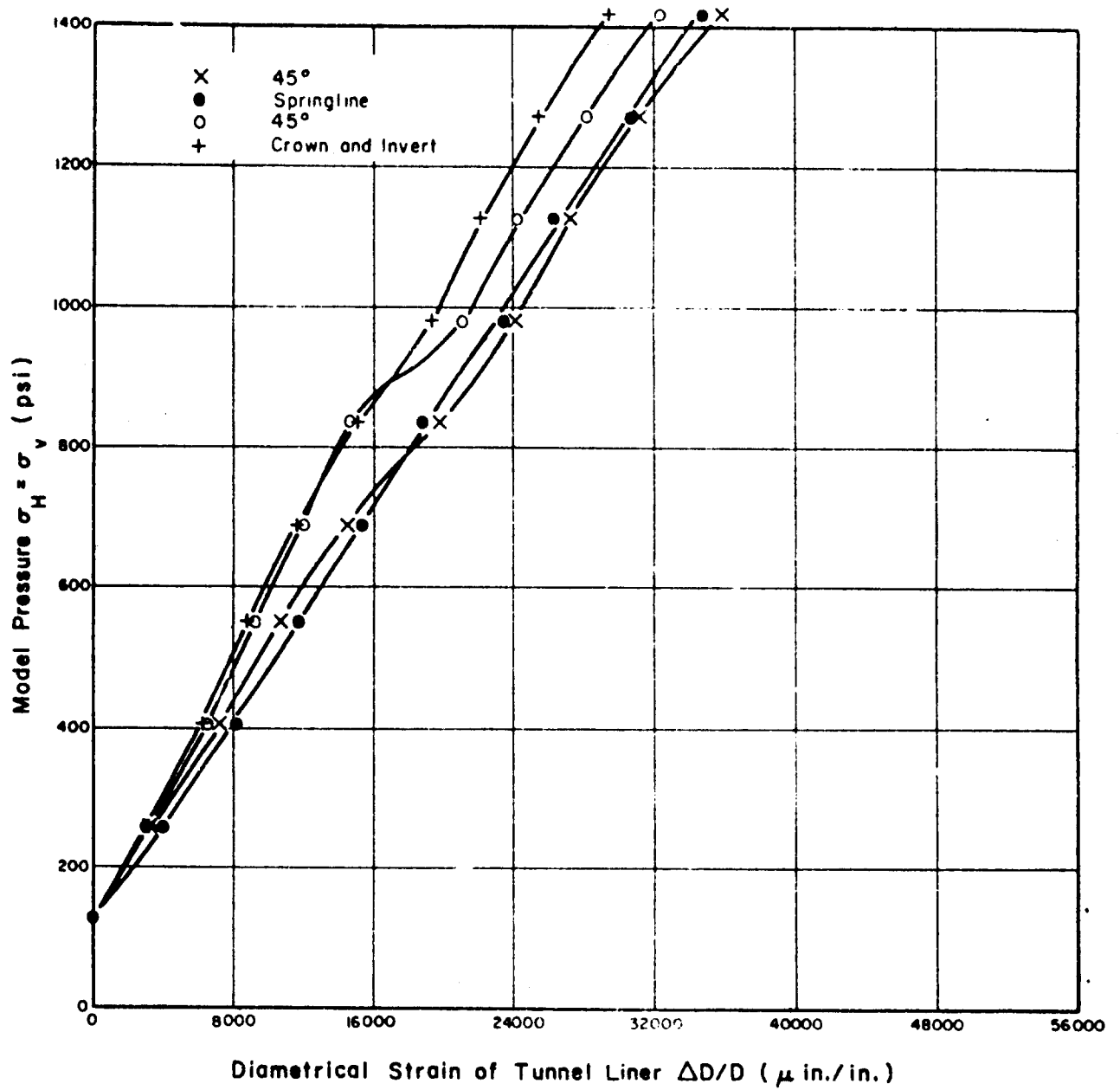


Figure 23. Diametrical strain of tunnel liner at four different diameters for JB #10.

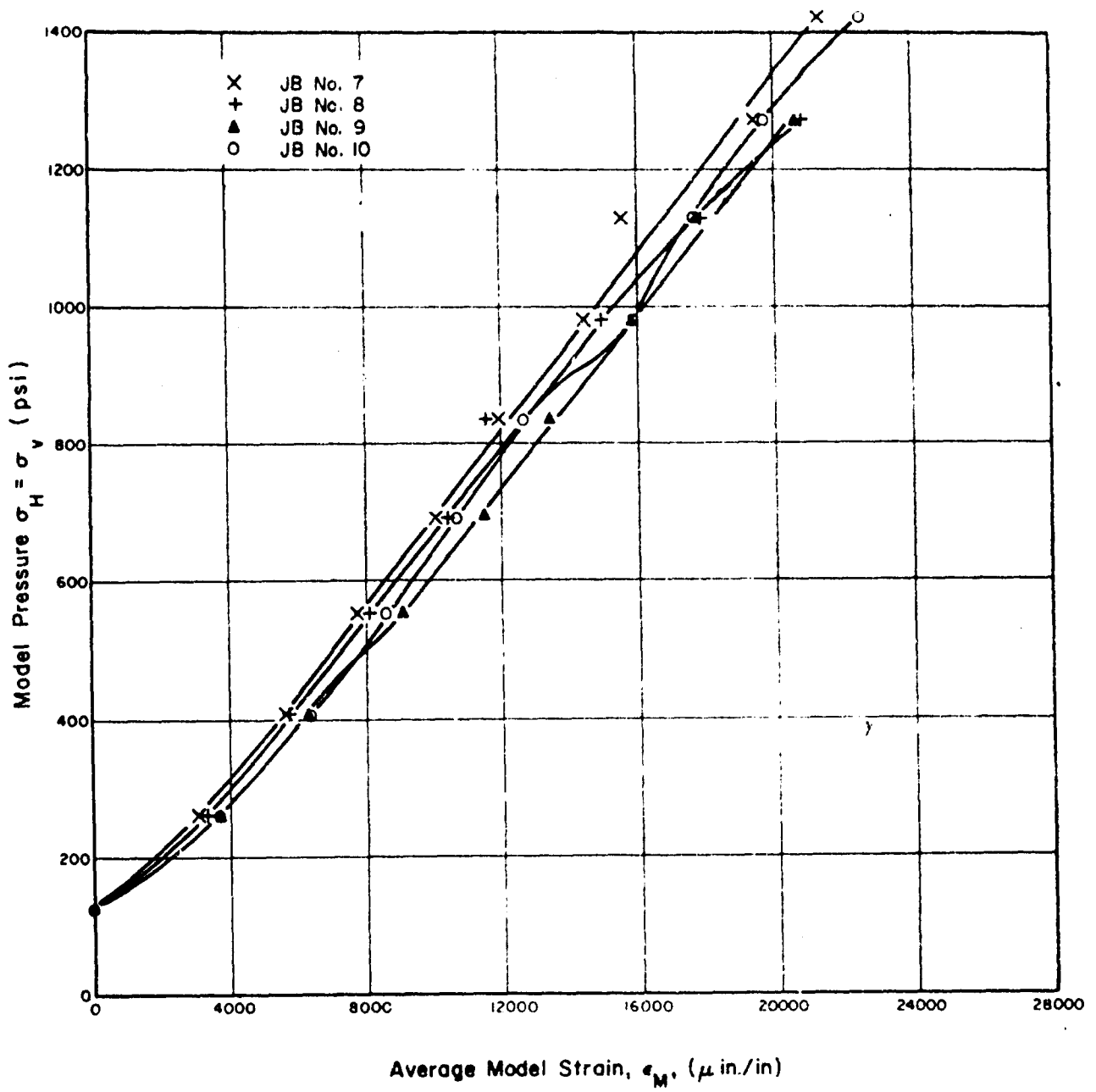


Figure 24. Average stress-strain curves for JB #7, JB #8, JB #9 and JB #10.

for each model obtained by averaging all four of the measured stress-strain curves. Each curve is adjusted to zero strain at a model stress of 125 psi to eliminate the effects of nonuniform seating movements. If the four models were all properly constructed with the same tolerances and model properties, then for a loading at a principal stress ratio $N = \sigma_h/\sigma_v = 1$ they should all have the same stress-strain curve. The four curves on Fig. 24 are remarkably similar; each shows additional seating movements up to a model pressure of about 300 psi and then is essentially linear with a slope ranging from 61,000 psi to 64,300 psi. The two models with joints oriented at 90° to the loading directions (JB #9 and JB #10) show slightly greater strains at similar model pressures than the two with joints oriented at 45° .

Fig. 25 is a plot of the average diametrical strain of the tunnel liners as a function of model pressure for each of the four models (JB #7 through JB #10). All of these models were tested at $N = 1$, and all had very nearly similar average stress-strain curves as seen in Fig. 24. Thus, the major differences between the four curves on Fig. 25 should be caused by differences in the stiffness of the liners and differences in the ratio of joint spacing to tunnel diameter. The joint spacing was 1 in. in all four cases, so the ratio of joint spacing, s , to tunnel diameter, D , was $1/4$ for JB #7, $1/6$ for JB #8 and JB #9, and $1/8$ for JB #10. It has been suggested by Hendron and Aiyer on the basis of field observations that a decreasing value of s/D should cause increased load on a tunnel liner at the same value of free field stress.

In Fig. 25, the curves for JB #8 and JB #9 are almost exactly coincident up to a model pressure of 1000 psi. These two models had the same stiffness ($Et/R = 16,700$ psi) and diameter liner and differed only in joint orientation. Joint orientation should have no effect for testing at $N = \sigma_h/\sigma_v = 1$ if the boundary conditions in the testing machine are as assumed.

JB #7 had a 4-in. diameter liner 1/8-in. thick ($Et/R = 25,000$ psi). Thus JB #7 and JB #10 both had the same calculated stiffness liner and about the same model stiffness. This is evidenced by the fact that the plot of pressure versus diametrical strain for these tests are nearly identical straight lines in Fig. 25 up to a model pressure level of 550 psi. Note also that the test results from JB #8 and JB #9 (Fig. 25) are also identical straight lines up to about 500 psi at a lower slope than tests JB #7 and JB #10 because the liner stiffness in JB #8 and JB #9 was only 16,700 psi. Above a

pressure level of 550 psi the curves for JB #7 and JB #10 (Fig. 25) diverge as the behavior of the jointed mass surrounding the tunnel becomes inelastic but the trend was surprising because it was thought that the 8 in. tunnel (JB #10) would show larger diametrical strains than the 4 in. tunnel (JB #7) with the same liner stiffness.

In Fig. 26 the curves of diametrical strain of the tunnel liner versus the average free-field strain for joint blocks 7 through 10 are shown. Note that at free field strains below 0.8% the strain concentration factor $\frac{(\Delta D/D)}{\epsilon_{ff}}$ for the tunnel liners in JB #7 and JB #10 ($Et/R = 25,000$ psi) are lower than the strain concentration factors for the tunnel liners tested in JB #8 and JB #9 ($Et/R = 16,700$ psi). At higher values of the free-field strain the test results of JB #7, #8, and #9 are nearly identical in having strain concentration factors $\frac{(\Delta D/D)}{\epsilon_{ff}}$ of about 2 and 2.5 at free field strains of 1.2% and 2% respectively. Test block JB #10 did not plot with the other results because the true free-field strains of the model were not measured in JB #10. The 8-in. diameter tunnel was so large with respect to the size of the model that the measured strains were affected by the large diametrical strains of the tunnel.

4 ANALYSIS OF TEST RESULTS

Hendron and Aiyer have analyzed the stresses and strains around a cylindrical tunnel in an elasto-plastic material with dilatancy for a uniform stress field ($N = \sigma_h/\sigma_v = 1$) under plane strain conditions. The loading conditions assumed in the analysis cited above are exactly the same as the conditions in the model tests conducted on this study. The main problem in applying the theory to the jointed models is to determine what strength properties should be used in the analysis to represent a jointed mass. Hendron and Aiyer give a correlation between the ratio σ_u/q_u and the ratio D/s for actual tunnels in jointed rock masses (Fig. 27), where σ_u is the equivalent unconfined compressive strength of the jointed rock mass around the tunnel, q_u is the intact unconfined compressive strength of the rock, D is the tunnel diameter and s is the effective joint spacing. The correlation is from field measurements of tunnel behavior. The models tested under this

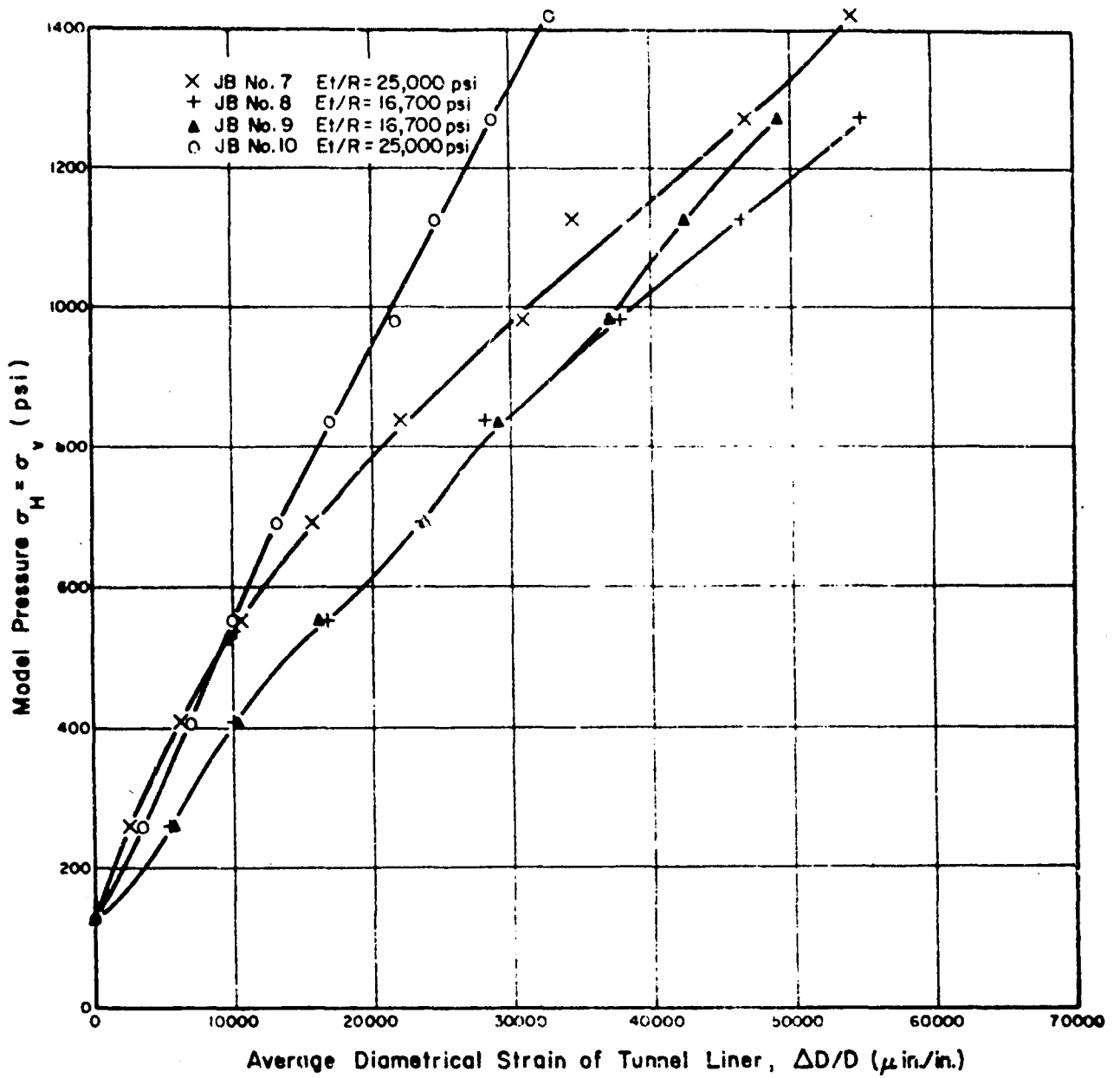


Figure 25. Average diametrical strain of tunnel liner as a function of model pressure for JB #7, JB #8, JB #9 and JB #10.

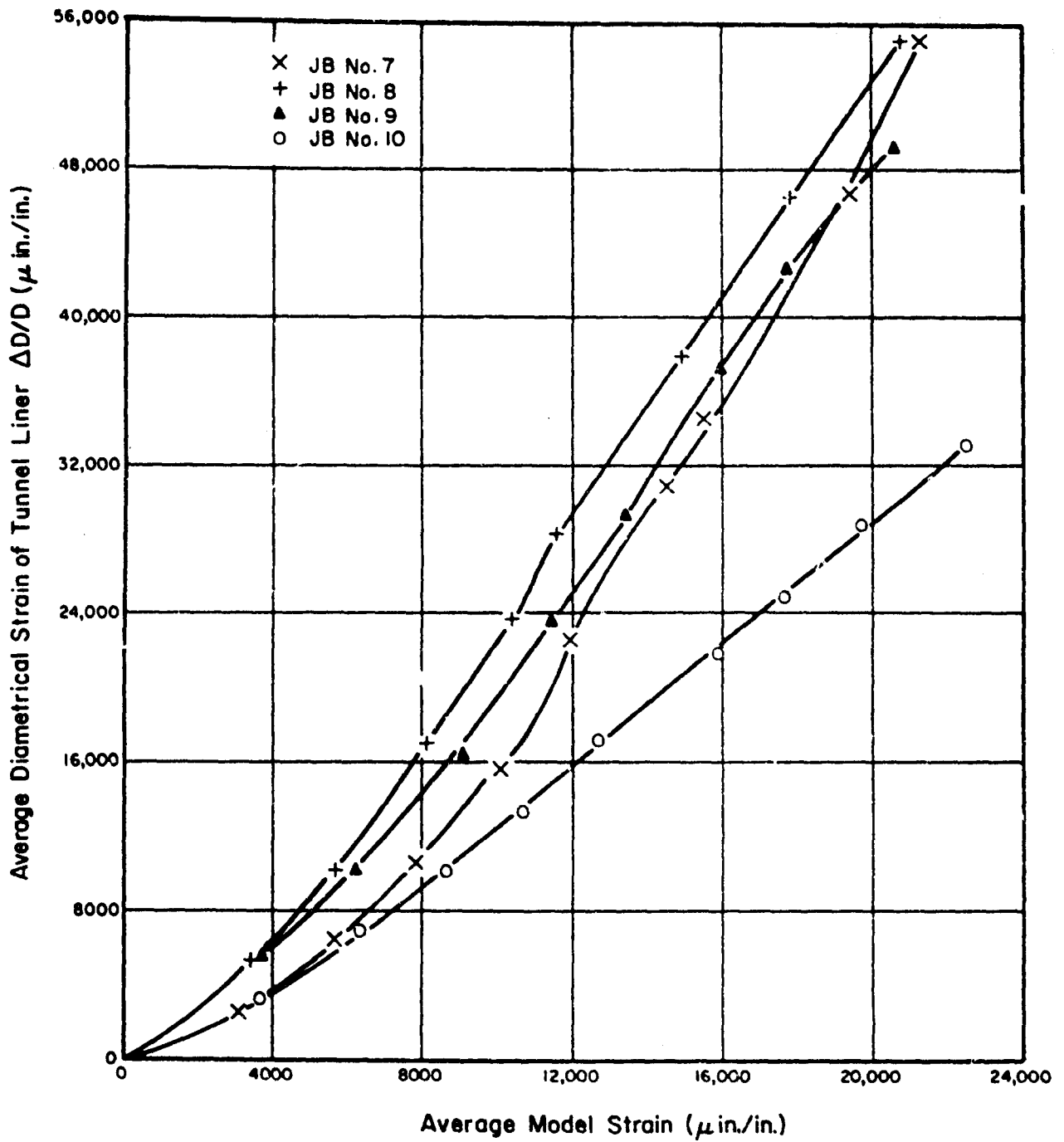


Figure 26. Dimensionless plot of average diametrical strain of tunnel liner as a function of average vertical strain of model for JB #7, JB #8, JB #9 and JB #10.

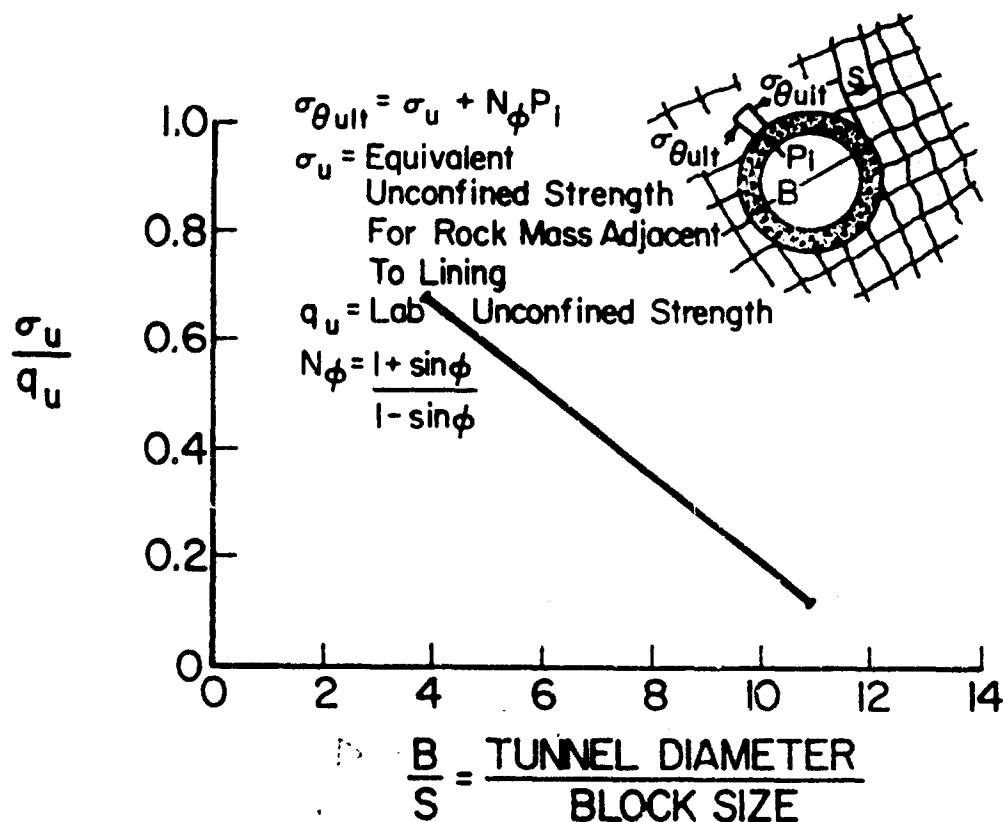


Figure 27. Ratio of insitu strength to laboratory strength as a function of tunnel diameter to joint spacing.

contract had values of D/s of 4, 6, and 8 with respective values of σ_u/q_u obtained from Fig. 27 of 0.65, 0.5, and 0.35. Since the model material has an intact unconfined compressive strength of 550 psi, these values yield σ_u values of 360 psi, 275 psi, and 190 psi respectively. The field correlations were from real tunnels where the joints were not exactly regular plane surfaces nor were they spaced evenly, and all oriented in two sets exactly parallel to the tunnel axis. Thus the field situation is not in general as unfavorable as the situation in the models and a lower value of σ_u/q_u would be expected for the models than for the field conditions.

From the model tests conducted on this study values of σ_u can be calculated using the theory above in conjunction with: (1) measured values of $\Delta D/D = \epsilon_{\theta}$, (2) measured values of E_m , (3) calculated values of the radial stresses between the liner and the medium from the liner properties and measured values of $\Delta D/D$

$= \epsilon_{\theta}$ and (4) known or estimated values of ν and ϕ for the jointed mass. Items (1) (2) and (3) above are easily obtained from measurements on the model during testing but the values of ν and ϕ for the jointed mass are not known precisely. The value of Poisson's ratio can be taken as about 0.25 based on previous experience but the estimation of this value is not critical since the results of the theory cited above are not very sensitive to the selected value of ν . The value of the angle of shearing resistance for the rock mass may be conservatively taken as the angle of friction along the joint surfaces, ϕ_j .²⁷

The value of the angle of shearing resistance along the joints, ϕ_j , is estimated from the results of direct shear tests on sawed joint surfaces shown in Fig. 7. The

²⁷ A.J. Hendron and A.K. Aiyer, *Stresses and Strains Around a Cylindrical Tunnel*

results of the direct shear tests on joint surfaces show that the value of ϕ_j decreases as the normal pressure on the joint surface increases. Thus for plastic behavior of the jointed model we should expect an effective value of ϕ_j less than the angle of internal friction, which was measured as 33° by triaxial tests.

The parameters used in the Hendron-Aiyer elasto-plastic analysis are E_m , μ , ϕ_j , σ_u , ϵ_θ , σ_r and p_0 . Where E_m , μ , ϕ_j and σ_u are effective plane strain properties of the jointed model mass, ϵ_θ and σ_r are strain and stress conditions at the point of interest and p_0 is the free field stress in the model ($p_0 = \sigma_h = \sigma_v$ for the model tests reported herein). Theoretical curves of the diametrical strain of the tunnel liner, $\Delta D/D$, as a function of the model pressure, $\sigma_h = \sigma_v = p_0$, have been calculated using measured values of E_m and assumed values of μ , ϕ_j and σ_u . With known values of the liner properties, Fig. 28, σ_r can be calculated as a function of $\epsilon_\theta = \Delta D/D$ of the liner. Then a value of p_0 can be calculated from the theory and theoretical curves of $\Delta D/D = \epsilon_\theta$ versus p_0 can be plotted. The actual experimental

curves from the model tests can be plotted on the same plot to get a comparison between theory and experiment. Such curves are plotted in Figures 29 and 30.

JB #8 and JB #9 were identical in all respects except that they had different joint orientations. Joint orientation should have no effect for testing at a principal stress ratio $N = \sigma_h/\sigma_v = 1$. Fig. 24 shows that indeed JB #8 and JB #9 did behave almost identically on a plot of diametrical strain of tunnel liner $\Delta D/D$ as a function of model pressure $\sigma_h = \sigma_v = p_0$. In Fig. 29, the results of the model tests JB #8 and JB #9 are plotted together with theoretical curves calculated from the Hendron-Aiyer analysis assuming the liner properties shown on Fig. 28, and the model properties listed on Fig. 29. The curves for JB #8 and JB #9 are essentially identical up to a model pressure of 1000 psi and are plotted as a single curve on Fig. 29. The theoretical curves in Fig. 29 are plotted assuming a value of $N\phi = 2$ which corresponds to a value of $\phi_j \cong 20^\circ$. The results of the direct shear tests shown in Fig. 7 show that the value of ϕ_j decreases with increasing normal

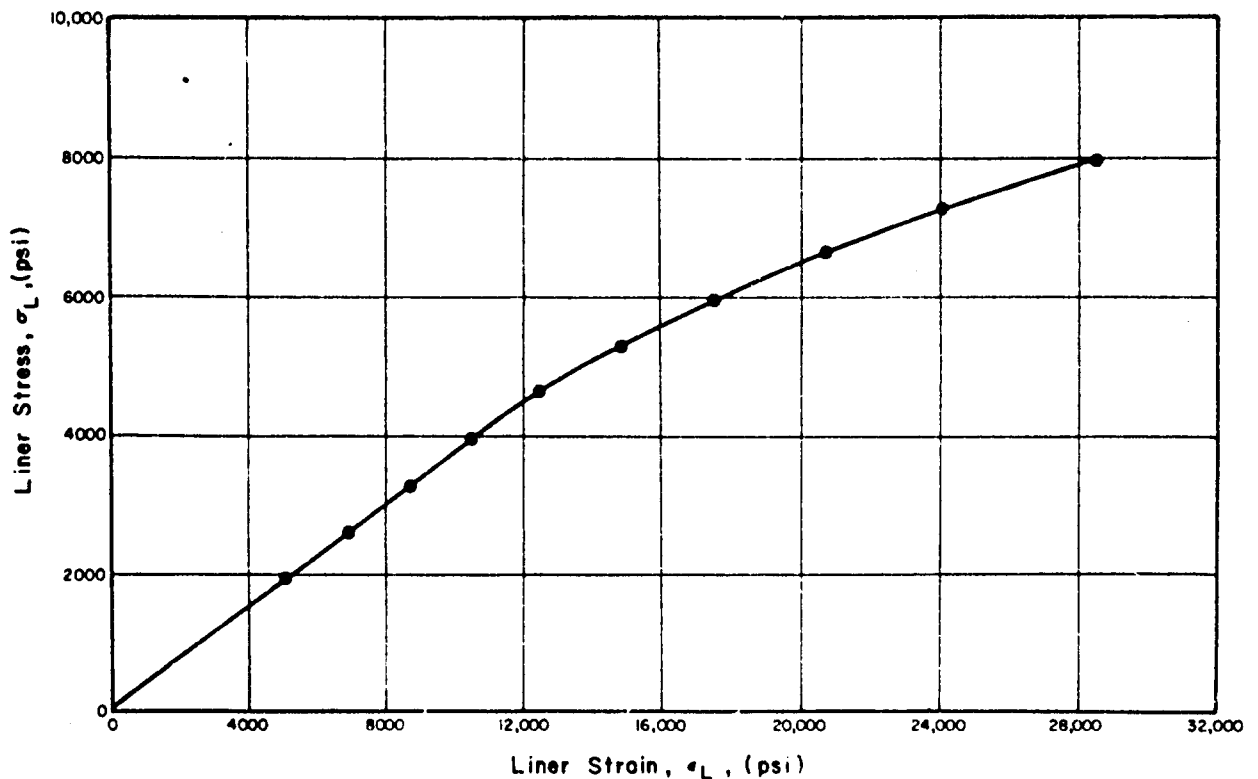


Figure 28. Stress-strain curve used for plexiglass liners.

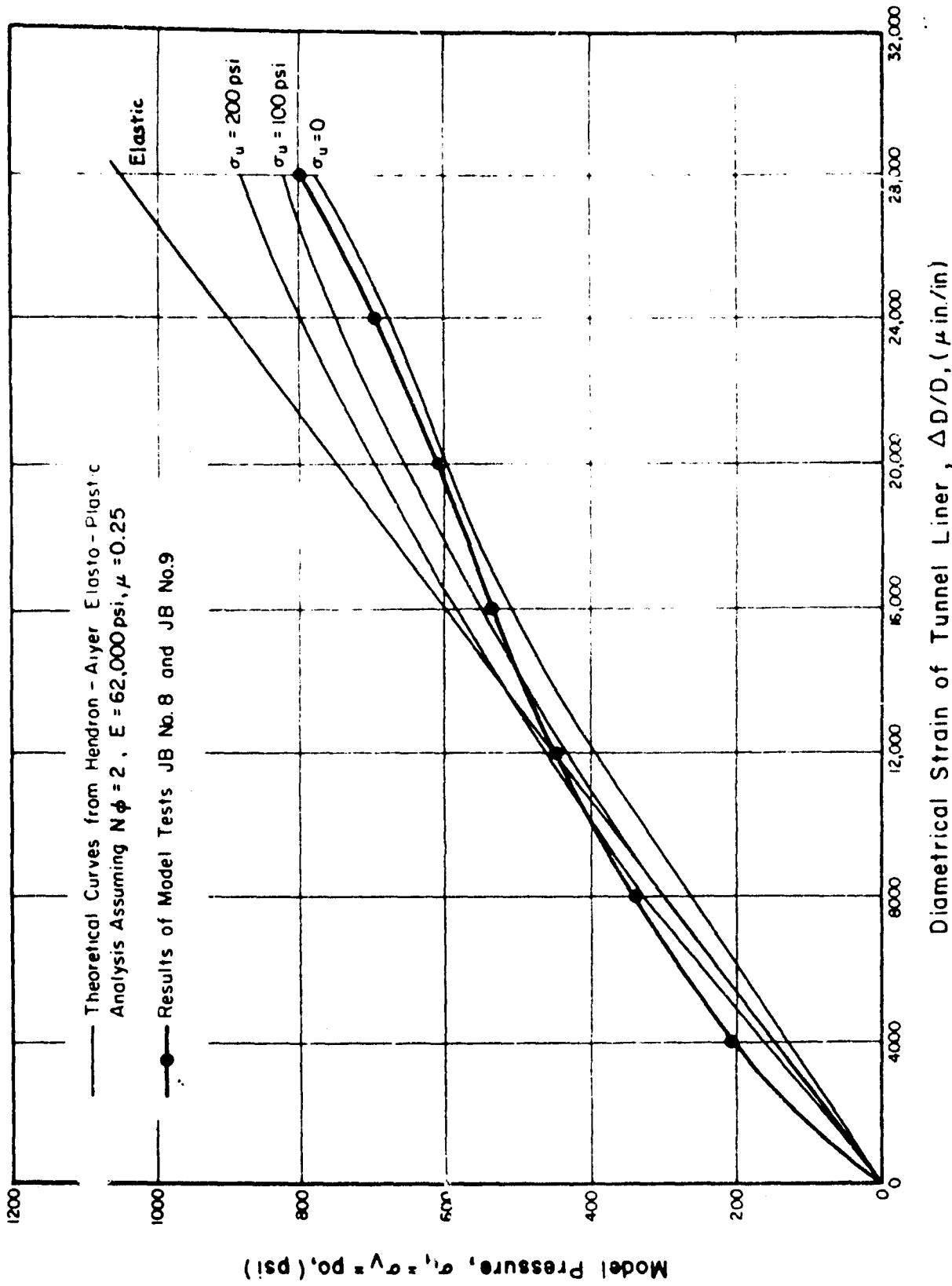


Figure 29. Diametrical strain of tunnel liner as a function of model pressure - measured results compared to theory.

pressure on the joints. The direct shear tests indicated that between a normal pressure of 50 psi and 400 psi, the value of ϕ_j decreased from 33° to 29° . The model pressures of interest ranged up to 800 psi and the material around the opening would also be subjected to a stress concentration due to the presence of the tunnel. Thus it was decided to compare the experimental results of the model tests to theoretical curves calculated using a value of $\phi_j \cong 20^\circ$. In Fig. 29, the experimental curve starts out well above the theoretical curves indicating that the effective value of ϕ_j at low pressure was considerably higher than 20° as should be expected. At a model pressure of 400 psi, the experimental curve crosses the theoretical curve for $N\phi = 2$, $\sigma_u = 200$ psi. With increasing model pressure, the experimental curve crosses over the theoretical curve for $N\phi = 2$, $\sigma_u = 100$ psi, and then becomes parallel to the theoretical curve for $N\phi = 2$, $\sigma_u = 0$. Thus the phenomenon occurring in the models could be considered to be a decreasing effective unconfined strength of the jointed mass with increasing model pressure at constant $N\phi$. As a matter of fact, the value of N also decreases with increasing model pressure and a more detailed analysis would take this effect into account quantitatively. However the model material properties used are estimates and sophisticated refinements of the analysis are not justified.

Fig. 30 is a plot similar to Fig. 29 with the experimental results of two model tests (JB #7 and JB #10) shown with theoretical curves calculated from assumed values of the model properties. JB #7 had two sets of joints spaced at 1 in. and oriented at 45° to the principal loading directions and had a 4-in. diameter tunnel lined with a 1/8-in. thick plexiglass liner. JB #10 had two sets of joints spaced at 1 in. and oriented parallel to the principal loading directions with an 8-in. diameter tunnel lined with a 1/4-in. thick plexiglass liner. These two liners have the same calculated circumferential stiffness ($E_t/R = 25,000$ psi) assuming the plexiglass was the same in each liner. The average measured model stiffness of JB #7 ($E_m = 64,300$ psi) was greater than that of JB #10 ($E_m = 61,000$ psi).

The experimental results of JB #7 and JB #10 plot very nearly on the same line up to a model pressure of about 500 psi above which they diverge rather sharply. The experimental curve for JB #10 starts out above all the theoretical curves and then at a model pressure of about 300 psi becomes coincident with the experimental curve for $N\phi = 2$, $\sigma_u = 300$ psi and follows that curve closely up to a model pressure of 950 psi. There, it begins to move toward curves for lower values of σ_u .

The experimental curve for JB #7 also starts out above all the theoretical curves, but it then crosses over all the experimental curves between model pressures of 400 psi and 550 psi.

5 CONCLUSIONS

The results of five model tests are reported and analyzed in this report. The tunnel liners used in these models were chosen so that the ratio of the circumferential tunnel liner stiffness to rock mass stiffness (E_t/R)/ E_m was similar to that for concrete liners in rock. The plexiglass liners used in this study had the further advantage that the ratio of the circumferential stiffness (E_t/R) to the flexural stiffness (EI/R^3) was nearly the same as for reinforced concrete tunnel liners. In the model tests reported here, none of the plexiglass liners buckled and two of them failed in circumferential compression as a real reinforced concrete liner would. Thus the use of plexiglass liners prevented a buckling mode of failure which had previously been experienced with aluminum liners.^{2,5}

The analysis of the data reported herein shows that elastic theory is not sufficient to predict the behavior of models loaded to high model pressures. In these tests, elastic theory was sufficiently accurate for calculating the diametrical strains of the lined tunnels up to diametrical strains of about 1.2%. For diametrical strains greater than 1.2%, calculations from elastic theory underestimate the diametrical strains of a liner. An elasto-plastic theory developed by Hendron and Aiyer was used to analyze the model behavior in the plastic range. Using experimentally measured strength and stiffness parameters for the model, the Hendron-Aiyer analysis could be used to estimate the diametrical strains of the tunnel liner in the plastic range of behavior.

The detailed analysis of the experimental data presented in the previous chapter shows that the procedure described below can be used for prediction of tunnel liner deformations ($\Delta D/D$, diametrical strains) for a tunnel liner in a jointed rock mass subjected to hydrostatic compression. The Young's modulus of the

^{2,5}A.J. Hendron et al., *Geomechanical Model Study... Report 3*

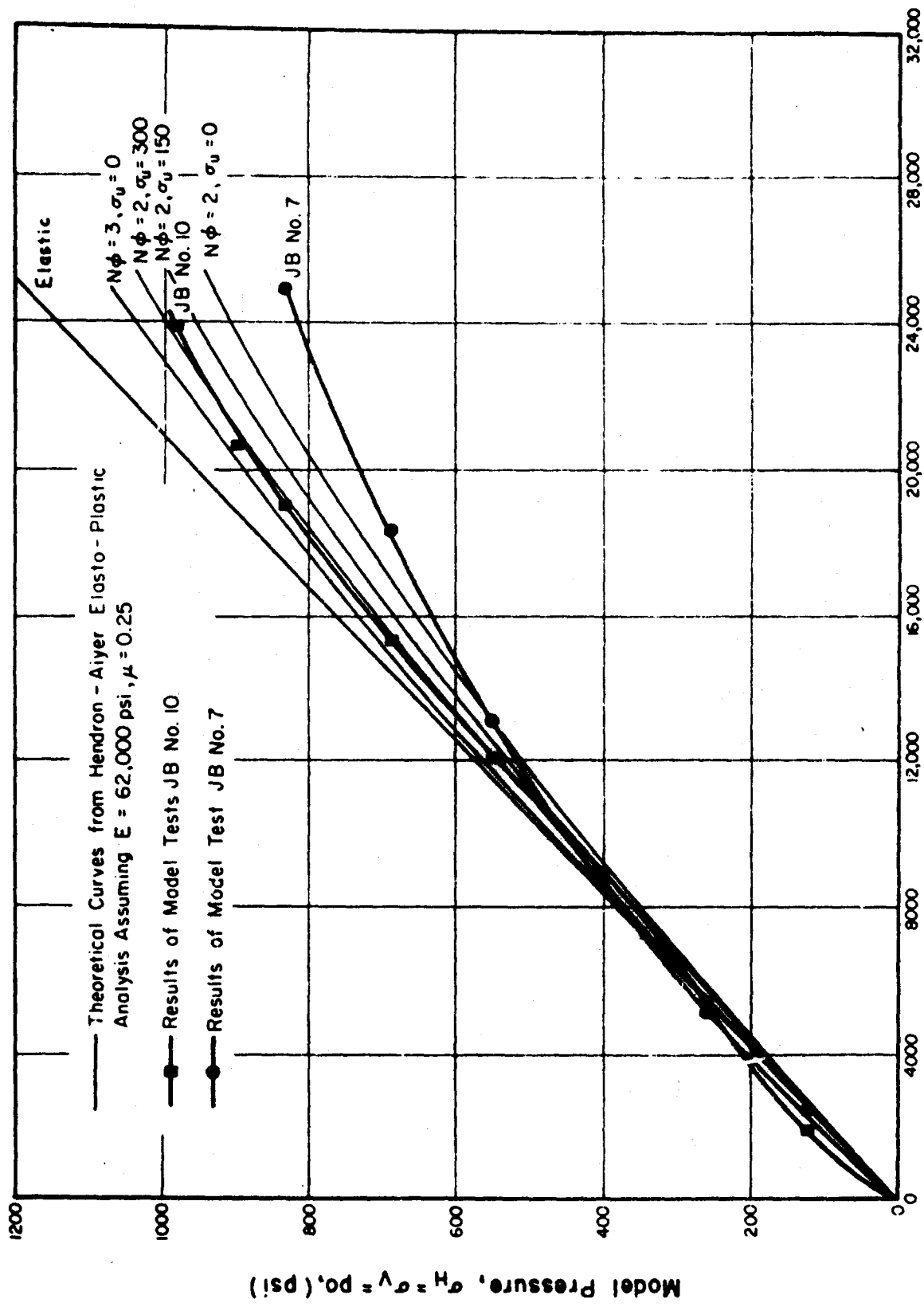


Figure 30. Diametrical strain of tunnel liner as a function of model pressure—measured results compared to theory.

jointed rock mass, E_m , as observed in these tests was about 1/10th of the Young's modulus, E , of the intact model material which composes the joint blocks. If the Young's modulus of the jointed mass, E_m , is used in an elastic analysis of the liner and jointed mass, it was found that the deformation of the liner would be predicted within about $\pm 10\%$ for diametrical strains ($\Delta D/D$), less than 1.2%. For strains above 1.2%, the elasto-plastic analysis given by Hendron and Ayer could be used to predict the liner deformations if the jointed medium was assumed to have the following properties:

- (1) The Young's modulus of the jointed medium, E_m , in the elastic range should be taken as about 1/10th the Young's modulus of the intact model material.
- (2) The angle of friction of the jointed medium,

ϕ_m , should be taken as the angle of shearing resistance along the joints, ϕ_j .

- (3) The effective unconfined strength of the jointed medium surrounding the tunnel, σ_u , should be taken as a fraction of the unconfined strength of the intact rock material as shown in Fig. 27, the fraction decreasing with an increase in the ratio of tunnel diameter to joint spacing as shown in Fig. 27.

If the above procedure is followed, the diameter changes of the structural liners can be predicted within $\pm 15\%$ for the test results presented in this report. It has been the writers' experience that the same procedure can be applied to concrete tunnel liners in rock. But, if this procedure is used for concrete liners in rock, elastic analyses should not be used beyond a diametrical liner strain of about 0.3%.

APPENDIX A: SIMILITUDE CONSIDERATIONS

Fundamental Considerations. In most physical phenomena considered in civil engineering and geology it is conventionally assumed that a "cause and effect" relationship exists between the various independent and dependent variables which influence and describe a phenomenon. This relationship is assumed to be expressed by some function

$$f(x_1, x_2, x_3, \dots, x_n) = 0 \quad [\text{Eq 1}]$$

where x_i are pertinent independent and dependent variables. The function $f(x_i)$ can usually be expressed explicitly for only the simpler phenomena. It may be determined from either theoretical considerations or empirical studies. Because the most basic physical laws (such as Newton's Laws) are dimensionally homogeneous; that is, their form does not depend upon the units of measurement, it can be hypothesized that the more complex function $f(x_i)$ is also dimensionally homogeneous, even though it is not explicitly known.

The theory of dimensional analysis, founded in the mathematical theories of algebra, is summarized in Buckingham's theorem,²⁹ which essentially states that from the dimensionally homogeneous function or equation describing a phenomenon, it is possible to develop a relationship in which the variables appear in a set of dimensionless products. (For a more complete discussion see texts such as Murphy or Langhaar.) In practice, dimensional analysis allows us to determine these dimensionless products, given the pertinent variables, even though we do not know the form of the function $f(x_i)$ which describes the phenomenon. Thus, from Equation 1, which is the basic function relating the pertinent variables x_i in a description of the phenomenon, we arrive by a dimensional analysis at

$$F(\pi_1, \pi_2, \pi_3, \dots, \pi_m) = 0 \quad [\text{Eq 2}]$$

as a description of the phenomenon. Each term π_i , often called a Buckingham pi term, is a dimensionless product of some number of the original x_i variables. Generally, the number m of independent pi terms is related to the number n of the x_i variables and to the number r of fundamental dimensions (such as mass, length, time, temperature) which are involved in the x_i variables by

$$m = n - r \quad [\text{Eq 3}]$$

²⁹H.L. Langhaar, *Dimensional Analysis*, p 18

There are several advantages which may be gained from the dimensional analysis. First, the relationship between the x_i variables in the π_i terms often gives valuable insight into the phenomenon being considered. Second, the phenomenon is described in terms of a fewer number of variables, only m pi terms instead of the n original variables. This reduction of variables is often important when studying the phenomenon experimentally since it usually reduces the number of experiments which must be conducted. A third advantage is that the dimensional analysis provides a theoretical basis for model studies, by which it may be possible to reduce even further the cost and time involved in studying the phenomenon being considered.

The function given in Equation 2 is dimensionally homogeneous and completely general. If the pi terms are independent and contain all of the pertinent variables x_i which influence and describe the phenomenon, then the function $F(\pi_i)$ completely describes the phenomenon, regardless of the scale of units with which the quantities x_i are measured, and regardless of the absolute magnitude of the x_i quantities. This means that if we wish to utilize models to study the behavior of a prototype, we can be assured that the behavior of the model duplicates the behavior of the prototype in all respects if each of the pi terms for the model is equal to the equivalent pi term for the prototype; that is, if

$$(\pi_i)_{\text{model}} = (\pi_i)_{\text{prototype}} \quad [\text{Eq 4}]$$

If such a condition exists, all requirements of similitude have been satisfied, the model is said to be "completely similar" to the prototype, and the phenomenon in the model is an exact replica of the phenomenon in the prototype.

Several major problems develop in the practical application of dimensional analysis to modeling. One is that it generally is technically impossible to insure that all of the x_i variables which influence the prototype are considered in the dimensional analysis and are accurately reproduced in the model by equating the π_i terms of the model and prototype. For satisfactory modeling it is necessary that the phenomenon be understood well enough to know what variables (x_i) are most significant and which pi terms (π_i) must be duplicated most rigorously so that the model gives the

most accurate simulation of the prototype which it is both possible and practical to attain.

In this approximation of the prototype by the model a second major problem arises from what are known as "scale effects." For example, as physical size of the model varies, the relative importance of different forces may vary also. Body forces such as weight due to gravitational attraction vary as the mass of the body, hence as the third power of linear dimensions, while surface forces such as pressures vary as area, hence as the second power of linear dimensions. Thus, as the physical size of a model is reduced, the influence of body forces decreases more rapidly than that of surface forces. It is possible that the behavior of the prototype may be strongly influenced by body forces, but when a model is made at a reduced size, its behavior may be strongly influenced by surface forces which are of lesser importance in the prototype. Careful consideration must be given to problems such as the selection of pertinent variables and the possibility of scale effects in developing a model testing program.

Selection of Significant Variables. The dimensions of mass M , length L , and time T are probably the most commonly used dimensions by which physical phenomena are described. An equally valid set of basic dimensions is force F , length L , and time T . For a static system such as is being considered, only force F and length L are involved. This is the set which will be used in the following analysis.

The significant variables associated with the behavior of an underground opening which will be considered in this study are given in Table A1. The reasons for the selection of these variables and the exclusion of others is discussed below. A number 1 in the dimensions column means that the variable is dimensionless, a pure member.

Free-field stresses. The prototype chosen for study is a segment of a long, straight, horizontal tunnel buried underground at a depth several times greater than the tunnel diameter. The most significant forces influencing the tunnel behavior are assumed to be those due to the free-field stresses which would exist at the location of the tunnel if it were not present. The two free-field stresses considered, σ_v and σ_h , are the vertical and horizontal stresses in a plane perpendicular to the tunnel axis (Fig. A1), and are assumed to be principal stresses (which they would be in an elastic half space with a horizontal surface). The magnitude of the third principal stress, σ_c , the horizontal stress parallel to the tunnel axis, will be considered later.

The vertical free-field stress σ_v could be due to the weight of the overlying material, and at any depth z below the surface it would be given by

$$\sigma_v = \gamma z \quad \text{[Eq 5]}$$

where γ is the average unit weight of the overburden. Following the arguments of Terzaghi and Richart,³⁰ and Deere,³¹ the horizontal free-field stress σ_h is assumed to be given by

$$\sigma_h = N\sigma_v = N\gamma z \quad \text{[Eq 6]}$$

The coefficient N relating σ_v and σ_h is intimately related to the present geologic environment and the previous geologic history of the site and may vary over a wide range of values.

The free-field stresses could also be due to the loads imposed by a nuclear detonation over a protective structure in rock. In this case the major principal stress would be the dynamic radial stress, σ_{rd} , of the direct induced ground shock emanating from the crater. The minor principal stress would be the dynamic tangential stress, σ_{td} , given by

$$\sigma_{td} = \sigma_{rd} \left(\frac{1-\nu}{1+\nu} \right) \quad \text{[Eq 7]}$$

where ν is Poisson's ratio of the rock mass. The ratio between the major and minor principal stresses, N , for this case could range from about 1/4 to 1.0.

Because the value of N for both static and dynamic stress fields varies over a large range, model tests to simulate either of these problems should be conducted at various values of N rather than at a specific value of N . Thus for purposes of dimensional analysis of the static problem considered here both σ_v and σ_h will be considered as independent variables.

Mindlin³² has developed rigorous solutions for stress distributions around a circular tunnel in an elastic half space under gravity loading with N values of 0, 1/2, and 1. His results (see Panek³³ or Caudle and

³⁰K. Terzaghi and F. E. Richart Jr., "Stresses in Rock About Cavities," *Cootechnique*, Vol. 3 (1952) pp 57-90.

³¹D. U. Deere, Discussion of "Failure of Homogeneous Rock Under Dynamic Compressive Loading," by G. B. Clark and R. D. Caudle, *State of Stress in the Earth's Crust*, W. R. Judd, ed. (Elsevier, 1964) pp 321-323; and "Geologic Considerations," *Rock Mech. in Eng. Pract.*, Stagg and Zienkiewicz, ed. John Wiley & Sons, 1968).

³²R. D. Mindlin, "Stress Distribution Around A Tunnel," *Proc. ASCE* (April 1939) pp 619-642.

³³L. A. Panek, *Stresses About Mine Openings in a Homogeneous Rock Body* (New York, 1951).

Table A1
Significant Variables

Variable		Dimensions
Free-field Stresses, assumed to be principal stresses		
σ_v ,	the vertical free-field stress	FL ⁻²
σ_h ,	the horizontal free-field stress	FL ⁻²
Intact rock properties		
c or q_0 ,	cohesion or unconfined compressive strength, use either one	FL ⁻²
ϕ ,	angle of internal friction	1
σ_t ,	tensile strength	FL ⁻²
E,	modulus of elasticity	FL ⁻²
ν ,	Poisson's ratio	1
Rock mass properties		
s,	spacing of joints	L
ϕ_j ,	angle of frictional resistance along joint surfaces	1
θ ,	orientation of joint planes with respect to principal planes	1
Geometry of the opening		
d or a,	internal diameter or radius of unlined opening, and D or R, diameter or radius of the lining	L
Support properties		
$E_l I/R^3$,	flexural stiffness of lining, where E_l is the modulus of the liner material and I is the moment of inertia of the liner wall per unit length	FL ⁻²
$E_l t/R$,	compression stiffness of lining, where t is the lining thickness	FL ⁻²
Response of system		
u,	radial deformations of the opening wall	L
ϵ ,	strain within the rock mass around the opening	1
σ ,	stress within the rock mass around the opening	FL ⁻²
T,	thrust in the lining, force per unit length	FL ⁻¹
M,	moment in the lining, moment per unit length	F

Clark^{3,4} for more detail) show that if the tunnel is at a depth of three tunnel diameters or more, the stress distribution around the tunnel can be approximated very closely by the distribution of stresses about a circular hole in a biaxially loaded elastic flat plate, as determined by the Kirsch equations (see, for example, Timoshenko and Goodier,^{3,5} or Obert and Duval^{3,6}). In

both cases the area in which stresses are significantly influenced by the tunnel has a width of about four times the diameter of the tunnel.

These observations allow a considerable simplification in modeling the stress field about the tunnel. The observation that the area influenced by the tunnel is about four tunnel diameters wide means that the stress distribution on a square whose sides are four tunnel diameters long, concentric with the tunnel, is very closely approximated by that illustrated in Fig. A1 where σ_v and σ_h are the free-field stresses at the location of the tunnel axis, and $\Delta\sigma_v$ and $\Delta\sigma_h$ are the changes in the free-field stresses between the top and the bottom of the zone due to the weight of the material within it.

^{3,4} R.D. Caudle and G.B. Clark, "Stress Around Mine Openings in Some Simple Geologic Structures," *University of Illinois Eng. Exp. Sta., Bull. No. 430* (1955).

^{3,5} S. Timoshenko and J.N. Goodier, *Theory of Elasticity* (McGraw-Hill, 1951).

^{3,6} L. Obert and W. I. Duvall, *Rock Mechanics and the Design of Structures in Rock*. (John Wiley & Sons, 1967).

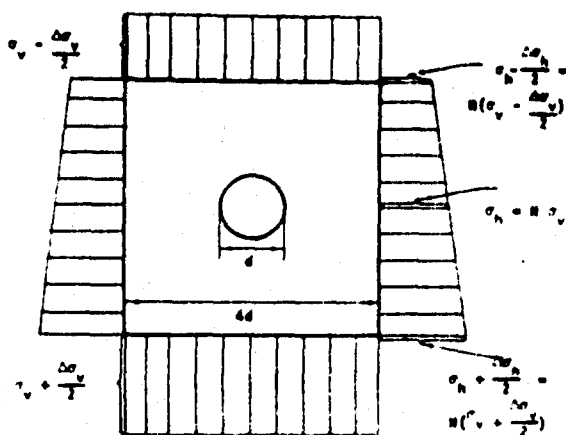


Figure A1. Stress distribution some distance from tunnel.

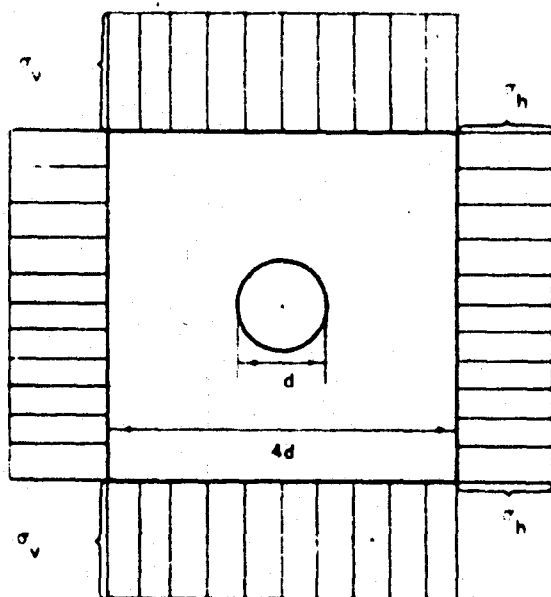


Figure A2. Approximate stress distribution some distance from tunnel.

The observation that Mindlin's solutions for tunnels buried at more than three tunnel diameters are closely approximated by Kirsch's solution means that the stress distribution of Fig. A1 can be approximated by that of Fig. A2 with small error. This means that for the elastic case the stress distribution around a tunnel underground at a depth of more than three tunnel diameters is more strongly influenced by the average

free-field stresses at the tunnel location than by the gravity forces on the material within the zone influenced by the tunnel. When modeling the static behavior of a tunnel in this situation only the average free-field stresses as illustrated by Fig. A2 need be modeled and the body forces can be neglected. On the basis of the preceding arguments the body forces and associated variables such as the density of the material are not considered in the list of significant variables for the present study. Thus, forces due to the weight of loosened rock around the opening are not being modeled.

Intact rock properties. A discussion of the failure mechanism of rock materials is beyond the scope of this report. The reader is referred to papers such as Jaeger,³⁷ Bieniawski,³⁸ Hendron,³⁹ and Hoek⁴⁰ as examples and discussions of recent work in this area. Regardless of the actual failure mechanism in rock materials, it is generally observed that some form of Mohr envelope can be fitted to observed experimental data and used to predict rock strength. In order to simplify the dimensional analysis and subsequent discussions, it will be assumed that the general curvilinear Mohr envelope can be approximated by a straight line in the compression pressure range of interest, so that the general Mohr failure criteria

$$\tau = F(\sigma) \quad [\text{Eq 8}]$$

can be replaced by the more specialized Coulomb-Navier failure criteria

$$\tau = c + \sigma \tan \phi \quad [\text{Eq 9}]$$

(For a more detailed discussion of failure criteria see Nadai,⁴¹ Seely and Smith,⁴² Jaeger,⁴³ and Obert and Duval.)

The two-independent Coulomb-Navier strength

³⁷ J.C. Jaeger, "Brittle Fracture of Rocks," *8th Symp. on Rock Mech.*, (AIME, 1967) pp 3-131.

³⁸ Z.T. Bieniawski, "Mechanism of Brittle Fracture of Rock," *Int. Journ. Rock Mech. and Mining Sci.* (October 1967) pp 395-430.

³⁹ A.J. Hendron, Jr., "Mechanical Properties of Rock," *Rock Mech. in Eng. Pract.*, Stagg & Zienkiewicz, ed. (John Wiley & Sons, 1968).

⁴⁰ E. Hoek, "Brittle Failure of Rock."

⁴¹ A. Nadai, *Theory of Flow and Fracture of Solids*, Vols I and II (McGraw-Hill, 1950).

⁴² F.B. Seely and J.O. Smith, *Advanced Mechanics of Materials* (John Wiley & Sons, 1952).

⁴³ J.C. Jaeger, *Elasticity, Fracture and Flow* (Methuen and Co. Ltd., 1962).

parameters are the cohesion c and the angle of internal friction ϕ . An alternate and equally valid pair are the unconfined compressive strength q_u , and the angle of internal friction ϕ . Either c or q_u , in conjunction with ϕ , are necessary and sufficient to define the failure state and describe the failure envelope in the compression range. In addition, the tensile strength σ_t must be defined, since Equation 9 is not valid in the tensile stress range. The complete failure envelope, then, is as shown in Fig. A3. A rigorous consideration of the actual curvilinear Mohr envelope does not change the basic conclusions of the dimensional analysis.

The elastic constants, the modulus of elasticity E and Poisson's ratio ν , relate stress and strain assuming the intact rock exhibits a quasi-elastic behavior at low and intermediate stress levels. In general this quasi-elastic range is followed by a range in which inelastic strains occur, and then by some form of failure such as fracture or plastic deformation (Fig. A4). No variables are included to describe the inelastic and plastic regions for two reasons: (1) because of the wide range of behavior exhibited by different rocks, and (2) because of the scarcity of real numerical description and data for this portion of the stress-strain curve. It is recognized that the other types of behavior exist. For example, a concave upward stress-strain curve is commonly observed at low stress levels for very porous rocks, for highly weathered rocks, and for thinly bedded or foliated rocks compressed perpendicular to the bedding or foliation. The initial quasi-elastic behavior is possibly more common, however, and is much more simple to consider and model.

Time-dependent behavior such as creep or viscous deformation is not considered here. These properties of real rock are so poorly known and understood that any attempt to consider them in modeling the behavior of underground openings must be considered a very questionable practice for the "present state of the art." The one exception to this statement would be in the case of underground openings in the evaporites: rock salt, potash, and possibly gypsum and anhydrite. For these rocks time-dependent behavior is so pronounced that it dominates the behavior. Indeed, because it is so pronounced it can be and has been studied enough so that intelligent attempts to model the time-dependent behavior of such rocks can be made (see for example Thompson and Ripperger⁴⁴).

⁴⁴ E. Thompson and E.A. Ripperger "An Experimented Technique for the Investigation of the Flow of Halite and Sylvanite," *Sixth Symposium on Rock Mechanics* (University of Missouri, 1964) pp 467-488.

Rock Mass Properties. The most important rock mass properties of a rock mass surrounding a tunnel are the spacing and orientation of the discontinuities and the strength along the discontinuities. Thus for purposes of dimensional analysis, the spacing of the joints or discontinuities, s , should be considered as an independent variable. The orientation of each joint set in a particular problem is also very important and must be considered as an independent variable. It is suggested herein to specify the orientation of the joint planes, θ with respect to the maximum free-field principal stress direction since the orientation will govern the ratio of normal and shear stresses on the joint planes.

The strength properties of the joint surfaces must also be considered. In the model tests conducted on this study the models were composed of planar joint surfaces free of irregularities. The shear strength along such a plane surface can be expressed by

$$\tau_j = \sigma_n \tan \phi_j \quad [\text{Eq 10}]$$

where σ_n is the normal stress on the plane surface and ϕ_j is a property of the joint surfaces which should be included in the dimensional analysis to represent the angle of shearing resistance along the planar joint surfaces.

Opening geometry. For this study, the opening is assumed to be of circular shape with internal diameter d (radius a). It is assumed that any lining of the opening is of diameter D (radius R) which is the same magnitude as the opening diameter d , and that the variables d , a , D , and R may be used interchangeably for the purposes of dimensional analysis. However, only one of these variables may be considered as an independent variable for the purposes of dimensional analysis, since they all define the same thing, the size of the underground opening.

Lining properties. "Unsupported" cylinders and rings: general expressions for the elastic deflection of rings and cylinders due to loads which do not vary with position along the axis are developed in numerous texts on strength of materials, the theory of elasticity, and structural analysis (such as Seely and Smith or Timoshenko and Gere⁴⁵). It is seen from these expressions that the deflection δ_p of a point on a long cylinder due to bending deformation caused by external loads P is given by

$$\delta_p = C_1 P R^3 (1 - \nu_0^2) / E_0 I \quad [\text{Eq 11}]$$

⁴⁵ S. Timoshenko and J. Gere, *Theory of Elastic Stability* (McGraw-Hill, 1961).

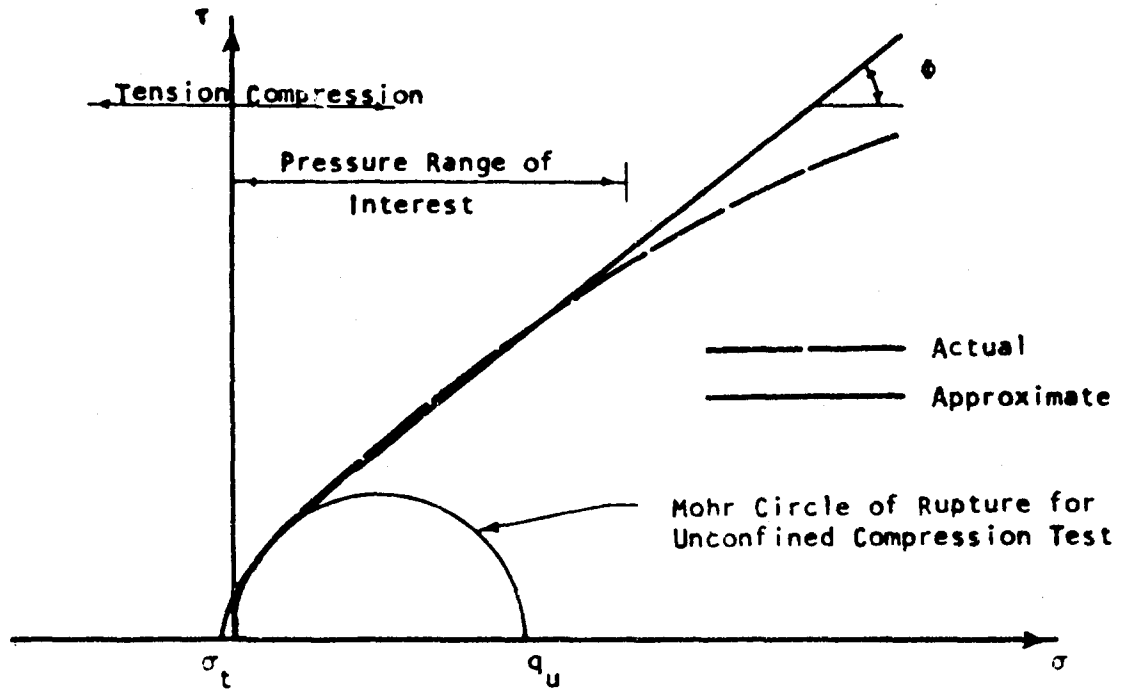


Figure A3. Failure envelope considered typical for rock.

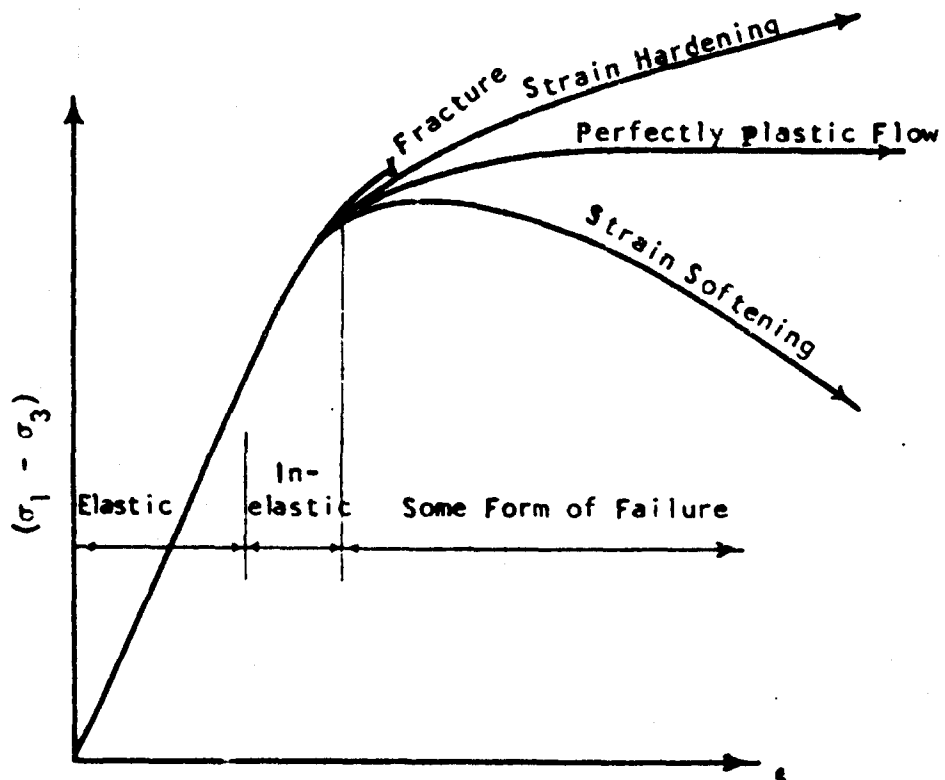


Figure A4. Stress-strain curve considered typical for rock.

and the deflection δ_c due to circumferential compression deformation is given by

$$\delta_c = C_2 P R(1-\nu_q^2)/E_q t \quad [\text{Eq 12}]$$

The quantities C_1 and C_2 are constants whose values depend upon the configuration of the applied loads and upon the location of the point in question. Lane⁴⁶ and Dorris⁴⁷ give tables of values of C_1 for different loading configurations. The flexural and compression stiffnesses of a long cylinder are the quantities $E I/R^3(1-\nu_q^2)$ and $E_q t/R(1-\nu_q^2)$ respectively. The term $(1-\nu_q^2)$ arises because of the restraint offered by the axial stress parallel to the cylinder axis in plane strain problems. In the case of a ring subjected to plane stress, this term vanishes and the bending stiffness becomes $E_q I/R^3$.

Buckling of unsupported rings and cylinders under uniform and non-uniform external loads and pressures is treated in a number of texts and papers such as Seely and Smith, Timoshenko and Gere, Boresi,⁴⁸ Bodner,⁴⁹ and Anderson and Boresi.⁵⁰ The conclusion reached in these investigations is that for a long, thin-walled cylinder, the critical external buckling pressure p_{cr} is given by an equation of the form

$$p_{cr} = C_3 E_q I/R^3(1-\nu_q^2) \quad [\text{Eq 13}]$$

where C_3 is a function of the loading configuration and the buckling mode. Note that the significant cylinder parameter is the bending stiffness $E I/(1-\nu_q^2)R^3$, which is reasonable since buckling is a bending phenomenon. As before, the term $(1-\nu_q^2)$ is due to restraint from the third dimension.

Cylinders and rings on elastic foundations: Hetenyi⁵¹ shows that for a ring on elastic foundation (i.e.,

with radial spring supports) which is subjected to any generalized radial loading P , the radial displacement δ of any point of the ring is of the form

$$\delta = F(P/E_q I/R^3, KR/E_q I/R^3, \theta) \quad [\text{Eq 14}]$$

where K is the modulus of subgrade reaction (the "spring constant" of the foundation), and θ is a measure of position on the ring. In the case of a long cylinder instead of a ring, the term $E_q I/(1-\nu_q)$ is substituted in place of $E_q I$. Note that this is $(1-\nu_q)$, not $(1-\nu_q^2)$ as previously, the reason being that the elastic foundation reaction is not continuous but consists of discrete springs.

Cheney⁵² and Luscher⁵³ analyzed buckling of radial spring supported rings and found the critical external buckling pressure to be

$$p_{cr} = 2(KR)E_q I/R^3 \quad [\text{Eq 15}]$$

As a first approximation in these analyses of cylinders and rings on elastic foundations, only bending deformations are considered, and deformations due to circumferential compression forces are ignored.

Cylinders supported by a continuous elastic medium: Hoeg⁵⁴ gives an elastic solution for stresses and displacements of a cylinder in an elastic medium considering $N = \sigma_h/\sigma_v$ as a variable for the cases of perfect bond and of free slip between the cylinder and the medium. He finds that the behavior is a function of the relative compressibility and flexibility of the cylinder and the medium as given by a flexibility ratio

$$F = \frac{1/6(1-2\nu/1-\nu)M}{E_q I/R^3(1-\nu_q^2)} \quad [\text{Eq 16}]$$

and a compressibility ratio

$$C = \frac{M/(1-\nu)}{E t/R(1-\nu_q^2)} \quad [\text{Eq 17}]$$

where M is the one dimensional constrained modulus of the medium and ν is the Poisson's ratio of the medium. Note that the significant cylinder parameters are the same as those for the unsupported cylinder.

⁴⁶ K.S. Lane, "Garrison Dam Test Tunnel, Evaluation of Results," *Trans. ASCE*, Vol 125, Pt 1, Paper 3022 (1960) pp 268-306.

⁴⁷ A.F. Dorris, *Response of Horizontally Oriented Buried Cylinders to Static and Dynamic Loading*, Technical Report No. AFWL-TR-65-116 (Air Force Weapons Laboratory, 1966).

⁴⁸ A.P. Boresi, "A Refinement of the Theory of Buckling of Rings Under Uniform Pressure," *Journal of Applied Mechanics*, Vol 22 (ASME, 1955).

⁴⁹ S.R. Bodner, "On the Conservativeness of Various Distributed Force Systems," *Journal of the Aeronautical Sciences*, Vol 25, No. 2 (1958).

⁵⁰ R.H. Anderson and A.P. Boresi, "Equilibrium and Stability of Rings Under Nonuniformly Distributed Loads," *Proc. of the Fourth U.S. Nat. Cong. of Applied Mech.*, Vol 1 (ASME, 1962).

⁵¹ M. Hetenyi, *Beams on Elastic Foundations* (University of Michigan Press, 1946).

⁵² M. Cheney, "Bending and Buckling of Thin-Walled Open-Section Rings," *Proc. ASCE, Journ. Eng. Mech. Div. EM5*, Paper 3665 (1963).

⁵³ U. Luscher, Study of the Collapse of Small Soil-Surrounded Tubes, Technical Report AFSWC-TDR-63-6 (Air Force Special Weapons Center, 1963).

⁵⁴ K. Hoeg, *Pressure Distribution on Underground Structural Cylinders*, Technical Report No. AFWL-TR-65-98 (Air Force Weapons Laboratory, 1966).

Cylinders in soil materials: On the basis of empirical data from tests of buried culverts, Spangler⁵⁵ developed the well-known "Iowa formula" in which the deformations of a thin-walled buried cylinder due to surcharge loading may be expressed in terms of $p/E_q I/R^3$ and $eR/E_q I/R^3$ where p is a measure of the surcharge pressure acting on the cylinder, and e is a passive deformation modulus of the soil. Watkins and Spangler⁵⁶ present arguments indicating that the quantity " eR " and not just " e " is a constant for a given soil.

Luscher⁵⁷ analyzes deformation data from tests on buried cylinders in terms of the parameters $p/E_q I/R^3$ and $E' E_q I/R^3$, where E' is a deformation modulus of the soil which he found to correlate with M , the one-dimensional constrained deformation modulus.

It is interesting to note that Spangler's Iowa formula can be written in a form which is very similar to the first term in the Hetenyi solution for the behavior of rings on elastic foundations.

Hoeg ran tests on cylinders buried in Ottawa sand which agreed well with predictions from his elastic solution for the behavior of a cylinder in an elastic medium.

Luscher⁵⁸ summarizes data on the buckling of cylinders in soil accumulated by a number of investigators and found that the bending stiffness $E_q I/R^3$ of the cylinder correlated with failure by buckling.

A review of the preceding discussions shows that the most significant cylinder parameter governing the behavior of a cylinder subjected to external pressures is the bending stiffness $E_q I/R^3(1-\nu_q^2)$. In the special case in which the external loading closely approaches a uniform radial pressure, the hoop compression deformation is more important than the bending deformations, and the important parameter becomes $E_q t/R(1-\nu_q^2)$. The quantity $(1-\nu_q^2)$ is quite close to unity and may be disregarded with little error.

Hence, for the purposes of dimensional analysis and modeling, the stiffnesses $E_q I/R^3$ and $E_q t/R$ are considered the significant parameters describing the tunnel lining, rather than the individual quantities E , I , R , and t . This has the great advantage of allowing the model lining to be made of any material, regardless of the prototype material, since it is necessary to consider only the structural stiffness properties of the liner and not the actual liner material properties. This assumes that the prototype lining is subjected only to stresses in the pseudo-elastic, working-stress range, so that the strength parameters of the liner material need not be modeled. This is a reasonable assumption for most tunnel linings. It must be noted, however, that the ratio between the two stiffnesses is distorted somewhat if the model lining is constructed of a material different from that of the prototype lining. This means that the response of a model lining will not reproduce with complete accuracy the response of a prototype lining constructed of a different material.

Variables describing the response of the system.

The radial movements of the tunnel wall are given by u , strains at points in the rock mass behind the wall are given by ϵ , and stresses within the rock mass are given by σ . The subscripts θ and r will be used with these variables to indicate the circumferential and radial directions, respectively.

The response of the tunnel liner is given by the displacements u , and by thrusts T and moments M in the liner. The thrusts and moments are given per unit length of tunnel: pounds per inch, and inch-pounds per inch. The actual stresses in the liner are not considered because they are of less fundamental significance than the thrusts and moments. The thrusts and moments are dependent only upon the more general, or "first-order," variable such as flexural and compression stiffness. The actual stresses, however, are also dependent upon less significant, or "second-order," details of the lining design.

Dimensionless Pi Terms. The behavior of the prototype tunnel is assumed to be determined and described with sufficient accuracy by the variables given in Table A2. These variables are the x_i terms of Equation 1, which then becomes

$$f(\sigma_v, \sigma_h, \epsilon \text{ or } q_u, \phi, \sigma_t, E, \nu, d \text{ or } a \text{ or } D \text{ or } R, \phi_j, \theta, s, E_q I/R^3, E_q t/R, u, \epsilon, \sigma, T, M) = 0$$

[Eq 18]

⁵⁵ M.G. Spangler, *The Structural Design of Flexible Pipe Culverts*, Bull. 153, Iowa Eng. Exp. Sta. (1941).

⁵⁶ R.K. Watkins and M.G. Spangler, "Some Characteristics of the Modulus and Passive Resistance of Soil, A Study in Similitude," *HRB Proc.* Vol 37 (1958) pp 576-583.

⁵⁷ U. Luscher, *Behavior of Flexible Underground Cylinders*, Technical Report No. AFWL-TR-65-99 (Air Force Weapons Laboratory, 1965).

⁵⁸ U. Luscher, *Behavior of Flexible Underground Cylinders*.

Table A2
Dimensionless Pi Terms

Loading:	$\sigma_h/\sigma_v, \sigma_v/q_u$
Intact rock:	$\sigma_t/q_u, \phi, E/q_u, \nu$
Rock mass:	$\phi_j, \theta, D/s$
Support properties:	ER^3/E_{qt} or $\sigma_v R^3/E_{qt}, ER/E_{qt}$ or $\sigma_v R/E_{qt}$
Response:	$u/D, \epsilon, \sigma/\sigma_v$ or $\sigma/q_u, T/\sigma_v R, M/\sigma_v R^2$

The next step in the determination of the similitude requirements governing a model study of this phenomenon is to perform a dimensional analysis; that is, to determine a set of pi terms as in Equation 2. By inspection of Table A1 and Equation 3 it is seen that there are $m = n - r = 18 - 2 = 16$ dimensionless pi terms which describe the phenomenon. Rigorous methods are available for determining a complete set of independent pi terms (see for example, Langhaar or Murphy). However, a complete set for the variables in Table A1 can be determined by inspection, and are given in Table A2.

Note that in several places in Table A2 two expressions are given as being equally valid. The principles of dimensional analysis state that in any given set, all pi terms are independent; i.e., no one pi term can be obtained by multiplying together any combination of the other pi terms of that set. But there are an infinite number of sets of independent pi terms which can be given for the n variables, any one set of which can be derived from any second set by multiplying terms of the second set together. For examples, either σ/σ_v or σ/q_u may be considered as one of the pi terms, but both cannot be considered as part of one set because they are not independent. One can be derived from the other by multiplication with other of the pi terms as follows:

$$\sigma/\sigma_v = \sigma/q_u \times q_u/\sigma_v \quad [\text{Eq 19}]$$

It was mentioned earlier that much insight into the phenomenon being considered could often be obtained from the relationships of the variables in the pi terms. The terms σ_v/q_u and σ_h/σ_v show that the free-field stress level relative to the strength of the material is important, and that the ratio of horizontal to vertical stress is of significance. The term D/s shows that the ratio of tunnel diameter to joint spacing is significant in the behavior of the tunnel. The ratios ER^3/E_{qt} and ER/E_{qt} ($E/E_{qt}/R^3$ and $E/E_{qt}/R$) show that the relative

stiffnesses of the rock mass and the liner are of importance in influencing the behavior. Alternately, from $\sigma_v R^3/E_{qt}$ and $\sigma_v R/E_{qt}$ it is seen that the behavior of the liner depends upon its stiffness relative to the applied stress. The development of thrusts and moments is best expressed in terms of the parameters $T/\sigma_v R$ and $M/\sigma_v R^2$. The importance of many of these terms, of course has been recognized for some time from other work, but this dimensional analysis is an independent substantiation of this importance.

Development of Modeling Laws. Using the pi terms just derived, Equation 2 becomes

$$F(\sigma_h/\sigma_v, \sigma_v/q_u, \sigma_t/q_u, \phi, E/q_u, \nu, ER^3/E_{qt} \text{ or } \sigma_v R^3/E_{qt}, \phi_j, \theta, D/s, ER/E_{qt} \text{ or } \sigma_v R/E_{qt}, u/d, \epsilon, \sigma/\sigma_v \text{ or } \sigma/q_u, T/\sigma_v R, M/\sigma_v R^2) = 0 \quad [\text{Eq 20}]$$

This is the dimensionless functional relationship describing the phenomenon. If the model study is to accurately reproduce the prototype field behavior, it is necessary that the pi terms as given in Table A2 and Equation 20 be identical for the model and the prototype, as indicated by Equation 4. This is, for example:

$$(\sigma_h/\sigma_v)_{\text{model}} = (\sigma_h/\sigma_v)_{\text{prototype}} \quad [\text{Eq 21}]$$

$$(\phi)_{\text{model}} = (\phi)_{\text{prototype}}$$

and so on for the rest of the pi terms.

If the symbol K_{x_i} is used to represent the ratio between the value of one of the x_i terms in the model and in the prototype, for example:

$$K_{\sigma_v} = (\sigma_v)_{\text{model}}/(\sigma_v)_{\text{prototype}} \quad [\text{Eq 22}]$$

then the requirements of similitude as given in Equations 4 and 21 dictate certain relationships which must exist between the K_{x_i} ratios. The K_{x_i} ratios are called the scale factors, and the relationships between them are called the model laws. The model laws for this phenomenon, as derived from the pi terms of Table A2 by simple algebraic manipulation, are given in Table A3.

The model laws of Table A3 show that all of the x_i quantities having the dimensions of length L scale in the same ratio K_L between the model and the prototype; all x_i quantities having the dimensions of stress FL^{-2} scale in the same ratio K_G ; and all dimensionless quantities such as strains and angles have the same magnitude in the model as in the prototype. Furthermore, the model laws show that the scale factors for

Table A3
Model Laws

Linear Dimensions L:	$K_L = K_d = K_u = K_D = K_R = K_s$
Stresses:	$K_\sigma = K_{\sigma_v} = K_{\sigma_h} = K_{q_u} = K_{\sigma_t} = K_E$ $K_{E_{qt}/R^3} = K_{E_{qt}/R}$
Strains and Angles:	$K_{\phi_j} = K_\theta = K_\epsilon = K_\nu = K_\phi = 1$
Response:	$K_T = K_\sigma K_L, K_M = K_\sigma K_L^2$

lengths and stresses, K_L and K_σ , are independent and may be chosen arbitrarily.

The inter-relationships between the scale factors K_T , K_M , K_σ , and K_L are not to be interpreted as restrictions upon this independency of K_L and K_σ but merely as a definition of the manner in which thrusts and moments scale between model and prototype.

If the model laws of Table A3 are satisfied, then the requirements of Equation 4 are satisfied and the model is "similar" to the prototype and behaves exactly as the prototype. By measuring the x_i quantities in the model, the x_i quantities of the prototype can be predicted through the scale factors. The accuracy with which the predicted prototype behavior matches the actual prototype behavior depends upon two factors:

- (1) The accuracy of the assumption that the x_i quantities of Table A1 are the quantities which determine and describe the phenomenon, and
- (2) The accuracy with which the model laws are satisfied.

Model Rock Material Requirements. Some very stringent limitations on the behavior of the model rock material are implicit in the modeling ratios given above. The model laws $K_{\sigma_t} = K_{q_u} = K_{\sigma_v} = K_{\sigma_h}$ and $K_\phi = 1$ require that on any dimensionless plot of strengths, the data for both the model and prototype rock materials must collapse onto a single curve. For example, if Fig. A5 were the Mohr envelopes for the prototype and model materials, then on a dimensionless plot of τ/q_u vs σ/q_u such as Fig. A6 the envelopes for the two materials must coincide. On any other dimensionless strength plot, such as $(\sigma_1 - \sigma_3)/q_u$ vs σ_3/q_u , the strength envelopes for the two materials must also coincide.

A similar relationship exists for the deformation characteristics of the model and prototype materials.

The modeling ratios $K_E = K_{q_u}$, $K_\epsilon = 1$, $K_\nu = 1$, and the strength requirements given above require that the materials have the same Poisson's ratio and that on all dimensionless plots of strains or deformations versus stress the curves for the two materials must coincide. For example, if Fig. A7 were the stress-strain curves for the model and prototype materials at comparable confining pressures; i.e., at a value of σ_3/q_u which is the same for both materials, then on a dimensionless plot of $(\sigma_1 - \sigma_3)/q_u$ vs ϵ , the curves for both materials must coincide as in Fig. A8. This means, for example, that in triaxial compression tests at comparable confining pressures, the materials must fail at the same strains. Hence, on a dimensionless plot of $\epsilon_{failure}$ vs σ_3/q_u , the data for the two materials must collapse onto a single curve.

In practice these requirements are almost impossible to satisfy. In a model study of a linearly elastic phenomenon, the strength modeling laws do not exist, and the deformation modeling laws are not so critical since the stress-deformation relationships are linear. For example, $K_\epsilon = 2$ might be allowed without seriously affecting the accuracy of the model. For a model study in which inelastic deformations and failure conditions are important, however, the model laws must be satisfied as nearly as possible. Patterns of stress and strain distribution in the prototype may change markedly as non-linear, inelastic deformations occur and as failure conditions are approached or reached. If the model laws are not satisfied and the model materials do not fulfill the requirements outlined above, the patterns of stress and strain distribution in the model may differ considerably from those of the prototype.

In modeling studies the most common solutions of this dilemma are either (1) to conduct tests in only the quasi-elastic, working-stress range, where the model material requirements are not so critical; or (2) to build the model from essentially the same material as the prototype, as is done in microconcrete model studies of reinforced concrete structures. These approaches are not feasible in geomechanical model studies of underground openings, however.

In the first case, underground structures are highly indeterminate so that local failures can develop without leading to complete failure of the structure. In fact, the economics of underground construction often demand that such local failures be tolerated. Hence, a study of the low stress, quasi-elastic behavior is not sufficient.

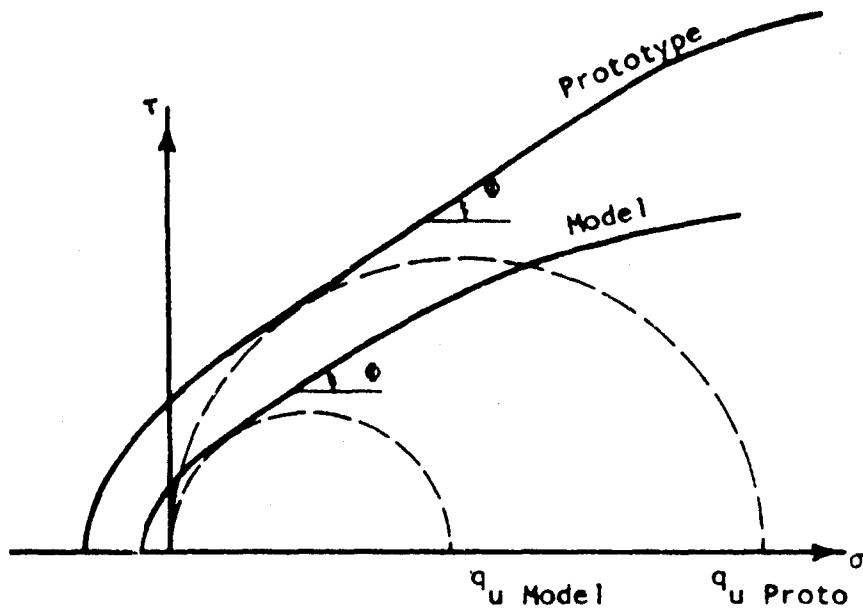


Figure A5. Prototype and model Mohr envelopes.

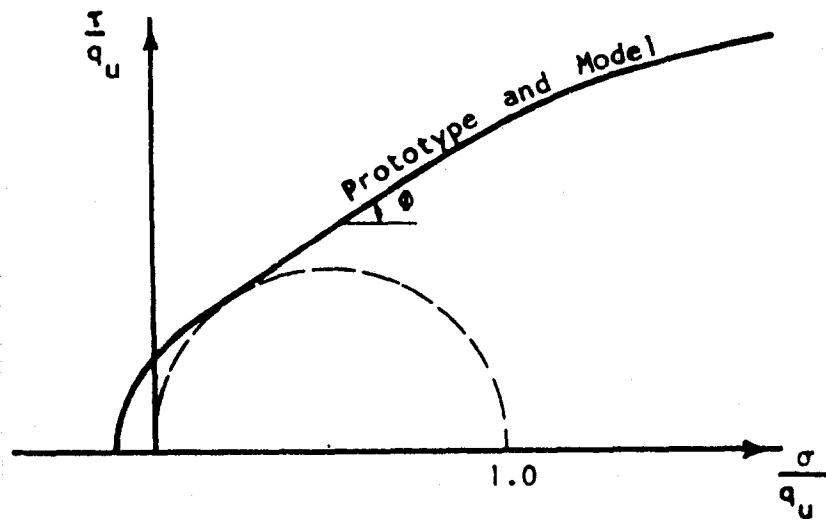


Figure A6. Dimensionless prototype and model Mohr envelopes.

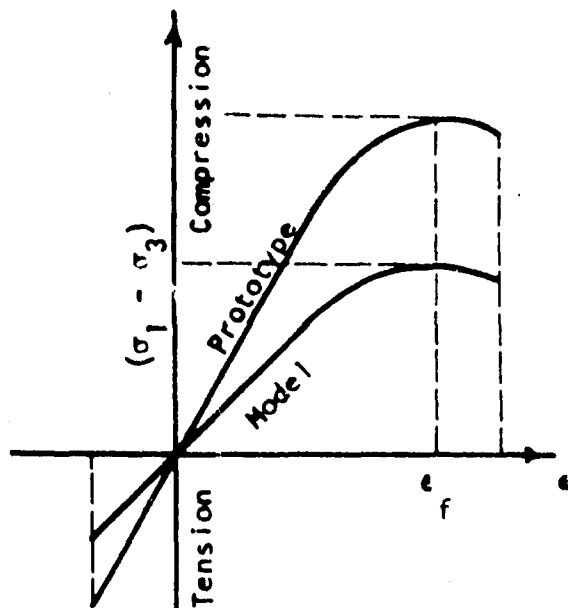


Figure A7. Prototype and model stress-strain curves.

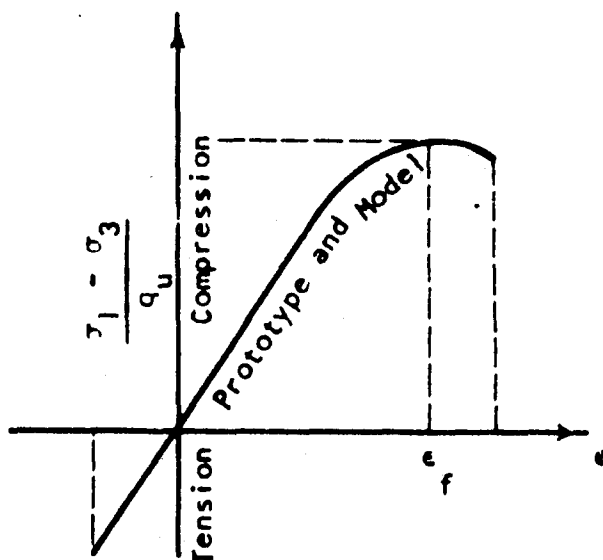


Figure A8. Dimensionless prototype and model stress-strain curve.

The second approach is not feasible for three reasons. First, discontinuities in the actual rock mass exist on a physical scale such that it is impossible to obtain samples of the rock mass small enough so that accurate model studies can be performed when the effect of mass discontinuities is being studied. Secondly, the

strength of the rock materials is generally so great that the size of models constructed of the prototype material which can economically be loaded to failure in the laboratory are too small to be of interest. Finally, it would be very difficult to get "identical samples" for testing from a real rock mass because most rock formations are not sufficiently homogeneous. Hence it is necessary to use artificial, low strength materials for the construction of geomechanical models.

Data for intact rock (for example, Deere and Miller,^{5,9} Deere,^{6,9} Hendron,^{6,1} Handin and Hager,^{6,2} Handin et al.,^{6,3} Corps of Engineers,^{6,4} and Robertson^{6,5} indicate that on the average, the properties of intact rock are such that the tensile strength is about five percent to ten percent of the unconfined compressive strength and the modulus of elasticity is about 250 to 500 times the unconfined compressive strength (E being the tangent modulus at fifty percent of q_u), while the angle of internal friction commonly varies between 25° and 60° , and ν is between 0.1 and 0.3. That is, for actual rock:

$$5\% < \sigma_t / q_u < 10\%; \quad 200 < E / q_u < 500;$$

$$25^\circ < \phi < 60^\circ; \quad 0.1 < \nu < 0.3$$

The material chosen for the construction of the model should also have properties within these ranges if similitude is to be achieved.

Test data indicate that rock specimens typically

^{5,9}D.V. Deere and R.P. Miller, *Engineering Classification and Index Properties for Intact Rock*, Technical Report No. AFWL-TR-65-116 (Air Force Weapons Laboratory, 1966).

^{6,9}D.V. Deere, "Geologic Considerations."

^{6,1}A.J. Hendron, "Mechanical Properties of Rock."

^{6,2}J. Handin and R.V. Hager, "Experimental Deformation of Sedimentary Rocks Under Confining Pressures: Tests at Room Temperature on Dry Samples," *Bull. A.A.P.G.*, Vol 41, No. 1 (January 1957) pp 1-50.

^{6,3}J. Handin, R.V. Hager, M. Friedman and J.N. Feather, "Experimental Deformation of Sedimentary Rocks Under Confining Pressure: Pore Pressure Results," *Bull. A.A.P.G.*, Vol 47, No. 5 (May 1963) pp 717-755.

^{6,4}*Tests for Strength Characteristics of Rock, Pile Driver Project* MRD Lab No. 64/90 (U.S. Army, Missouri River Division Laboratory [MRD], Sept 1964); *Tests for Strength Characteristics of a Schistose Gneiss*, MRD Lab No. 64/493 (May 1965); *Strength Parameters of Selected Intermediate Quality Rocks*, MRD Lab No. 64/493 (July 1966).

^{6,5}F.C. Robertson, "Experimental Study of the Strength of Rocks," *Bull. G.S.A.*, Vol 66 (October 1955) pp 1275-1314.

fail in unconfined compression at axial strains of 0.2 to 1.0 percent. In triaxial compression at confining pressures equal to their unconfined compression strength, rock specimens reach a peak stress difference ($\sigma_1 - \sigma_3$) at axial strains which may range widely, from around one percent for dense igneous rocks up to ten percent to twenty percent or more for ductile shales or evaporites. Rocks commonly exhibit dilation during shear, possible exceptions being very porous sedimentary or volcanic rocks whose porous structure collapses during

shear, or some evaporites which may fail by intercrystalline gliding with no volume change. A "general rock modeling material" should exhibit dilation during shear to satisfy similitude.

Typical stress-strain curves for a wide range of rock types are given in the references listed above. The modeling material chosen should possess stress-strain curves which are of the same shape as those of a typical rock, as in Fig. A4.

APPENDIX B: DESCRIPTION OF MODEL LOADING APPARATUS*

Lateral Loading Elements. The design criteria for the system of applying the lateral pressures, σ_v and σ_h , to the model were that it be able to apply a uniform pressure up to 1,000 psi on the 24" x 8" faces of the model for a total reaction of 192,000 pounds, and that it be able to deform up to one-quarter inch as the model was loaded. Although large, irregular deformations of the faces were not anticipated, a nonuniform concave outward deformation was anticipated for two reasons: (1) the presence of the tunnel, and (2) restraining friction along the adjacent loading faces. Hence, the lateral loads had to be applied by a flexible loading system which could adjust to the irregular model deformations, rather than by a rigid loading head.

It was decided that the load should be actively applied to all four lateral sides, rather than actively loading the model on two adjacent sides and pushing it against a passive reaction on the opposing sides. Although this increased the complexity of the loading system, it was done to maintain loading symmetry in the model so that friction between the model and the longitudinal and lateral loading heads would be symmetrical about the tunnel.

The loading system which was chosen is a completely mechanical one whose basic operation is quite similar to a system used by Hoek^{6,6} on small models 6" x 6" x 1". It consists of a pyramid of increasingly larger triangular elements produced by welding angle irons and flat plates together, as shown in Fig. B1. Two such sets of elements are used to apply the load to each lateral face of the model, as shown in Fig. B2. The load is applied by a hydraulic jack against the transition head element and distributed down through the pyramid to the model, which is in contact with the smallest triangular elements, Element No. 3. At the contact between the elements, grooves 1/16-in. deep with a 1-in. radius are cut into the plates and the angle corners are rounded on a 1/2-in. radius. The purpose of the grooves and rounded corners is threefold: (1) to allow the elements to rotate with respect to each other and

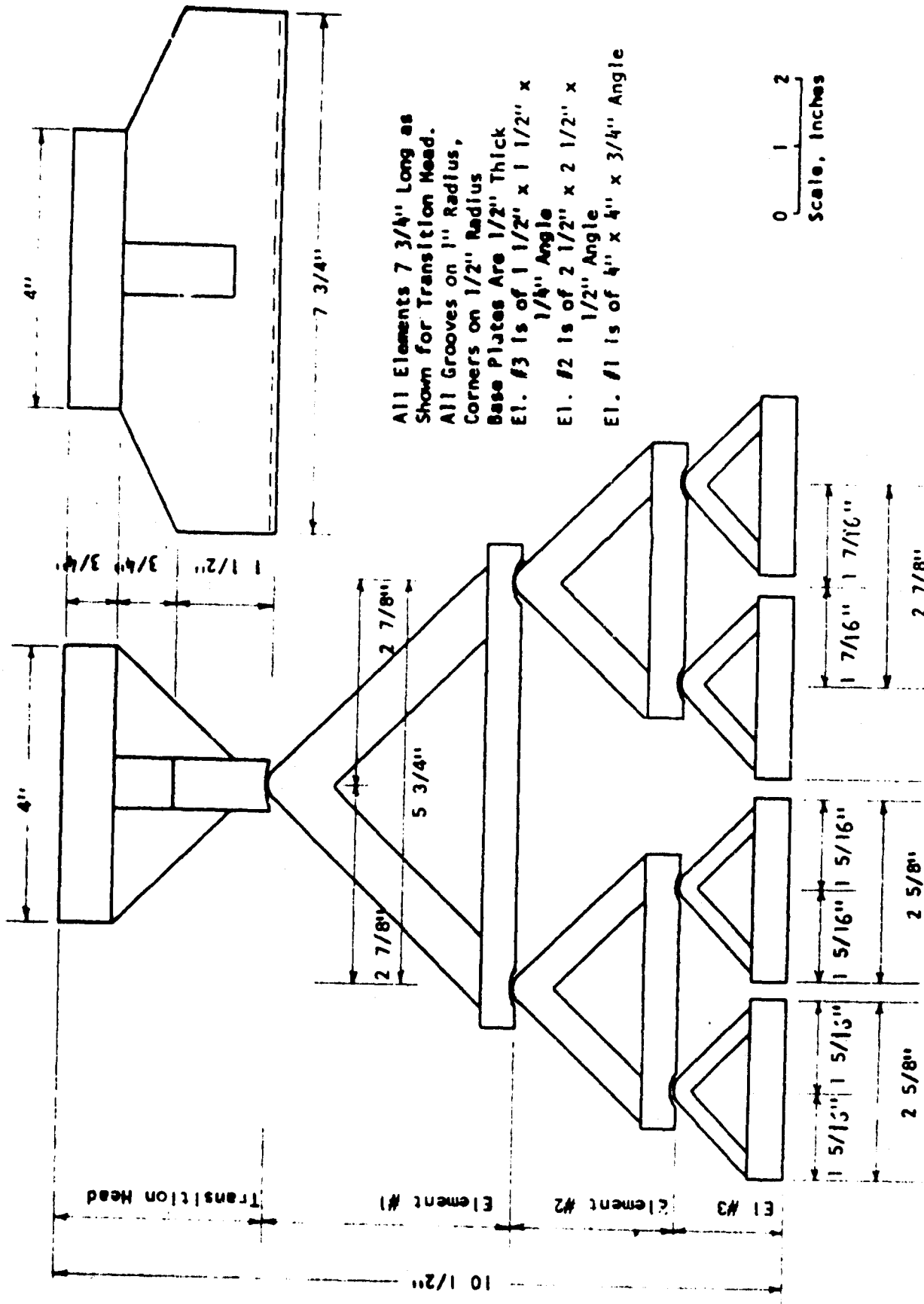
to adjust to any irregular deformations of the model while carrying equal loads, (2) to aid in aligning the elements, and (3) to provide a large enough bearing area at the contacts to prevent local yielding of the steel and flattening of the contacts. Even so, high contact stresses exist, and a high yield strength steel (T-1 steel) was used for the transition heads and the angles of Element No. 1. This system of applying the lateral loads was chosen for two reasons: (1) the successful operation of the similar loading system used by Hoek,^{6,7} and (2) the simple, completely mechanical nature of the system, which suggested that it would be very dependable and rugged.

Load Distribution Characteristics of the Triangular Element Lateral Loading System. The load distribution characteristics of the triangular loading element assembly were studied in some detail to determine how well they satisfy the lateral boundary condition; that of a uniform lateral stress distribution some distance from the tunnel. It is recognized that the stress distribution on the face of the model will be quite irregular due to the finite width and the finite stiffness of the loading elements. The philosophy guiding the design of the elements was that they should be relatively narrow, stiff, and closely spaced, and that each should apply the same total force to the model even if it deforms unevenly. Then, within a short depth into the model, approximately equal to the width of the elements, the actual stress distribution would deviate only slightly from the average stress applied to the boundary. To check the behavior of the loading apparatus, three things were done. First, one set of loading elements was instrumented to determine the loads being carried by the smallest triangles, under uneven deformations of the assembly. Second, concrete blocks the size of the actual model blocks, 24" x 24" x 8", both with and without tunnels, were tested in biaxial compression. These were sprayed with a brittle lacquer coating on an unloaded 24" x 24" face to study the strain distribution in the block. Third, before testing the first model tunnel, a solid block of the model material without a tunnel was tested with internal instrumentation

^{6,6} E. Hoek, *Rock Fracture*.

* After Heuer and Hendron, *Geomechanical Model Study Report 2*

^{6,7} E. Hoek, *Rock Fracture*.



All Elements 7 3/4" Long as Shown for Transition Head.
 All Grooves on 1" Radius,
 Corners on 1/2" Radius
 Base Plates Are 1/2" Thick
 El. #3 Is of 1 1/2" x 1 1/2" x 1/4" Angle
 El. #2 Is of 2 1/2" x 2 1/2" x 1/2" Angle
 El. #1 Is of 4" x 4" x 3/4" Angle

Figure B1. Detail of lateral triangular loading elements.

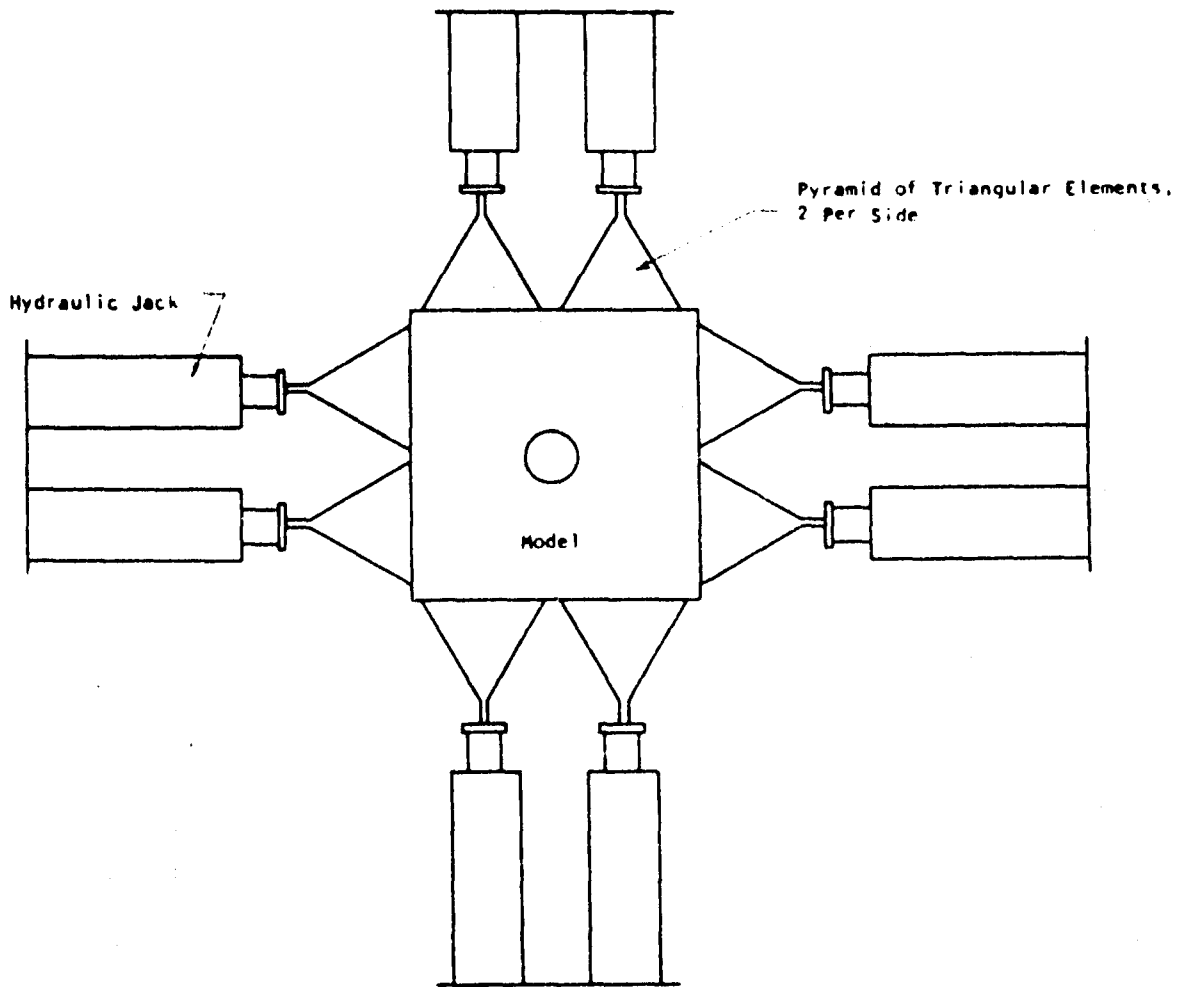


Figure B2. Sketch of lateral loading element assembly (not to scale).

to measure the strain field which was produced within the block. These studies led to the conclusion that the lateral loading system was performing satisfactorily and fulfilling the design requirements and boundary condition.

Load Distribution As Measured by the Instrumented Elements. One set of triangular elements as shown in Figure B4 was used for this study. An electrical resistance strain gage (SR4 Gage, Type A-7) was placed on the center of each leg of each of the four small triangular elements (Element No. 3) as shown in Fig. B3. The two gages from each element were wired into opposite arms of a four-arm Wheatstone bridge and monitored by a strain indicator. Each of the small triangular elements was then loaded individually with the transition head to obtain a calibration curve showing SR4 gage reading versus total load carried by the individual element. The

entire pyramid of triangular loading elements and transition head was then loaded and at successive stages of loading the strain indicated by the SR4 gages on each of the small elements (No. 3) was recorded and compared with the calibration curves to determine how much of the total applied load was being carried by each individual element.

This method of monitoring the loads carried by individual elements is not satisfactory for general usage, although it was sufficient for the purpose of the immediate investigation. The problem with this method is that it is very sensitive to bending moments in the triangle legs, which are in turn caused by bending of the bottom flat plate of the element at the contact with the model. This system of instrumentation is thus quite sensitive to pressure distribution on the base of the elements. Ideally, the instrumentation should be

sensitive only to the average expansion in the legs of the angles. This might be achieved, for example, by placing another A-7 gage on the back of each angle leg, opposite each existing gage and then wiring it in series with the opposing existing gage on into an adjacent arm of the Wheatstone bridge. The back of the angle legs is inaccessible, however, so this could not be done.



Figure B3. An instrumented No. 100 angle leg.

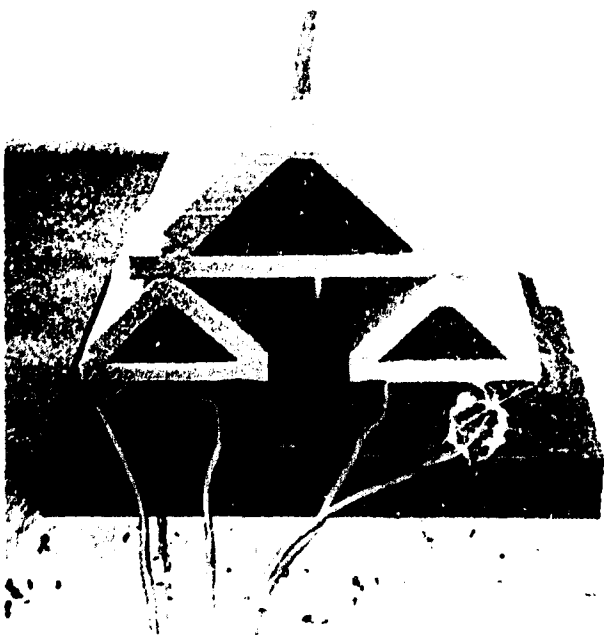


Figure B4. Entire set of instrumentation for one element.

For the immediate investigation, this difficulty was solved as shown in Fig. B4. A steel bar $1/2'' \times 1/8''$ was placed under each edge of each element and these in turn were placed upon a $1/8$ in. strip of rubber. Rubber strips of different stiffness were used to induce differential movement of the elements during loading. The use of narrow strips under the edges of the elements eliminated the problem of pressure distribution across the base. In addition the elements were placed upon a $12'' \times 8'' \times 1-1/2''$ steel plate which could be moved freely so that the individual elements could be centered in the test machine for calibration, and then the whole assembly could be centered for loading. In this way the whole loading assembly could be tested with the small elements in exactly the same position and with exactly the same base conditions with which they were calibrated.

The results of the tests on the whole assembly are shown in Fig. B5. The maximum variation between elements is approximately plus or minus 2.3 percent of the total assembly load and was generally around plus or minus one percent. The variation between the load carried by each element is almost equal to the variation in the calibration of the individual elements, so that within the accuracy of this method of measurement, the elements are carrying equal loads. This was measured during tests in which significant movement of the whole assembly and significant relative movements of individual elements were recorded as shown in Fig. B5.

In summary, this study showed that this lateral loading assembly can accommodate substantial differential movements of its base while distributing the total load equally across the base.

Longitudinal Restrain and Reaction Frame. The method of applying the longitudinal restraint and the method of supplying the lateral jacking reactions are intimately related in the design of the loading machine and must be considered together. As discussed previously, a condition of plane strain should be approximated in the model. Three methods of achieving this result were listed:

- (1) A uniform pressure against the longitudinal faces, controlled to null any longitudinal expansion which tends to develop.
- (2) Rigid heads against the longitudinal faces, tied rigidly together across the model.
- (3) Rigid heads against the longitudinal faces, with a controlled load applied to them to null

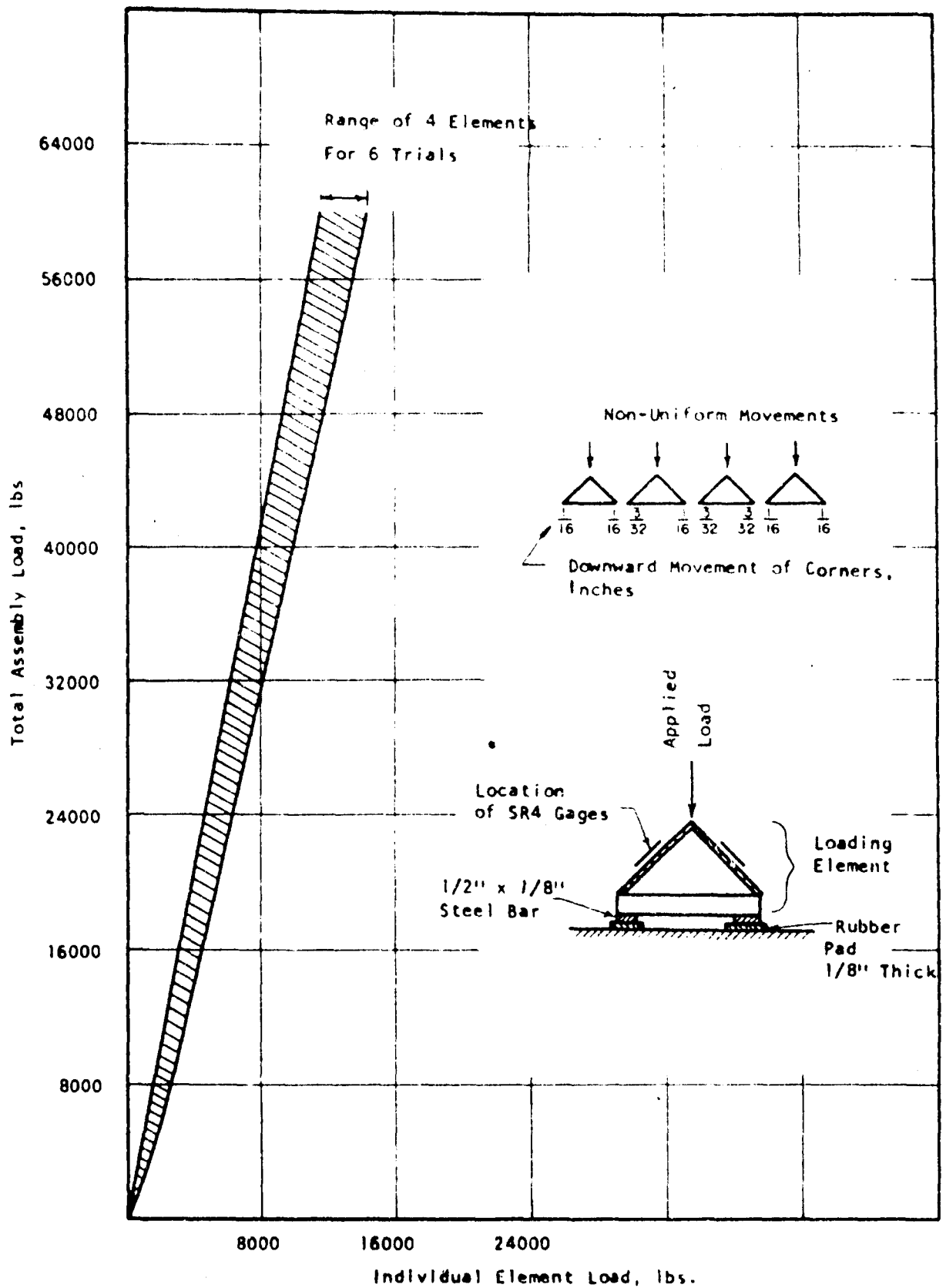


Figure B5. Calibration of lateral loading elements.

any longitudinal expansion which tends to develop.

Uniform Restraining Pressure System. It is believed that the uniform pressure method would not satisfy the boundary condition satisfactorily. Dilation of the material is expected in failure zones which develop around the tunnel, with some expansion occurring in the longitudinal direction. More pressure would be required to null longitudinal strains in these regions than in regions away from the tunnel which are still behaving elastically. A uniform nulling pressure would then be too low to prevent expansion in the plastic zones and/or too high to exactly null strains in the elastic zones. Hence, the longitudinal faces would not remain plane during the loading, but would warp. Thus, the system is unsatisfactory.

Rigid Heads Tied Across Model. The second method suggested has the obvious advantage of greatly simplifying the test procedure. Once the model is in testing position, the longitudinal heads are brought into contact with it and tied together across the model, probably at the corners of the model. Then during the lateral loading the model is restrained from longitudinal expansion by the rigid heads and ties. This would eliminate the need for monitoring and regulating the longitudinal deformations and loads. A serious problem which must be given careful consideration with an apparatus of this sort is the difficulty of seating with the restraining heads against the model. Because of the very small longitudinal expansion which would occur even in the plane stress condition, the restraining heads

must be seated very carefully and tightly. Otherwise, the expansion of the model which would occur before intimate contact with the restraining loads was developed would be of the same order of magnitude as the total expansion during the test. In such a case the actual test condition would approximate plane stress more closely than plane strain. In spite of this problem, the anticipated simplicity of the testing procedure with an apparatus of this sort is very attractive and the design of such a system was carefully considered.

To be acceptable, the calculated deformation of such an apparatus should not exceed about 10 percent of the plane stress expansion of a model block. Such an apparatus proved too massive to be practical. The problem of adequately seating a model in an apparatus of this design remains unsettled. Furthermore, such an apparatus, representing a sizable investment, would not have the adaptability and general capabilities of the design finally chosen. For these reasons, it was decided that rigid heads tied together across the model were not a satisfactory design.

Controlled Rigid Longitudinal Heads. The next system considered is shown schematically in Fig. B6. The bottom frame and lateral reactions would be combined into a single unit. The top head would consist of a grill work as shown in Fig. B7 with a 1-in. bottom cover plate in contact with the model and a 1/2-in. top cover plate. Hydraulic jacks would force the head against the model to null longitudinal expansion of the model.

Calculation of the deformation of this "rigid"

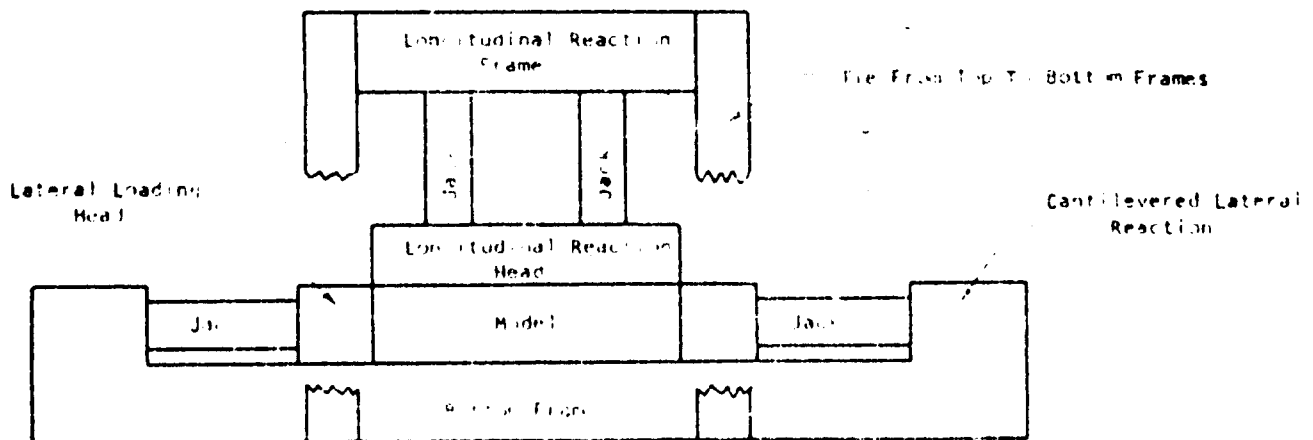
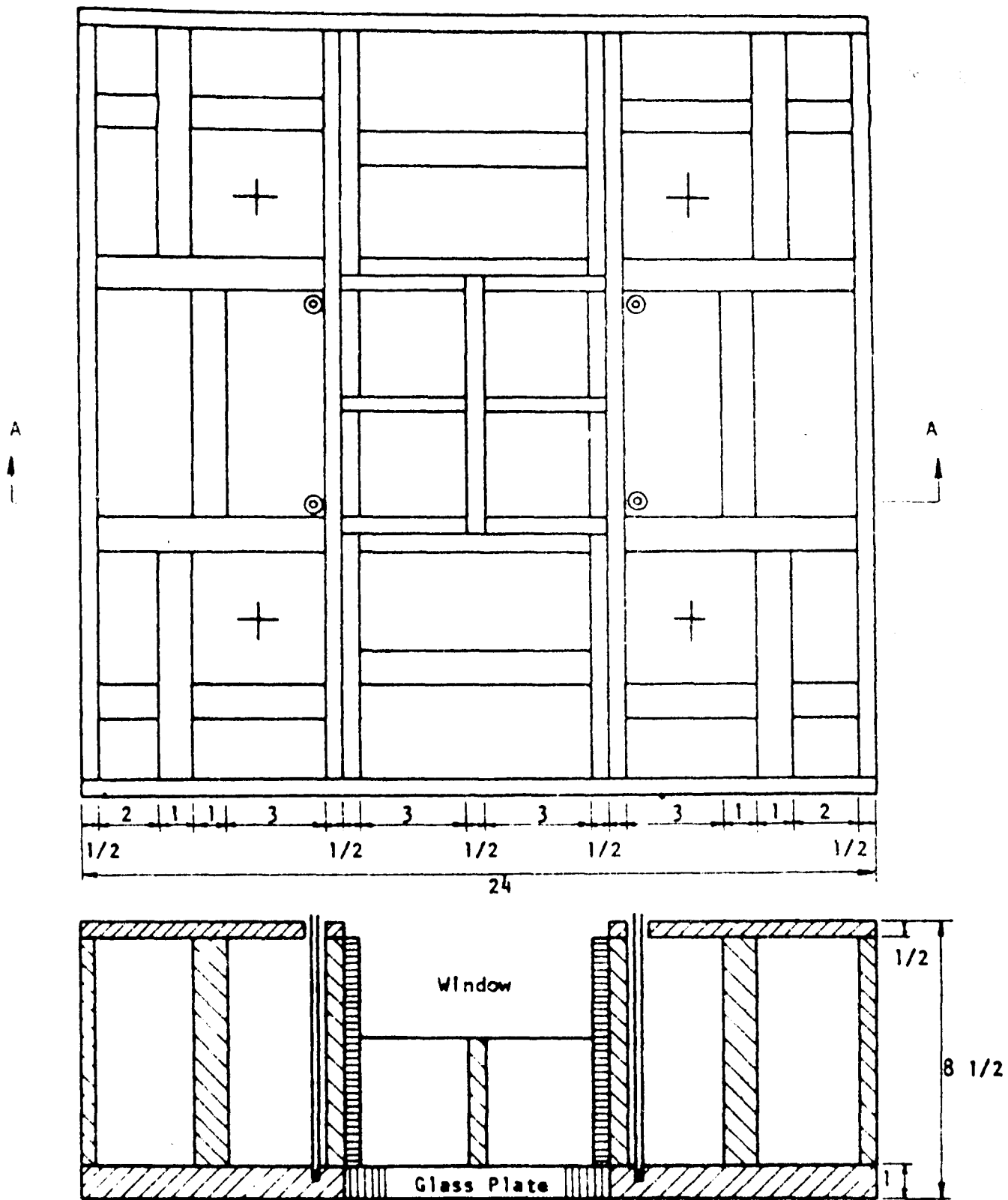


Figure B6 Sketch of possible cantilevered lateral reaction system (not to scale).



Section AA

Figure B7. Plan and section of top head. Window is 1" x 8" x 8" plate of LOF Tutlex glass. In plan view, crosses mark centers of hydraulic jacks, circles represent 1/2" holes in top plate to receive 1/4" rod threaded into bottom cover plate.

head, assuming a uniformly distributed load from the model and point loads from the jacks, indicates that waviness of the surface in contact with the model would be less than plus or minus 10 percent of the longitudinal model expansion which would occur in the plane stress case, considering both shearing and bending deformations. This was considered satisfactory and was actually an overestimate since the jack reactions would be spread over the area of the jack bases and would not be point loads.

The difficulty with this design was that the support for the lateral jacks was not symmetrical, but was cantilevered off the bottom frame. This produced bending stresses and a convex upward curvature in the bottom frame under the base of the model, which was intolerably large. A number of schemes were considered for reducing this curvature but calculations for all schemes showed that the maximum deformation of the center would be up to 20 percent of the plane stress deformation, unless steel sections much larger than shown were used. The conclusion reached is that an eccentric support of the lateral reactions was unsatisfactory.

Utilizing experience gained from previous considerations, a final design was arrived at in which the

reactions were symmetrically supported and deformation of the reaction frame was not a major problem. This design is shown in Figures B8 and B14. Overall views of the apparatus are shown in Figure B8 and B9. The lateral loads were applied by the pyramids of triangular elements discussed previously, which were arranged as shown in Fig. B10. The reactions for the lateral jacks were supplied as shown in Fig. B11. The horizontal 1 3/4-in. rods were removed while positioning the model in the loading frame and setting up the test. These rods had the same cross-sectional area as the horizontal 3" x 3" x 7/16" angle iron ties, and the axis of the lateral jacks was spaced vertically midway between the centroid of the rods and the centroid of the angles, in both the σ_v and σ_h directions. Hence, bending moments in the lateral reaction frame were kept to a minimum. Moreover, the lateral reaction system was independent of the longitudinal system, and deformations and moments in the lateral system had no effect upon the longitudinal deformations.

The top longitudinal loading head was the same as shown in Fig. B7. Note that this head contained an 8" x 8" glass window allowing observation of the tunnel during the test. The bottom restraint was a passive element, the 2' x 2' x 2' concrete cube as shown in Figures B12 and B13. The reactions were supplied by

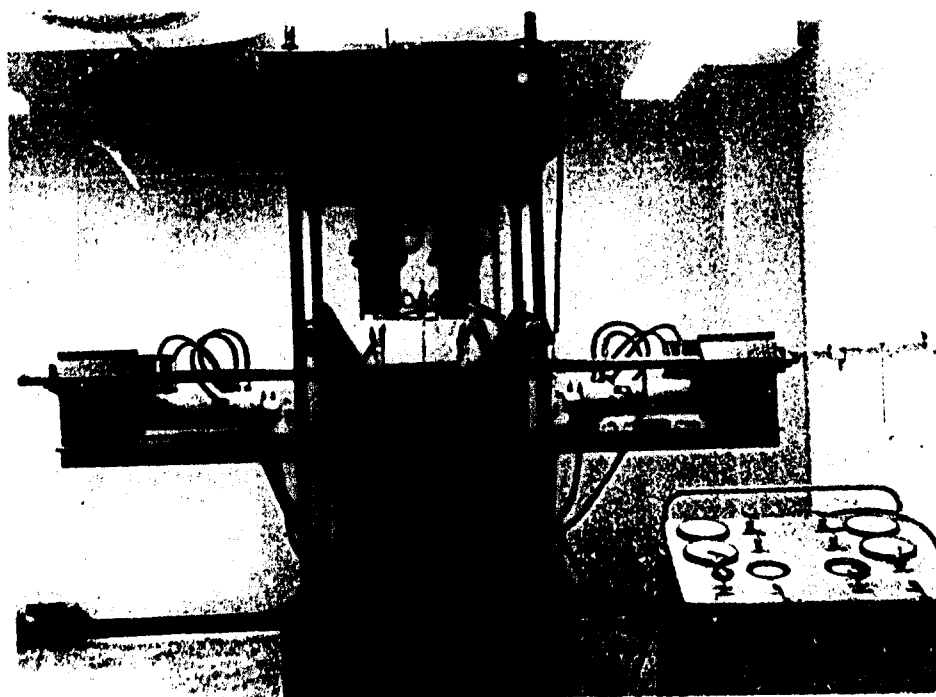


Figure B8. Loading machine.

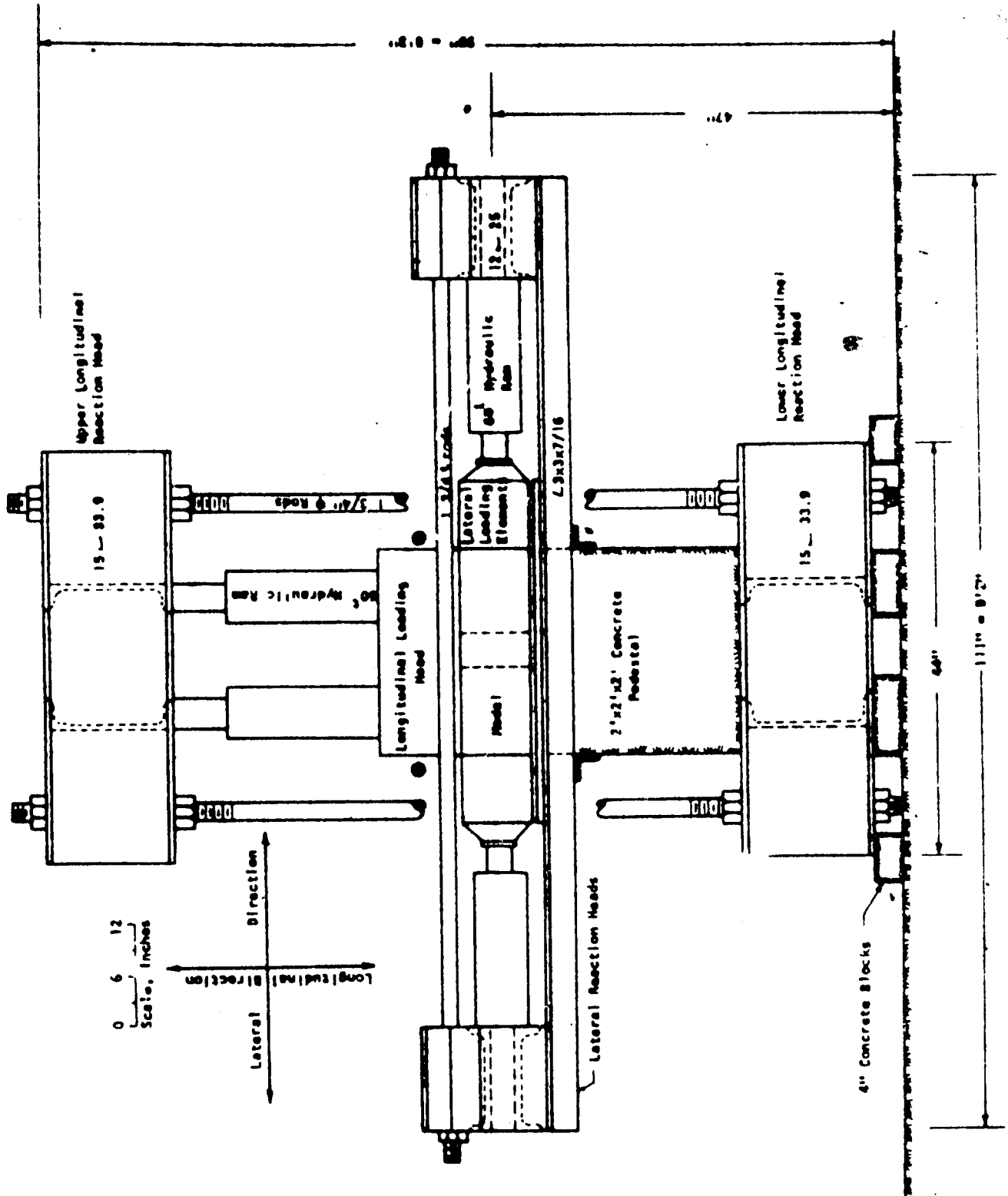
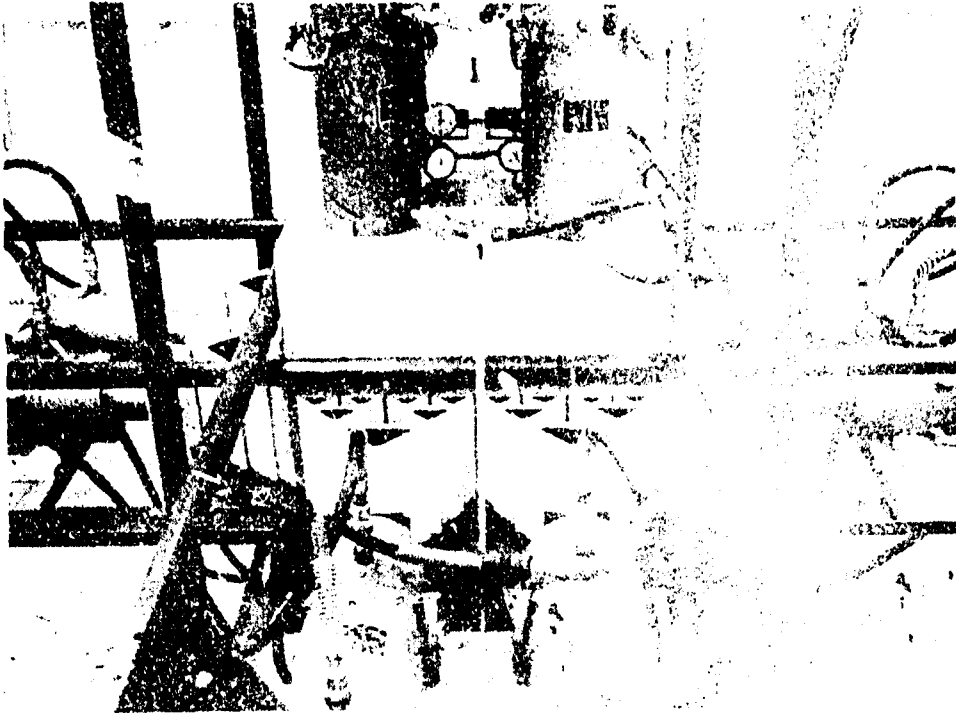


Figure B9. Loading frame assembly.



Best Available Copy

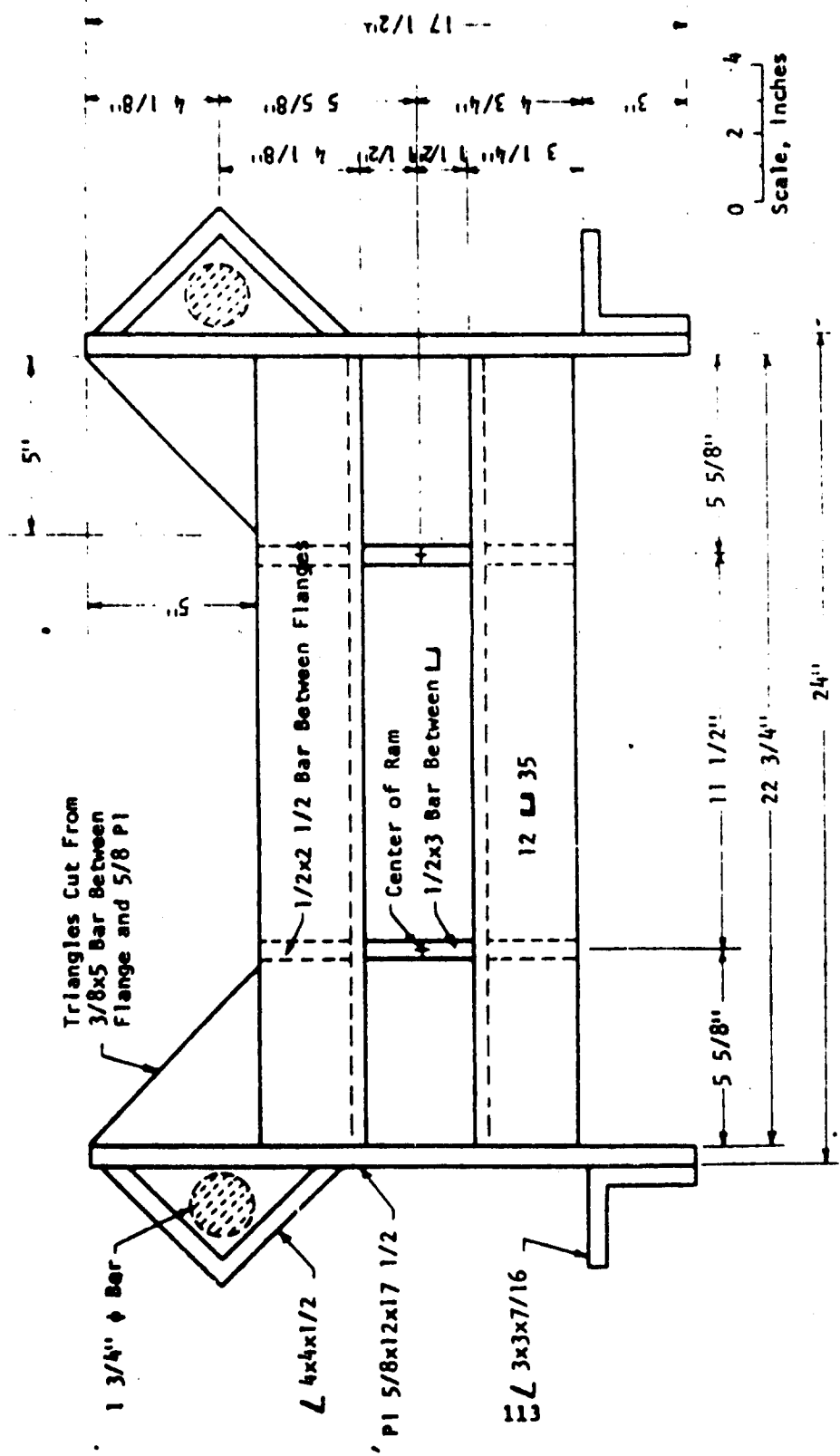


Figure B11. Longitudinal end reaction in σ_y direction.



Figure B12. Lower longitudinal reaction head and concrete pedestal.

top and bottom longitudinal reaction heads as shown in Fig. B14, which were tied together by the four vertical 1 3/4-inch diameter rods. While considerable deformation of these top and bottom reaction heads occurred, it was of no significance because the model did not rest directly against them. The model was shielded from irregular deformation of the bottom frame by the 2-ft concrete cube, while being loaded from the top by the hydraulic jacks acting against the top loading head. The system designed for monitoring the longitudinal strains is discussed later in the section on instrumentation of the model.

For those members in which deformation was not a controlling factor, the reaction frame was designed for an extreme fiber stress of 20,000 psi in both tension and compression in the rolled steel sections, which were of A36 steel. The horizontal and vertical tie rods

were subjected to higher stresses in the threaded sections, and were of higher yield steel.

In an attempt to ensure seating of the loading heads (and longitudinal deformation measuring points) against the model, the following procedure was used: The top 3/8-in. aluminum plate beneath the model (Fig. B13) was the bottom of the mold in which the model was compacted, hence it fitted tightly against the model. The bottom 3/8-in. steel plate was cast directly against the concrete cube. As the model was put in testing position a thin film of plaster (approximately 1/16-in. thick) was placed between the 3/8-in. plates to ensure complete contact between them. Another thin film of plaster was placed between the top loading head and the model to ensure a tight, continuous fit. Then, when testing was begun, a 30 psi longitudinal seating load was applied before the lateral loads were applied.

The hydraulic jacks used were twelve Simplex RC-6010 double-acting 60 ton hydraulic rams. They were actuated by the pressure console seen in Fig. B8. The console was driven by air pressure and featured two independent hydraulic systems each capable of producing pressures of 10,000 psi from an air pressure of 100 psi. The four jacks applying the σ_v loads to the model were driven by one of the consoles' hydraulic systems, while the four applying the σ_h loads were driven by the other system. A hydraulic pressure of 7,150 psi was required to develop the average stress of 1,000 psi against the model. In the initial tests of model blocks without tunnels, the four longitudinal hydraulic jacks were driven from one common hand pump. It was observed that any tendency of the longitudinal loading head to rotate could not be controlled with this system, and further testing was done with an individual hand pump for each jack, ensuring positive control of the longitudinal loading head movements.

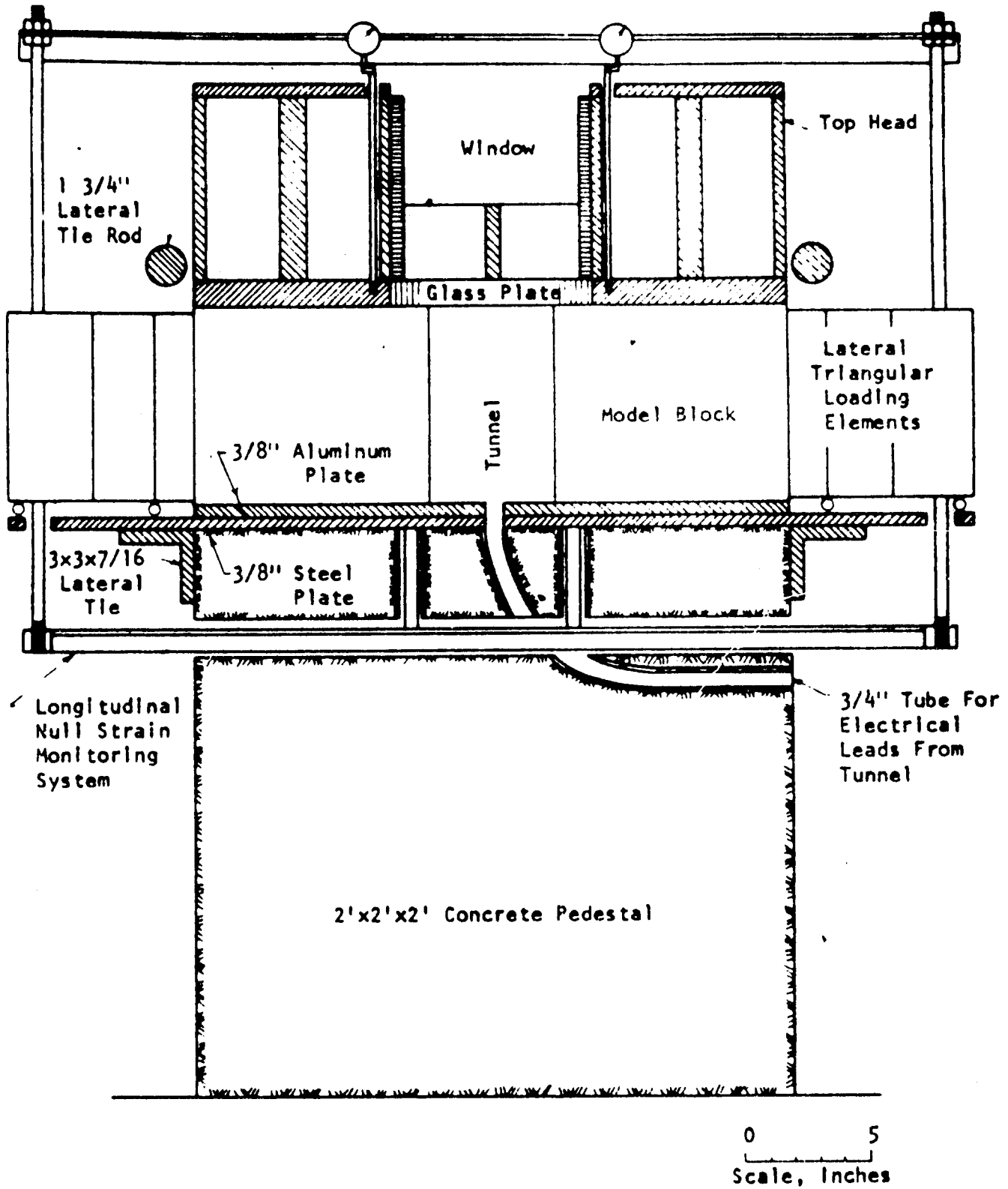


Figure B13. Schematic diagram of base and loading element assembly.

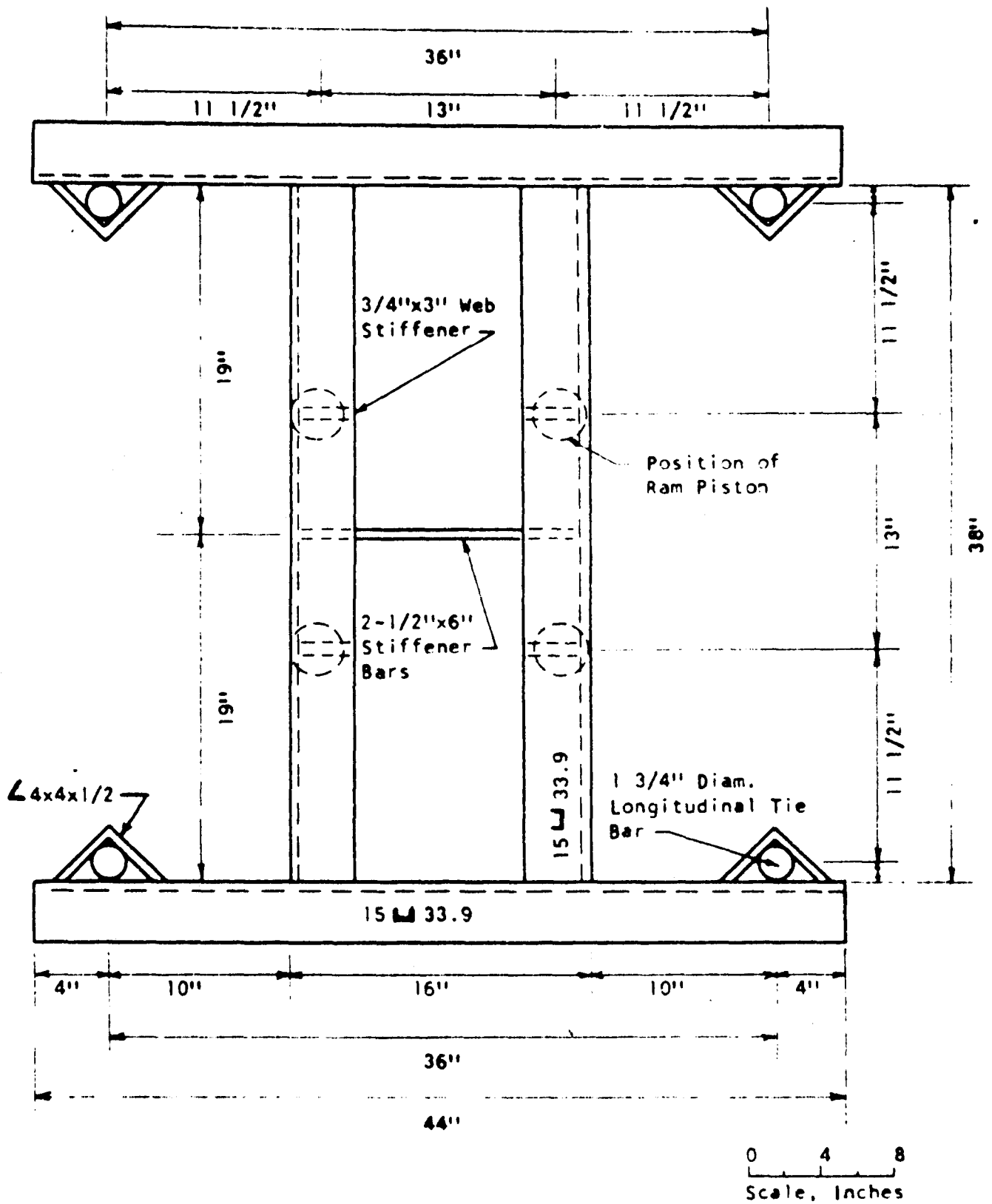


Figure B14. Top longitudinal reaction head.

REFERENCES

- Anderson, R.H., and Boresi, A.P., "Equilibrium and Stability of Rings Under Nonuniformly Distributed Loads," *Proc. of the Fourth U.S. Nat. Cong. of Applied Mech.*, Vol 1 (ASME, 1962).
- Barron, K., and Larocque, G., "Development of a Model for a Mine Structure," *Proc. Rock Mech. Symp.* (McGill University, Montreal, 1962) pp 145-190.
- Bieniawski, Z.T., "Mechanism of Brittle Fracture of Rock," *Int. Journ. Rock Mech. and Mining Sci.* (Oct 1967) pp 395-430.
- Bodner, S.R., "On the Conservativeness of Various Distributed Force Systems," *Journal of the Aeronautical Sciences*, Vol 25, No. 2 (Inst. of the Aeronautical Sci., Inc., 1958).
- Boresi, A.P., "A Refinement of the Theory of Buckling of Rings Under Uniform Pressure," *Journal of Applied Mechanics*, Vol 22, (ASME, 1955).
- Caudle, R.D., and Clark, B.G., "Stresses Around Mine Openings in Some Simple Geologic Structures," *Eng. Exp. Sta., Bull. No. 430* (University of Illinois, 1955).
- Cheney, M., "Bending and Buckling of Thin-Walled Open-Section Rings," *Proc. ASCE, Journ. Eng. Mech. Div.*, EM5, paper 3665 (1963) pp 17-44.
- Strength Parameters of Selected Intermediate Quality Rocks*, MRD Lab No. 64/493 (Corps of Engineers, Missouri River Division Laboratory [MRDL], July 1966).
- Tests for Strength Characteristics of Rock, Pile Driver Project*, MRD Lab No. 64-90, (MRDL Sept. 1964).
- Tests for Strength Characteristics of A Schistose Gneiss*, MRD Lab No. 64/126 (MRDL, May 1965).
- Deere, D.U., Discussion of "Failure of Homogeneous Rock Under Dynamic Compressive Loading," by G.B. Clark and R.D. Caudle, *State of Stress in the Earth's Crust*, W.R. Judd, ed. (Elsevier, 1964) pp 321-323.
- Deere, D.U., "Geologic Considerations," *Rock Mech. in Eng. Pract.*, Chap 1, Stagg and Zienkiewicz, ed. (John Wiley and Sons, 1968).
- Deere, D.U., and Miller, R.P., *Engineering Classification and Index Properties for Intact Rock*, Technical Report No. AFWL-TR-65-116, (Air Force Weapons Laboratory [AFWL], 1966).
- Dorris, A.F., *Response of Horizontally Oriented Buried Cylinders to Static and Dynamics Loading*, Technical Report No. 1-862, Corps of Engineers, Waterways Experiment Station [WES] 1965).
- Everling, G., "Model Tests Concerning the Interaction of Ground and Roof Support in Gate-Roads," *Int. Journ. Rock Mech. and Min.Sci.*, Vol 1, No. 3 (1964) pp 319-326.
- Fumagalli, E., "Communication Sur Les Materiaux Pour Modeles Statiques De Barrages En Beton," *5th Int. Cong. on Large Dams*, Vol IV, c. 26 (Paris, 1955) pp 1039-1074.
- Fumagalli, E., "Model Simulation of Rock Mechanics Problems," *Rock Mechanics in Engineering Practice*, Chap II, Stagg and Zienkiewicz ed. (John Wiley & Sons, 1968).
- Fumagalli, E., *Modeles Geomecaniques des Reservoirs Artificiels: Materiaux, Technique D'essais, Ex-empler de Reproduction Sur Models*, ISMES Pub. No. 26 (Bergamo, Italy, Oct 1964).
- Fumagalli, E., "The Use of Models in Reinforced Concrete Structures," *Mag. of Conc. Res.*, Vol 12, No. 35 (July 1960) pp 63-72.
- Goodman, R.E., "On the Distribution of Stresses Around Circular Tunnels in Non-Homogeneous Rocks," *Proc. 1st Int. Cong., Int. Soc. of Rock Mech.*, Vol 2 (1966) pp 249-255.
- Goodman, R.E., Taylor, R.L., and Brekke, T.L. "A Model for the Mechanics of Jointed Rock," *Proc. ASCE*, Vol 94, No. SM3 (May 1968) pp 637-659.
- Handin, J., and Hager, R.V., Jr., "Experimental Deformation of Sedimentary Rocks Under Confining Pressures: Tests at Room Temperature on Dry Samples," *Bull. A.A.P.G.*, Vol 41, No. 1 (January 1957) pp 1-50.
- Handin, J., Hager, R.V., Jr., Friedman, M., and Feather, J.N., "Experimental Deformation of Sedimentary Rocks Under Confining Pressure: Pore Pressure Results," *Bull. A.A.P.G.*, Vol 47, No. 5 (May 1963) pp 717-755.
- Hendron, A.J., Jr., "Mechanical Properties of Rock,"

- Rock Mech. in Eng. Pract.*, Chap 2, Stagg & Zienkiewicz, ed. (John Wiley & Sons 1968).
- Hendron, A.J., Jr. and Aiyer, A.K., *Stresses and Strains Around a Cylindrical Tunnel in an Elasto-Plastic Material with Dilatancy*, Technical Report on contract No. DACA 45-69-C-0100 (Omaha District, U.S. Army Corps of Engineers, January 1971 [In Publication]).
- Hendron, A.J., Jr., Engeling, P., Aiyer, A.K. and Paul, S., *Geomechanical Model Study of the Behavior of Underground Openings in Rock Subjected to Static Loads, Report 3* (U.S. Army Engineer Waterways Experiment Station [WES] [in publication]).
- Heuer, R.E., and Hendron, A.J., *Geomechanical Model Study of the Behavior of Underground Openings in Rock Subjected to Static Loads: Report 1, Development of Modeling Techniques*, Contract Report N-69-1 (WES, October 1969).
- Heuer, R.E. and Hendron, A.J., *Geomechanical Model Study of the Behavior of Underground Openings in Rock Subjected to Static Loads: Report 2, Tests on Unlined Openings in Intact Rock*, Contract Report N-69-1 (WES, 1971).
- Heuer, R.E., *Geomechanical Model Study of the Behavior of Underground Openings in Rock Subjected to Static Loads*, Ph.D. Thesis (University of Illinois, 1971).
- Hetenyi, M., *Beams on Elastic Foundations* (University of Michigan Press, 1946).
- Hobbs, D.W., "Scale Model Studies of Strata Movement Around Mine Roadways, Apparatus, Technique, and Some Preliminary Results," *Int. Journ. of Rock Mech. and Min. Sci.*, Vol 3, No. 2 (May 1966) pp 101-128.
- Hobb, D.W., "Scale Model Studies of Strata Movement Around Mine Roadways I, The Dependency of Roadway Closure upon Rock Strength; II, The effect of Dinting; III, The Effect of Slotting A Solid Rib," *Int. Journ. of Rock Mech. and Mining Sci.*, Vol 5, No. 3 (1968) pp 219-251.
- Hoeg, K., *Pressure Distribution on Underground Structural Cylinders*, Tech. Report No. AFWL-TR-65-98 (AFWL, 1966).
- Hoek, E., *Rock Fracture Under Static Stress Conditions*, Nat. Mech. Eng. Res. Inst., Council for Sci. and Ind. Res., SCIR Rept. MEG 383 (Pretoria, South Africa, Oct. 1965).
- Hoek, E., "Brittle Failure of Rock," *Rock Mech. in Eng. Prac.*, Chap 4, Stagg and Zienkiewicz, ed. (John Wiley & Sons, 1968).
- Jeager, J.C., *Elasticity, Fracture, and Flow* (Methuen and Co. Ltd, London, 1962).
- Jeager, J.C., "Brittle Fracture of Rocks," *Failure and Breakage of Rock, 8th Symp. on Rock Mech.* (A.I.M.E., 1967) pp 3-131.
- Lane, K.S., "Garrison Dam Test Tunnel, Evaluation of Results," *Trans. ASCE*, Vol 125, Pt 1, Paper 3022 (1960) pp 268-306.
- Langhaar, H.L., *Dimensional Analysis and Theory of Models* (John Wiley & Sons, 1951).
- Luscher, U., *Behavior of Flexible Underground Cylinders*, Technical Report No. AFWL-TR-65-99 (AFWL, 1965).
- Luscher, U., *Study of the Collapse of Small Soil-Surrounded Tubes*, Technical Report AFSWC-TDR-63-6 (Air Force Spec. Weap. Center, 1963).
- Mandel, J., "Tests on Reduced Scale Models in Soil and Rock Mechanics, A Study of the Conditions of Similitude," *Int. Journ. Rock Mech. and Min. Sci.*, Vol 1, No. 1 (1964) pp 31-42.
- Mindlin, R.D., "Stress Distribution Around A Tunnel," *Proc. A.S.C.E.* (April 1939) pp 619-642 (Also in *Trans. A.S.C.E.*, Vol 105, pp 1117-1140, 1940).
- Murphy, G., *Similitude in Engineering* (Ronald Press, 1950).
- Nadai, A., *Theory of Flow and Fracture of Solids*, 2 Vol (McGraw-Hill, 1950).
- Obert, L., and Duvall, W.I., *Rock Mechanics and the Design of Structures in Rock* (John Wiley & Sons, 1967).
- Panek, L.A., *Stresses About Mine Openings in a Homogeneous Rock Body*, New York, (1951).
- Preece, B.W., and Davies, J.W., *Models for Structural Concrete* (C.R. Books Ltd., London, 1964).
- Reyes, S.F., *Elastic-Plastic Analysis of Underground Openings by the Finite Element Method*, Ph. D. Thesis (University of Illinois, 1966).
- Robertson, E.C., "Experimental Study of the Strength

- of Rocks," *Bull. G.S.A.*, Vol 66 (October 1955) pp 1275-1314.
- Rocha, M., "Model Tests in Portugal," *Civ. Eng. and Pub. Work Rev.*, Vol 53, No. 619 (Jan. 1958) pp 49-53; and No. 620 (Feb 1958) pp 179-182.
- Rocha, M., "Structural Model Techniques Some Recent Developments," *Stress Analysis* Chap 16, Zienkiewicz and Hollister, ed., (John Wiley & Sons, Ltd., 1965).
- Seely, F.B., and Smith, J.O., Jr., *Advanced Mechanics of Materials* (John Wiley & Sons, 1952).
- Spangler, M.G., *The Structural Design of Flexible Pipe Culverts*, Bull. 153, Iowa Eng. Exp. Sta. (1941).
- Terzaghi, K., and Richart, F.E., Jr., "Stresses in Rock About Cavities," *Geotechnique*, Vol 3 (1952) pp 57-90.
- Thompson, E. and Ripperger, E.A., "An Experimented Technique for the Investigation of the Flow of Halite and Sylvinite," *6th Symp. on Rock Mech.* (Univ. of Missouri at Rolla, 1964) pp 467-488.
- Timoshenko, S., and Gere, J., *Theory of Elastic Stability* (McGraw-Hill, 1961).
- Timoshenko, S., and Goodier, J.N. *Theory of Elasticity* (McGraw-Hill, 1951).
- Watkins, R.K. and Spangler, M.G. "Some Characteristics of the Modulus of Passive Resistance of Soil. A Study in Similitude," *HRB Proc.*, Vol 37, (1958) pp 576-583.
- Zienkiewicz, O.C., "Continuum Mechanics as an Approach to Rock Mass Problems," *Rock Mech. in Eng. Pract.*, Chap 1, Stagg and Zienkiewicz, ed. (John Wiley & Sons, 1968).